ABSTRACT

QIN, HANTANG. Development of High Resolution Rapid Prototyping Method for Flexible Electronic Devices Based on Electrohydrodynamic Inkjet Printing. (Under the direction of Drs. Yuan-Shin Lee and Jingyan Dong).

This research focuses on developing micro level rapid prototyping methods to fabricate conductive patterns for low-cost flexible electronic devices. The fabrication techniques presented in the study provide significant replenishments for additive manufacturing community by investigating metal nanoink and rapid prototyping methods for flexible substrates.

In recent years, flexible electronics and rapid prototyping both demonstrate attractive features and have been rapidly developed. However, there are two main challenges before rapid prototyping can be applied for flexible electronics: (1) how to achieve high resolution features, and (2) how to acquire micro patterns with great electrical performance on flexible substrates.

In the research, a rapid prototyping method based on electrohydrodynamic jet (e-jet) printing was developed for fabrication of flexible electronic components using silver nanoink. Silver nanoink was first characterized in the study for patterning of sub-20 μm features by controlling input parameters with the help of material deposition mechanism and sub-micro position system.

Residual charges and electrical performance of printed pattern were two main challenges for e-jet printing other than resolution issues. These two challenges were critical before this rapid prototyping method can be used for flexible electronics, especially where highly insulated substrates such as polyethylene terephthalate (PET) film were used. AC-pulse modulated voltage was introduced in the study to overcome residual charge problems

for higher resolution and pattern accuracy. The printing speed was coupled with AC-voltage frequency to neutralize charges of printed droplets by consequently printing equally positive charged and negative charged droplets. Curing process and electroless copper deposition were investigated to improve the electrical performance of printed patterns.

The prototyping method was further investigated to device fabrication and system integration. An array of microelectrodes for capacitive touch screen applications using the proposed rapid prototyping method was discussed in the end. Pre-treatment process for substrate film will be future research work to fabricate micro electrodes with high electrical performance and fine cross-section profile control. Based on my proposed rapid prototyping method, the capacitive sensor was fabricated and tested in order to demonstrate the capability and versatility of my approach. The printed silver microelectrodes are potential replacements for traditional indium-tin-oxide (ITO) electrodes for future flexible display technologies. The proposed fabrication technique is capable of rapid prototyping of electronic components for flexible electronic, medical sensors, wearable devices, and radio frequency identification devices.

Development of High Resolution Rapid Prototyping Method for Flexible Electronic Devices Based on Electrohydrodynamic Inkjet Printing

by
Hantang Qin

A dissertation submitted to the Graduate Faculty of
North Carolina State University
in partial fulfillment of the
requirements for the degree of
Doctor of Philosophy

Industrial Engineering

Raleigh, North Carolina

2016

APPROVED BY:

_____	_____
Dr. Yuan-Shin Lee Chair of Advisory Committee	Dr. Jingyan Dong Co-Chair of Advisory Committee
_____	_____
Dr. Paul H. Cohen	Dr. Roger Narayan

DEDICATION

To my parents, Zhaoqing Qin and Yunping Miao, who have worked very hard to support me to achieve my goal.

To my wife, Dr. Xiaolei Shi, whose sacrificial care for me and our child makes it possible for me to complete this work.

To my daughter, Charlotte Y. Qin, who is indeed a treasure for me.

To my advisors, professors, and all of my friends, without whom none of my success would be possible.

BIOGRAPHY

Hantang Qin was born in 1990, in Dingtao, Shandong, China. He moved to Jinan, capital of Shandong, in 2003, and finished his high school at Jigang High School in 2008. He received the bachelor's degree in Electrical Engineering and Automation from Zhejiang University, China in 2012. He was accepted as a 3+X student at North Carolina State University in 2011, and received his en-route master degree in 2014. He finished his Ph.D. study in Industrial Engineering in July, 2016.

Hantang's research area focuses on novel additive manufacturing processes, rapid prototyping methods and tools, and manufacturing systems based on electrohydrodynamic inkjet printing for flexible electronics and optoelectronics. The fabrication method he proposed is capable of rapid prototyping of capacitive sensor arrays using metal nanoink for optoelectronics and flexile touch screens to replace high-cost and fragile ITO films. His research interests include micro/nano fabrication, manufacturing, automation, CAD/CAM systems, 3D printing and rapid prototyping for flexible electronics, multi-material and multi-scale fabrication based on additive manufacturing and topography optimization applications.

.

ACKNOWLEDGMENTS

I would like to express my sincere appreciation to my advisor, Dr. Yuan-Shin Lee and Dr. Jingyan Dong for their continuous support, guidance and encouragement throughout my academic and research work at North Carolina State University. I would like to express my deep gratitude to Dr. Paul H. Cohen, for his help and suggestions in my research and my teaching in the department. I would like to thank Dr. Roger Narayan, for his selfless support in my research. I would like to thank Dr. Cassie Castorena for serving in my doctoral dissertation committee, Dr. Harvey West and Mr. Daniel Leonard for their helps and suggestions in my research.

I sincerely thank my research group members: Dr. Xiaofeng Qin, Yi Cai, Peter Prim, Jia Deng, Xiangcheng Kong, Yiwei Han, and Hengfeng Gu for their valuable suggestions, advice, and help during group meetings and working in the research office. I deeply enjoy every moment we spent together at Daniels Hall 412, Daniels Hall 101, and the gym. I also would like to thank my friends for their continuous support and encouragement.

TABLE OF CONTENTS

LIST OF TABLES

LIST OF FIGURES

CHAPTER 1 INTRODUCTION

1.1 Motivation

The advancement of flexible electronics has been expanded from development of single-crystal silicon flexible solar cell arrays to organic light-emitting diode (OLED) displays on plastic substrate for the past five decades. In recent years, the rapid development of this field has attracted significant interests of finding and applying feasible techniques for large-area electronics with applications in flexible displays, novel medical sensors, and electronic papers. The ultimate goal for flexible electronics will always be lighter, more portable, more flexible, more stable, and less expensive to manufacture compared to traditional rigid substrate based technologies. A wide variety of materials from polymeric to inorganic materials have been used to fabricate devices on flexible media, while these varieties also encompass plenty of performance benchmarks. Electrical and mechanical characteristics of materials, system performance and processes involved to make the device will finally determine successful applications.

Finding any suitable manufacturing processes to fabricate flexible electronic devices is part of industrial engineering, not only verifying feasible concepts, but also calibration of manufacturing variables, as well as reducing cost. It is exactly the intent of this research to propose novel rapid prototyping methods for flexible electronics and validate them, providing a starting reference for these methods and potential applications. If we focus on the micro wires or interconnectors, and transistors on flexible substrates, there are many micro fabrication processes generally can be applied such as photolithography on sheets by batch

processing, chemical deposition and etching, imprinting on web by roll-to-roll manufacturing, atomic force microscopy for surface modification, additive printing, direct laser micromachining, etc., each of which has advantages and disadvantages. But if we consider rapid prototyping of micro patterns on flexible substrate, we will find that additive printing and direct micromachining seem to be best suitable for the following reasons. First, the cost could be tremendously reduced, by simplifying fabrication steps compared with lithography or electron beam micromachining that require vacuum environment. Second, additive printing and direct micromachining are theoretically capable of printing and machining all kinds of materials, including organic conductors, semiconductors, insulators, polymers, metals, wax, etc. It is the challenge at this moment for researchers to figure out how to apply direct printing or micromachining into fabrication of devices, e.g., thin film transistors (TFT). Third, additive printing and direct micromachining are roll-to-roll compatible process, which can be adapted as high throughput process with the help of multi-heads. Fourth, additive printing and laser micromachining use device and materials efficiently, and do not require vacuum environment. Fifth, more materials become available for additive printing, generating new opportunities. For example, metal nano ink composed of metal nano particles may reduce process temperature of printing and sintering to values acceptable for polymer substrates. They may replace traditional indium-tin-oxide (ITO) in capacitive touch screen technology.

However, there are still issues that remain to be resolved for additive printing before it can be used for flexible electronics. The resolution of patterns printed by traditional jet printing cannot fully satisfy the requirements for wires and interconnectors of flexible

electronics where high resolution is required. The liquid drop generated by traditional jet printing is typically greater than 20-30 μm, much larger than resolution requirements for certain applications. It's impossible for traditional inkjet printing to print high-quality gate dielectrics or other components for flexible electronic devices. Meanwhile, the operational stability of printed devices and related mechanical and electrical performance still need to be further investigated. A main issue is calibration and process control for different ink materials, and on different substrates. Though inkjet printing has been used in both printing etch masks for vapor deposition and direct deposition of materials, the integration of printing steps into conventional fabrication process hasn't been realized yet. It is important to understand the fundamental of achievable feature resolution, variables, and placement of droplets on different substrates. The mechanical and electrical properties of fabricated devices need to be tested at device level.

On the other hand, new issues of quality and efficiency in direct micromachining also need to be considered. Photo ablation of laser micromachining is totally different from traditional machining. This is a much more complex systems, with input processing variables including laser parameters (laser power, types, beam energy profiles, wave lengths), substrate properties especially for flexible electronics (threshold, reflection and absorption rate), focal distance of laser beam, feed rates and path overlaps. Although researchers have studied on laser ablation for a long time, the model and experiments on newly developed flexible substrates still need to be conducted. The cleaning of debris and residual contaminations generated by laser are challenges in order to improve edge resolution of fabricated patterns.

1.2 Research objectives and scopes

The research focused on developing rapid prototyping methods for flexible electronic devices by proposing and conducting novel advanced micro manufacturing techniques to fabricate high-resolution conductive patterns on flexible substrates. The work started from the fundamental study on jet printing parameters applying electrohydrodynamic theory in the lab built platform in order to understand how these parameters correlated to one another. These parameters include frequencies and amplitudes of applied voltage, size of nozzles, and plotting speeds. Residual charge issue of traditional e-jet printing has been successfully addressed by introducing AC-pulse modulated voltage into the printing mechanism. After calibration, the electrical properties of printed patterns were investigated. Another main challenge for e-jet printing was electrical performance of printed patterns. To further improve the conductivity of printed patterns, post treatment processes were conducted. The study has investigated post curing process for printed patterns. Curing can be used for applications where high temperature was tolerated. Electroless copper deposition was adapted to selectively grow a copper shell out of printed silver seeds. In this way, not only uniform and surface roughness can be improved, but I can also improve stability, connectivity and conductivity of the patterns. Capacitance touch sensors were fabricated and tested for system integration. Mechanical and electrical performance of fabricated devices were tested to demonstrate possibilities of applying the technique into diverse applications. For future research, a pre-treatment process either by micromachining or laser ablation will be a good topic helping better control thickness and cross section profile of printed patterns, and also for potential 3D structure. By fabrication of microgrooves on substrates first, I will be able to

selectively deposit silver ink into these grooves, helping me to better control thickness and cross section of micro wires. These works provide useful references for future research to investigate rapid prototyping of flexible electronic devices.

In summary, it is important to propose a rapid prototyping method for flexible electronic devices. The novel process or a combination of processes must be capable of fabricating high-resolution electronic components or devices that meet all functional requirements. I investigated new flexible technologies and showed the path to industrialist by developing necessary concepts, calibration, and process control, offering them a choice of new fabrication techniques and potential applications. The novelty on additive printing and direct micromachining are challenging and beneficial to current society. Direct micromachining and copper deposition combined with e-jet printing showed great potential to be further applied and integrated into additive manufacturing, or other mechanical and industrial science fields.

1.3 Fabrication approach

As a matter of fact, because of the varieties of parameters that may potentially affect final performance of printed components, the fundamental parameter study of e-jet printing, electroless copper deposition and device testing were required before developing any micro devices. In this section, the proposed approach was introduced and discussed in details to fabricate micro patterns or micro channels on substrates. The processing parameters, variables and critical issues were discussed and further investigated in the following chapters.

The whole fabrication is shown in Figure 1.1. The proposed processes were all compatible to roll-to-roll manufacturing and potential used as industrial manufacturing standard processes. The research focused on improving current jet printing process by introducing electrohydrodynamic theory. To achieve better electrical performance of printed conductive component, direct micromachining was proposed to pattern substrate first with micro grooves followed by selective silver nano ink deposition. Another key technique was post treatment of printed silver seeds through electroless copper deposition to form a copper shell outside silver seeds.

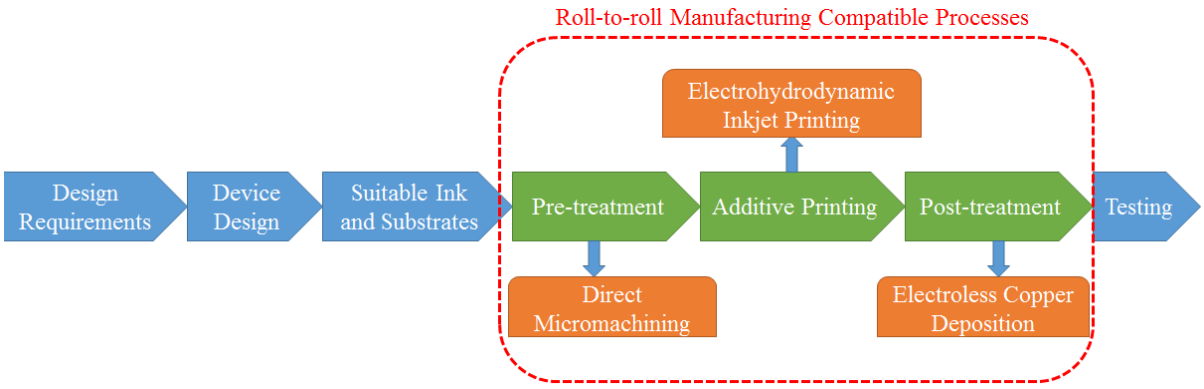

Figure 1.1 Overall proposed fabrication approaches

As shown in Figure 1.1 with a full development circle of electronic devices, all work began with device design that will fulfill certain requirements for their functions. Ink and substrate will then be identified based on function, resolution, and specific applications. The ink can be polymer, wax, metal ink, and bio materials. The substrate can be rigid glass slides, silicon based substrate, flexible polymer film, paper, etc. The roll-to-roll manufacturing compatible process was shown in the red dot circle. Pre-treatments of substrates include

cleaning, etching, or micromachining. Direct micromachining was a process that based on laser ablation or micromachining that was capable of patterning on substrates before additive printing. In this way, the patterned grooves can help solve the low aspect ratio problems of e-jet printing. Additive printing based on e-jet printing could selectively deposit functional ink onto substrates. Silver nano ink was used in the work, however, there are other options such as silver nano paste, copper or gold based nano ink. Post-treatment of e-jet printed components was also necessary for better electrical performance of printed micro patterns. It can be a simple curing process for devices with high temperature threshold, or electroless copper deposition for components with low temperature thresholds. They were discussed in details in the following chapters.

There were several research topics in this dissertation from fundamental study in e-jet printing parameters, silver nano ink to the application in flexible substrates on micro-machined surface. The issues were organized in the following chapters and described in the following section.

1.4 Organization of dissertation

This dissertation has been divided into six chapters and the remaining sections of this dissertation were presented as follows:

Chapter 2 reviewed pertinent literatures with the objective of placing the research in the context of work that has been done before, with a highlight on novel rapid prototyping methods based on jet printing and solution-processable materials such as nano metal ink.

Chapter 3 discussed e-jet printing in details with my results of the study, which supports the feasibility of proposed techniques. A capacitive touch sensor pattern was presented in the section to demonstrate the capability of my methods for rapid prototyping of high resolution electronic components on flexible substrates, as a potential technique to replace ITO electrodes in traditional capacitive touch screen applications.

Chapter 4 focused on improving conductivity of printed patterns. Detailed study of curing and electroless copper deposition on printed silver seeds was described.

Chapter 5 investigated fabrication technique in device level. Projected capacitive sensor was fabricated in different designs. Mechanical and electrical performance test were conducted on the sensors to demonstrate versatility of the technique in diverse applications. The capability of our methods was fully investigated for rapid prototyping of microelectrodes arrays on flexible substrates as capacitive sensors.

Chapter 6 draw the conclusions and clarified future research topics. Publication and presentations from the dissertation was listed in details.

CHAPTER 2 LITERATURE REVIEW

The chapter began with literature reviews on flexible electronics with focus on projected capacitive displays, electrohydrodynamic inkjet printing, electroless copper deposition and direct micromachining. Some critical issues of current existing techniques were discussed in the last section of this chapter. This chapter provided several important backgrounds relating to my proposed techniques and current researches related to fabrication of highly conductive features.

2.1. Flexible electronic devices and additive printing

Flexible electronics has been rapidly developed in the last few years and has the potential to take place as next technology revolution in electronics; similar to the way integrated circuits was back in 1960s to take place discrete components. Flexible electronics are not only flexible in mechanical properties, but also flexible functionalities in all kinds of applications, ranging from personal devices (wearable devices[1, 2]), electronic memory devices [3] to large area sensors (biomedical sensor arrays [4], solar cells [5, 6], flexible displays [7, 8]), and radio-frequency identification devices [9]. The flexible electronics began with single-crystalline silicon solar cells for use in extraterrestrial satellites back to 1960s [10, 11]. A bendable display with text image was shown in Figure 2.1 (a), and a prototype of Samsung's flexible smartphone was demonstrated at international Consumer Electronics Show in 2013 as shown in Figure 2.1 (b). The ultimate goals of flexible electronics are always lightweight, flexible, easy-to-integrate, low-power, and energy independent [12].Display industry has been driving new development of flexible screens for portable devices. At the same time, chemical and biological sensor arrays are another great

opportunities for human healthcare systems and flexible electronics.

(a)  (b) 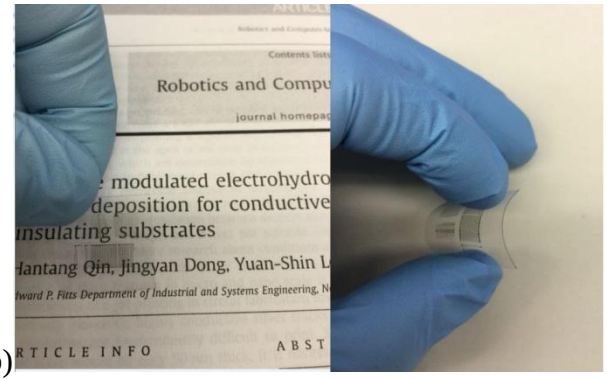

Figure 2.1 (a) Bendable display [13] with text image, (b) prototype of microelectrodes arrays showing transparency and flexibility

The concept of flexible electronics can be traced back to 1960s when the first flexible solar cell arrays were fabricated by thinning single crystal silicon wafer cells down to 100 μm followed by assembling on flexible plastic substrate [10, 11] . When we talk about flexible as a terminology today, it contains the qualities like bendable, lightweight, non-breakable, large-area flexible electronics, roll-to-roll manufacturing, elastic, wearable, and conformal shape. Historically, the flexible silicon solar cells has opened a new area of photovoltaics and much of initial work in large area flexible electronics has centered on this topic. The breakthrough of introducing roll-to-roll fabrication of hydrogenated amorphous silicon (a-Si:H) on organic polymer substrates [14] helped expansion the techniques into industry. Today, a-Si:H solar cells are routinely made by roll-to-roll processes as a common industrial standard.

Almost at the same time fifty years ago at 1960s, flexible thin-film transistors (TFT) was brought into reality by Brody when he tried to fabricate TFT on papers and showed potential applications in display area [15]. He and his group made TFTs on a wide range of flexible substrates and invented the active matrix TFT display technology by producing the world's first active matrix liquid crystal display in the 1970s [15]. A lot of groups in research area and industry companies began focusing on large area electronic for display applications ever since. The flexible displays have expanded dramatically in the past few decades with new materials and fabrication processes proposed.

Recently, the concept of flexible electronics has been adapted into new applications and researchers have been focused on flexible displays medical sensors, wearable devices, and radio frequency identification (RFID), most of which are touch sensor based technologies. Touch sensors are based on various techniques, including resistive, capacitive and infrared sensors. Resistive is one of the oldest types of touch sensors, produced since mid-1970s. They are most pressure-sensitive or analogy-resistive film touch panels, which features a glass screen and a film screen separated by a narrow gap, each with a transparent electrode layer attached. Pressure contacts the electrodes in the film to electrodes on the glass, resulting in flow of electrical current, where voltage change is detected and contact point is identified. These touch sensors owned the largest market share because of very low cost and ease of implementation despite poor durability and optical performance [16]. Scanning infrared touch sensors are based on the concept of determining position by the interruption of one or more of a series of light beams and thus interruption the excitation of a phototransistor that is illuminated by the beam. If the touch sensor is touched, the infrared light will be

blocked and not come back to the infrared imaging sensors. However, their design cost is high, and initial calibration is difficult and complex [17]. Acoustic touch sensors mainly include surface acoustic wave (SAW), and acoustic pulse recognition (APR) technology. These technologies all depend on some aspects of propagating mechanical waves on the surface, capturing and analyzing those waves to determine a touch position. It is difficulty to realize multi-touch for acoustic sensors, and it is limited to relative low resolution [18]. Compared to these mechanisms mentioned above, capacitive sensing represents second widely used sensing method. Touch activity is identified by detecting minor changes in electrical current generated by contact with a finger or changes in electrostatic capacity. Substrates for capacitive touch sensors may be glass or flexible polymers, or combination of them. [19] They are usually constructed both as narrow stripes of conductors. Interdigitated electrodes are among the most commonly used structures. The change in capacitance caused by proximity of finger near an intersection is 1pF or less, and effect on adjacent electrode may be less than 0.1 pF. [20] The analysis of capacitance changes at or near intersections of electrode reports the touch action if change in capacitance exceeds the system threshold. Capacitive sensors shows excellent sensitivity with activation, and they are unaffected by most contaminations.

Projected capacitive technology is a technology based on capacitive coupling effect, which can detect anything that is conductive or has different dielectric effects from air [21]. The technology has been widely used in modern touch screens. A basic construction of a typical projected capacitive touch screen includes a top layer touch surface (chemically strengthened cover glass with holes and slots cut into), optical bonding adhesives, touch

sensor arrays (usually glass separator with indium tin oxide deposited on both sides), and bottom LED/LCD screen [12], as shown in Figure 2.2. Projected capacitive technology shows advantages such as multi-touch, excellent optical properties, and long life. Projected capacitive touch sensors are easy to be integrated into systems using scanning algorithm, which eliminates coordinate drift and complicated calibration for display [22]. Projected capacitive touch sensors can be adapted into both glass and plastic, allowing them to have the flexibility to be contoured. Most touch applications are immune to most chemicals and extreme temperatures because sensors are usually sealed to meet the requirements.

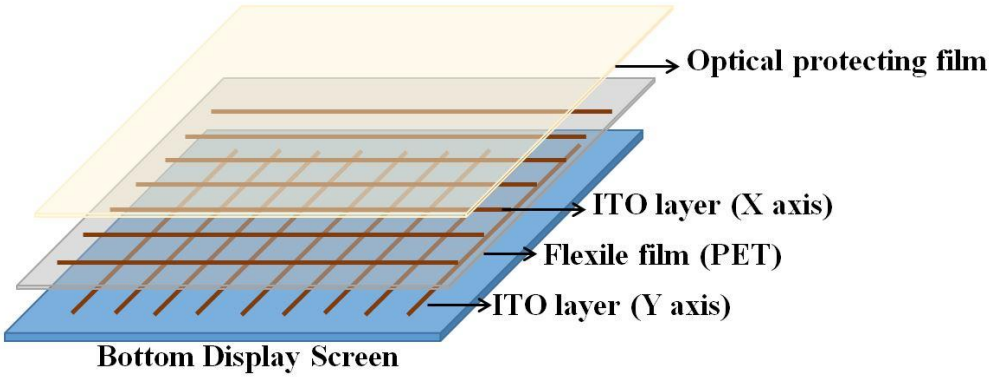

Figure 2.2 Schematic of structures in projected capacitive touch screens: row and column stack up layers

However, there are several challenges to most projected capacitive sensors before they can be used into flexible devices. First, they are relatively expensive in fabrication and it is hard to build large-area screens. It is mostly because of the expensive fabrication process for depositing electrodes sensor arrays. Electrodes patterns are most commonly deposited on

surfaces by physical vapor deposition, electron beam deposition, or sputter deposition techniques, which are all costly layer deposition processes that require vacuum. Second, indium tin oxide (ITO) is currently the most popular material as transparent electrodes for optoelectronic devices because of its good electrical conductivity and optical transparency. However, indium is scarce resource on earth. On the other hand, its high mechanical fragility makes it hard to be used for flexible electronic devices. As a result, the demand for alternative electrodes that can replace ITO has been critical. There are many materials that have been introduced, including carbon nanotubes [23-25], graphene [26, 27], conducting polymers [28, 29], and metal nanoink. Among them, metal nanoink has drawn attention because several advantages over other materials.

Metals possess highest conductivity among all other materials at room temperature due to their high free-electron density. At the same time, ultra-thin and ultra-small metal patterns demonstrate decent optical transparency at micro and nano scale. Transparent thin metal film and metal grids have been reported in optoelectronic devices where light must pass through while current or voltage needs to be applied as a replacement of ITO [30, 31]. The properties of these transparent metals are extremely important for device performance. For example, the brittleness properties of electrodes are crucial for flexible devices. The optical transparency and electrical resistance are another two most important parameters. To achieve the highest performance in optical transparency and resistance, metal-based nanostructures need to be fabricated at micro scale while maintain their highest electrical conductivity at room temperature.

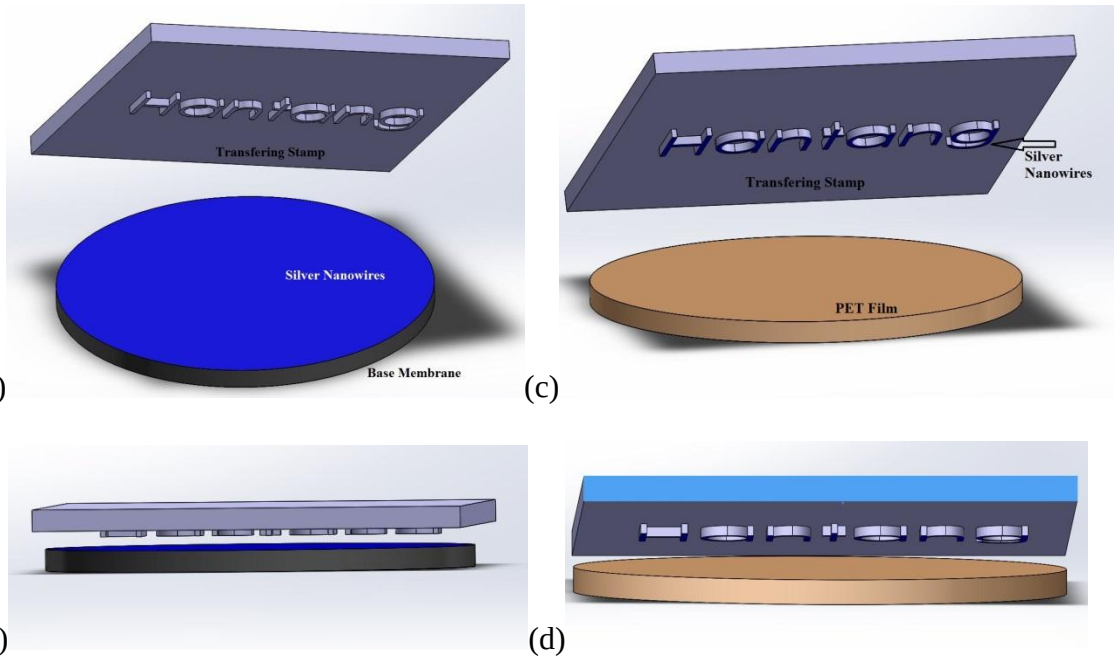

(a) (c)

(b) (d)

Figure 2.3 Fabrication of conductive patterns based on PDMS stamp [32]: (a) pressing of the PDMS stamp against the silver nanowire film, (b) stamp and peeling off, and (c) pressing the stamp on receiving substrates, (d) transfer pattern onto PET film

There are several approaches that have been reported where metal nanowire ink was used to fabricate transparent conductive electrodes. Lee et al. demonstrated solution-processed transparent electrodes consisting of random meshes of metal nanowires that can be used in organic solar cells [33]. De et al. reported transfer of deposited silver nanowire films to PET substrate with optical transmittance as high as 92% [34]. Madaria et al. [32] improved a facile plydimethylsiloxane (PDMS) assisted dry transfer printing technique, which was originally used for printing carbon nanotube thin films [35], as shown in Figure 2.3. These reports represent significant advancement of researchers trying to replace ITO with metal

nanoink. However, the silver nanowires required a relative high annealing temperature [33], and there were poor adhesion problems [34]. The inevitable extra fabrication of PDMS stamps also increased cost of the process, and reduced the flexibility of fabrication, making it impractical for rapid prototyping of sensor arrays. It still remained a challenge for researchers to find out rapid prototyping method of sensor arrays for flexible optoelectronic applications.

There is also a tremendous gap in terms of fabrication between flexible electronics and modern semiconductor technologies. Flexible electronics are most time large area electronics, which require large device dimensions and different types of substrates. This is different from integrated silicon based chips of modern CMOS technology which focus on minimizing area, improving device densities and reducing sizes. The challenge for modern flexible electronics is finding new solutions for large area electronic applications with full mechanical and electrical function while reducing costs compared to traditional small area covered silicon based fabrication processes. The scaling of flexible electronics has pushed the technical and cost limits of conventional materials and device processing. Plenty of research groups are focusing on alternative patterning and fabrication method to replace conventional process such as photolithography and vacuum deposition while meet high-performance, resolution, manufacturing needs and cost requirements. Among them, additive printing shows its potential to be the best fabrication process and rapid prototyping method for future flexible devices. It can be scaled to very large scales with full microelectronic function. Additive printing is noncontact jet printing process that is capable of fabricating both silicon based and polymeric based TFTs and electronic components. However, feature resolution of traditional inkjet printing is limited by the size of droplets which is typically

above 30 μm in diameter. By incorporated with roll-to-roll fabrication, additive printing can definitely help to reduce process and material cost for flexible electronic fabrication to be used for wireless technology, photovoltaic, RFID and displays.

It is necessary to find out a method for rapid prototyping of conductive electrode patterns on substrates which can be used as sensor arrays for flexible optoelectronic devices. The term rapid prototyping first referred to layer-based approaches that made prototypes of products by combining planar layers of materials for 3-dimensional structures back to 1980s when stereolithography (SL) [36], powder sintering [37], and sheet lamination [38] were developed and came into market. Rapid prototyping has been expanded to new areas with the help of filament extrusion based methods and droplet based deposition. Directly printing approaches, especially those based on ink jet printing in high-resolution fabrication situation, demonstrate attractive features in their application. First, inkjet printing is noncontact, which means any substrates can be processed. Materials can be deposited on planar or curved substrates, as long as there is a stand-off distance between print head and substrate. Second, inkjet printing is capable of depositing a wide range of materials given appropriate print heads. Third, the printing process is scalable. Multiple print heads has been reported to print wider pattern or several materials at the same time [39]. Fifth, inkjet printing is flexible in position for customized product. [40] The location can be changed in real time to adjust with distortion or alignment of substrate to ensure high quality patterns. It also shows potential for mass production and low cost operation [41]. These features of inkjet printing make it particularly attractive for rapid prototyping of such flexible sensor arrays. However, there

were still gaps to be filled for current technologies. Most of complex, multi-functional metal or alloy inks have to be characterized first before they can be adapted into real applications.

2.2. Electrohydrodynamic inkjet printing

In the last few years, there was a significant interest in finding feasible direct printing techniques for fabrication of micro-scale electronic devices with increasing applications in electronics, biotechnology and micro systems. The term direct printing refers to approaches where patterns or structures can be obtained directly without the use of masks, liquid etching or other variable fabrication processes. Directly printing approaches, especially those based on ink jet printing in high-resolution fabrication situation, demonstrate attractive features in their application. For instance, they have the ability to pattern directly on substrate regardless of the mechanical property of substrate, compared with other pattern method like photolithography. Printed electronics and systems offer an attractive alternative to conventional technologies by enabling the creation of large areas , multiple tracks and mass production at low cost [41]. At the same time, rapid control of printing trajectory with programming based print control system offers great flexibility for the technique [40]. Direct write technologies thus are the low cost, high speed, noncontact, flexible and environmental friendly process.

Conventional ink jet printing approaches are based on thermal or acoustic formation and ejection of liquid droplets through nozzles [42]. The fabrication processes has been successfully applied in electronics, drug delivery systems [43], micromechanical devices [44, 45] and other areas. The maximum resolution using thermal or acoustic theory is 20-30 μm,

resulted from the fact that the diameters of the droplets are typically bigger than 10 μm[46]. Even though with assistant technique, e.g., by combing lithography into these ink jet printing to confine the liquid flow [47], it remains a challenge to for electronics research and industry community to achieve the sub-micrometer level in fabrication process.

(a)  (b) 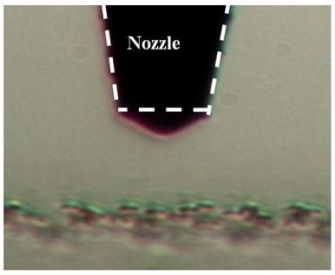

(c) 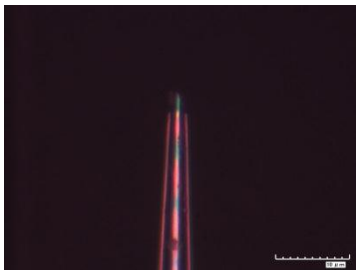

Figure 2.4 (a) E-jet printing working at cone-jet mode using polycaprolactone (PCL) polymer ink [48], (b) meniscus of e-jet printing using silver nanoink, (c) tip of the needle used

The electrohydrodynamic mechanism was first proposed by Zeleny back in 1917 [49]. The multiplicity of electrohydrodynamic spraying modes has been studied ever since and different functioning modes such as cone-jet, multijet, microdripping, simple jet and ramified jet was reported [50]. Electrospraying and electrospinning using the mechanism has already been commercialized. Electrohydrodynamic jet (e-jet) printing is a pattern method using electric fields to generate fluid flows to deliver inks to a substrate working in cone-jet mode. Figure 2.4 (a) showed the cone-jet shape and jet printed filaments in the previous work of our

lab at NC State to fabricate 3D polymer scaffolds with sub-10 μm structures using e-jet printing.

When a liquid is supplied to a sufficiently high electrical potential, the liquid will form a stable cone at the tip of the nozzle and emits a jet on its summit. The technique that uses electric fields instead of thermal or acoustic offers some advantages of patterning compared with other direct write technologies. First, the dimension of droplets could be reduced dramatically (40 nm - 1.8 μm) using electrohydrodynamic printing to optimize physical properties of the liquid droplet by controlling parameters [51]. Second, the diameter of the nozzle used could be larger than nozzles of other jet printing techniques. This would avoid blockages of particles of liquid.

Manufacturing within electronic industry is demanding requiring smart fabrication technique for metallization and conductive micro-interconnects. Plenty of researches have been focused on metallic-organic compounds. To date, metal nanoparticles such as Au, Ag and Cu have been studied as promising functional materials for conductive inks, since they exhibited high conductivity and stability. As the size of metal particles decrease to nanometers, the melting point falls dramatically due to high surface energy. As a result, the curing and sintering process to form denser structure for the printed patterns can take place at a low temperature, which is compatible with polymer substrate. By changing the property of ink, Ahn et al. even succeeded in printing 3D structure on substrate with a customized highly viscous ink [52].

However, before e-jet printing can be adapted to any applications, there were still plenty of obstacles remained to be overcome. First, e-jet printing is a patterning method that uses a fine jet generated at the apex of ink cone of an electrospray in cone-jet mode [53], which are determined by experimental parameter, such as electric field, conductivity and viscosity of fluids and flow rate [54]. Numerical analysis of formulations and relationships are hard to develop among many parameters. Lee et al.(2012) have tried to propose a formulation between droplet size, surface tension and applied voltage, but it was not suitable for jet formation situations [55]. More researches about conditions and parameters for e-jet printing needed to be conducted. Second, fabrication of filaments in micro and nano scale was attractive for applications of e-jet printing in circuit fabrication as well as biomedical fields. However, highly conductive silver tracks with such high resolution were tremendously difficult to print. Since single printed layer would be only 50 nm thick, it was necessary to print multi-layers for better conductivity. On the other hand, multi-layers would play a negative role on resolution. Smaller diameter of nozzle was another key factor for high resolution, while blockage of the nozzle was unavoidable and conductivity of the silver line would be poor with thinner thickness [56]. The fabrication technique have to be verified at device and system level to demonstrate its capability as electronic components.

Conductive microtracks have been obtained by direct printing of metallic organic ink using nanoparticles and subsequent thermal decomposition [57-59]. However, the line width of the tracks obtained by direct printing of metallic-organic ink was relatively large, typically greater than one hundred microns. Very recently, Wang had reported metallic pads and conducting tracks with 150 μm line width printed on Si substrates, showing excellent

resistivity [60]. Youn et al. put emphasis to make high resolution micro patterning using e-jet printing and succeeded in fabricating silver line with width down to 6 μm on silicon substrate using tilted-outlet nozzle instead of conventional nozzle [61]. Lee et. al. reported depositing silver tracks onto polyimide film by e-jet printing, obtaining conductor lines with resistivity about three times than bulk silver (0.0016 Ω·μm) but poor resolution (200 μm in width and 0.3-5 μm in thickness) [51, 62]. Besides, few researches have reported conductive silver tracks printed on highly insulating materials such as Ajinomoto build-up films (ABF).

2.3. Electroless copper deposition

Copper has been selected for interconnector in integrated circuits and electronic packages because of its low resistivity and high electro migration resistance. Electroless deposition of metals such as copper, silver, gold and nickel have been developed since 1990s and been widely used for production of fine metal patterns in printed circuits [63]. The planar process of electroless copper deposition on electronic device fabrication was shown in Figure 2.5. Photo resist was first deposited on to bottom level dielectric materials with patterns determined by etching masks. The pattern was etched on to bottom materials, followed by a deposition process that deposit catalytic metal onto whole area. The photoresist was then removed and only grooves that needed to be filled with copper was left. Copper will selectively grow into those grooves catalyzed by catalytic metal.

The process occurs by a redox process in which the cation of metal to be deposited is reduced by a reducing agent at the surface of catalysts or induced areas used to initiate the deposition. The redox process generally takes place only on catalyzed area, such as activated

surface or metal seeds like silver or palladium, which functions as catalyst [64]. Selective deposition can be achieved by producing patterned catalysts. Hidber et al. reported patterning surfaces with palladium catalyst by microcontact printing of colloids, which enabled selective copper metallization by electroless deposition on areas of surface activated by deposited colloids. They generated metallic features with sub-micron dimensions and film thicknesses greater than 1 μm [65].

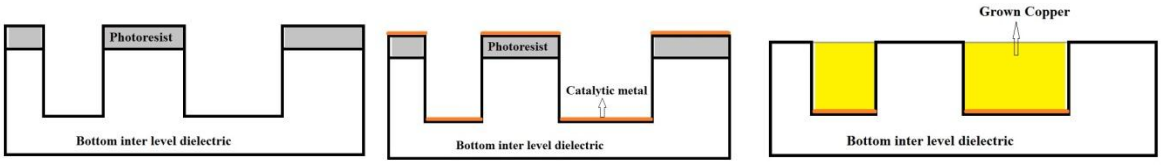

Figure 2.5 Planar process of electroless copper deposition on electronic device fabrication [66]

Generally, electroless metallization is cost-effective compared with sputtering, chemical vapor deposition, and evaporation, since it does not require vacuum equipment or high power supplies. The elimination of expensive palladium or expensive metal catalyst would reduce the cost of electroless plating. Some other catalysts were currently drawing attention. A critical aspect of the process was how to form these seed particles on the substrate, where particles have excellent uniformity and adhesion. The traditional reducing agent in electroless copper has been formaldehyde whose oxidation can be catalyzed by many noble metals, such as Au, Ag, Pt, Ru, Ni, and Co [66].

Silver was selected in my research due to its catalytic properties, cost and good adhesion to substrates. Uzunlar et al. investigated a procedure composed of a H_2SO_4 surface pretreatment, two-step Sn/Ag nano-colloidal catalyst seeding, and immersion in traditional formaldehyde electroless copper bath. The H_2SO_4 activated the epoxy surface for sensitization of Sn. The tin-silver activation in the bath resulted in Sn and Ag products in form of Sn/Ag nano-colloidal catalyst for further copper deposition [67]. Dellas et al. used a frequency tripled laser to pattern silver seed lasers. They fabricated copper line with width of 150 μm, thickness of 2 μm and electrical resistivity of 0.005 Ω*μm [68]. Kao et al. reported copper plating using printed lines of nano sized silver seeds on aluminum substrates, and acquired copper film on silver tracks with width 100 μm and 200 μm, with film thickness of 3.6 μm and electric resistivity about 0.0018 Ω*μm, very close to bulk copper (0.00168 Ω*μm) [69].

Electroless deposition of metal is based on the reaction between copper particles and a chemical reducing agent in the electrolyte. The process is initiated by a catalyst on the substrate surface. Once the target metal is precipitated out at the first place, the process transforms into autocatalytic process. The precipitation will keep going on where the catalytic seeds and precipitated metals oxidize reducing agent [66]. The catalytic activity of electroless copper deposition is directly related to oxidation of the reducing agent in the electroless bath. The role of catalyst is to facilitate the dissociative adsorption of reducing agent (i.e. formaldehyde in this case) resulting in an adsorbed anion radical and adsorbed atomic hydrogen. The oxidation of adsorbed anion radical generates an electron, and the adsorbed atomic hydrogen recombines or becomes ionized.

Traditional electroless plating baths are typically composed of a metal salt such as metal ion sources like $CuSO_4$ and $AgNO_3$, chelating agent to prevent formation of undesired compounds, and a reducing agent. The reactions are typically catalyzed only on noble metals, including Pt, Pd, Ag, Au, Rh, or Ir. The current challenges in electroless copper deposition include high cost of Pd-based catalysts.

2.4. Direct micromachining/laser ablation

The demand for micro products and micro components has been increasing in the past decades and will keep growing in the future in IT industry, medical and biomedical products. Silicon based manufacturing technologies are relatively highly developed because of the need for electronics industry. On the other hand, metals, polymers and ceramics based micro manufacturing still face plenty of challenges. It is continuously necessary to create novel fabrication methods and operational basis for industrial production of micro products. Figure 2.6 shows the production process in terms of machining. Material is processed into parts followed by assembly to product. This production flow also applies on micromachining. The miniaturization is able to proceed into micro level based on existing machining methods when the equipment precision can be improved and unit removal can be precisely controlled [70].

Figure 2.6 Production process flow for machining

There are currently many types of fabrication process proposed by researchers for micromachining. The most simple and popular micromachining method is mechanical force based fabrication based on material removal from workpiece, such as cutting, grinding, ultrasonic machining, and punching. Mechanical force based micromachining directly contact the workpiece during fabrication, resulting in a better control of machining trajectory and better machined surface control. On the other hand, since this method is based on elastic deformation of tolls and/or workpiece, the machining force may affect accuracy and machinability is limited. [71]

Another popular micromachining method is melting and vaporization based fabrication with the help of excessive heat selectively on workpiece, such as electrical discharge machining (EDM), electron beam machining (EBM), etc. These techniques have also been adapted for additive manufacturing of powders. For machining point of view, the useless section of workpieces is melted or vaporized by heat. One key element of melting based micromachining is concentration of energy for a high temperature at certain points on workpiece. One main advantage of this type of micromachining is that it can fabricate on workpiece regardless of its mechanical property such as fragility, and the noncontact feature of these techniques can help protect toll and workpiece. However, this noncontact feature also makes it hard to control final accuracy and surface roughness of final product. The heat affected zone on the parts might also be a potential problem. [72]

One technology that coming from melting based micromachining, but slightly different in material removal mechanism, is ablation based methods. Ablation based

micromachining uses beams with very high energy which exceeds atoms binding energy of workpiece, to decompose the working material and remove them from workpiece. In some cases, the energy and removal is so high that the vaporization skips melting phase. Most commonly used power source include excimer laser and femtosecond laser. One main advantage of ablation based method compared with melting based method is that the heat affected one was reduced on the machined surface. The machining shape can have better accuracy and lesser defects. One major drawback of ablation based micromachining is the use of mask patterns during fabrication and relatively high energy cost.

(a)

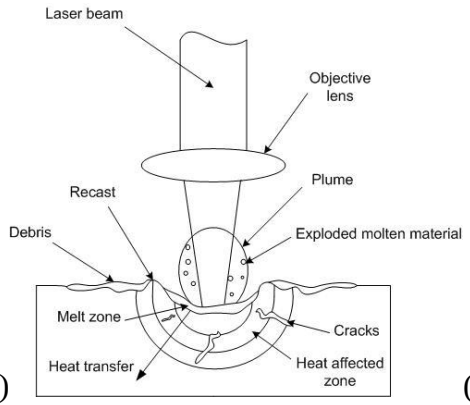

(b)

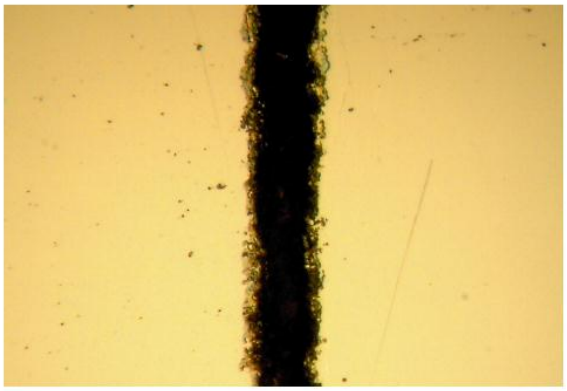

Figure 2.7 (a) Schematic diagram of laser ablation [75], (b) microgrooves on silicon wafer [76]

In the previous research from our group at NC State [73-76], laser ablation has been adapted to fabrication of microgrooves for biomedical devices and microfluidic systems. Figure 2.7 (a) shows a schematic diagram of laser ablation, and Figure 2.7 (b) shows

microgrooves on silicon wafer with the help of surface coating with poly(ethylene glycol) diacrylate [74, 75]. It is a continuous work in our lab to research on excimer laser for new applications, expanding from microfluidic systems and silicon wafers to polymer films and flexible electronics.

2.5. Challenges to be solved

Flexible electronics are attractive topics and have fancy applications, such as projected capacitive displays, wearable devices, and RFID. For current display technology, the expensive fabrication process cost and small-area limitations have motivate researchers to find new ways to replace traditional deposition process for fabrication and prototyping of electrical components. Indium tin oxide is currently the most popular transparent electrodes for optoelectronic applications but its high mechanical fragility and scarce resources property make it hard to be used for flexible electronic devices. It is our obligation to find out alternative ways that can replace these traditional fabrication methods for future applications.

The large area properties and polymer based substrate of flexible electronics is against modern semiconductor technologies which focusing on minimizing area and improving device densities. The scaling of flexible electronics has also pushed the technical and cost limits of conventional materials and device processing. A method for rapid prototyping of conductive electrode patterns on substrates is necessary for research of low cost manufacturing process. Metals possess highest conductivity and decent optical transparency at micro and nano scale to replace ITO electrodes among all other materials at room temperature. The optical transparency and electrical resistance are another two most important parameters. To achieve the highest performance in optical transparency and

resistance, metal-based nanostructures need to be fabricated at micro scale while maintain their highest electrical conductivity at room temperature.

Directly printing approaches, especially those based on ink jet printing in high-resolution fabrication situation, demonstrate attractive features for rapid prototyping of flexible electronics. Direct printing shows the advantages such as noncontact, capable of depositing wide range of materials, scalable using multiple printing heads, and flexible in position. However, each of printing inks has to be characterized first before they can be adapted into real applications. Process control of e-jet printing and characterization of each ink needed to be investigated. Meanwhile, numerical analysis of parameter relationships needs to be developed. Residual charge problems and curing temperature issues need to be addressed before this technology can be adapted for rapid prototyping of flexible electronics. Device fabrication and system integration needs to be investigated to demonstrate efficiency of proposed methods. In the following chapter, a new rapid prototyping method was proposed and investigated to address all these challenges.

2.6. Summary

In this chapter, I reviewed pertinent literatures of flexible electronics with focus on projected capacitive touch applications, e-jet printing, electroless copper deposition, and micromachining. The electrohydrodynamic ink jet printing and laser micromachining with direct-writing capabilities shows its flexibility to fabricate micro patterns on materials. The microstructures can be applied directly as micro-electro-mechanical systems (MEMS) or connecters for PCB boards and chips. The chapter reviewed electrohydrodynamic ink jet printing, electroless copper deposition and laser micromachining, showing their possibilities

to be combined together to fulfill needs. The flow in the chapter showed a roadmap of how my dissertation research was conducted.

The next following chapters began with description of proposed techniques. Then, the results were discussed to show advantages and capabilities of my research and help to verify the concept. After that, conclusion, achievements, and future work were discussed in the end. The following chapters described the experimental approaches in the study in details.

CHAPTER 3 RAPID PROTOTYPING BASED ON E-JET PRINTING

As discussed in the literature review, e-jet printing is a promising approach to achieve higher printing resolution. The fabrication process advantages over other rapid prototyping method include: (1) ability for direct patterning, (2) better controllability, (3) cheap cost, (4) large area printability, (5) potential for mass production with multi heads. On the other hand, there are still several challenges remaining to be solved before it can be generalized. The characterization of each functional ink needs to be conducted first before they can be used for high-resolution applications, including plenty of parameters such as voltage, nozzle, plotting speed, performance test etc.

In this chapter, the fundamental study of e-jet printing using silver nanoink is investigated to verify the concept that e-jet printing has the capability to fabricate high resolution conductive patterns for flexible electronics.

3.1 E-jet printing mechanism

Figure 3.1 presents a schematic of e-jet printing process. As we can see from Figure 3.1, the e-jet printing system proposed in this research consists of a three-axis (XYZ) stage, a dispensing system with pressure regulator, a nozzle, substrates, and a high AC voltage power supply. The controllable parameters during fabrication include pressure applied to syringe, height between nozzle and substrate, applied voltage potential between nozzle tip and substrate, surface thickness, and plotting speeds of the three-axis stage.

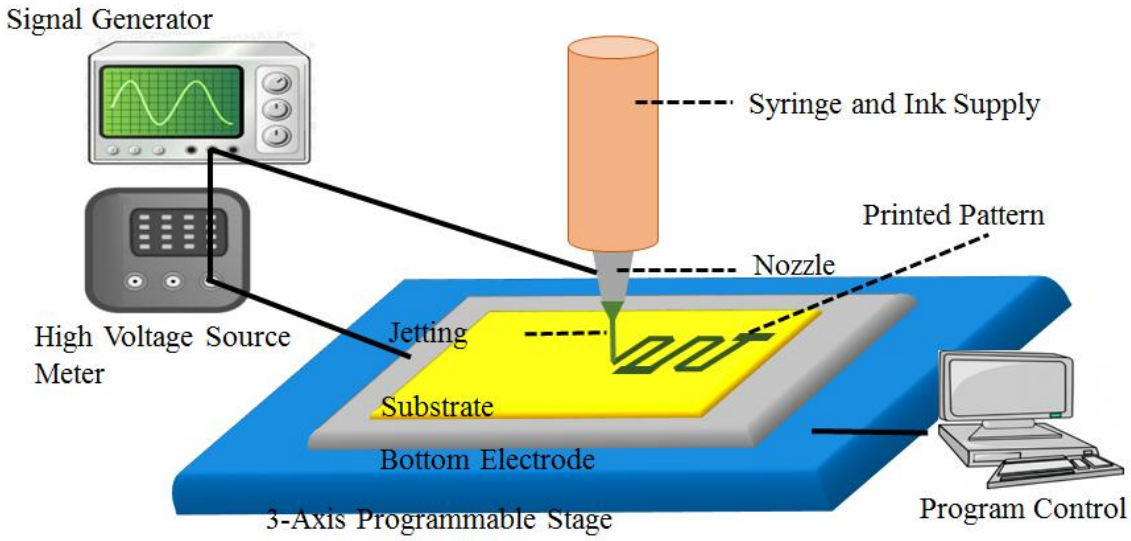

Figure 3.1 Schematic of electrohydrodynamic jet printing setups

The mechanism of electrohydrodynamic theory was first examined by Zeleny back to 1917 [49]. However, we would like the e-jet printing to function in cone jet mode [50]. A voltage applied to the nozzle tip causes mobile charged particles to accumulate at the tip of the nozzle, forming a meniscus until at some point when the electrical force overcomes the surface tension of the meniscus and jet forms and transfers into cone jet mode. Referring to our platform shown in Figure 3.1, the nozzle is functioning as an electrode, and used to generate the jet containing organic silver nanoparticles, which are supplied by a syringe to the nozzle. Desired voltage is generated, amplified and applied between nozzle and electrode. Waveform of the AC voltage is fixed while amplitude and frequency can be adjusted. The three-axis stage can be programmed to provide relatively displacement in X-Y directions between substrates and nozzle, simultaneously controlling plotting speed of nozzle and

trajectory of tracks. Note that the fabrication process is capable of on demand printing multi-layers on substrate by programming the movement of 3-axis stage.

In the last few years, several research works were presented on patterning of metal nanoparticles through e-jet printing on glass and silicon substrate [62, 77-80] and droplet analysis using different forms of voltage [81-84]. In the study, AC voltage was adapted because direct printing of highly conductive silver tracks on insulating materials in electronic industry would be a major application in the future. As shown in Figure 3.2, situations are different printing on insulating substrate using DC voltage, since the substrate will never transmit or neutralize any charges of droplets and inks. The charged ink accumulates on the substrate and then affected the whole electric field between nozzle and substrate. Two scenarios happened: (1) the jet is affected by net charge of previously printed ink, resulting in deflection; (2) the jet is completely stopped, resulting in discontinuous tracks. A solution to address this problem is to use AC voltage instead of DC, so that it is possible that silver tracks can not only be printed on glass substrate but highly insulating materials.

(a) 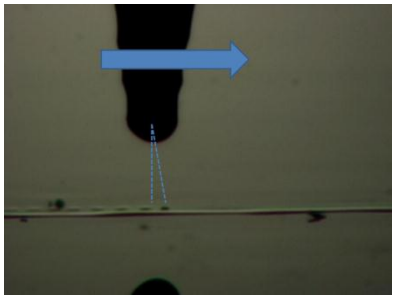 (b) 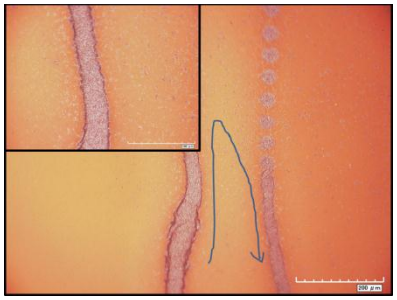

Figure 3.2 E-jet printing using DC voltage on insulating materials

AC modulation, was initially introduced in literature 2009 by Nguyen and Byun [56]. In our earlier works presented in [48, 85-87], a lab setup on e-jet printing with precision table control was reported. The mechanism of fabrication process of e-jet printing in this study using AC-pulse modulated voltage is shown in Figure 3.3. The figure shows a circle of AC signal with different stages. Due to the AC voltage signals, positive and negative charged particles are induced on the meniscus of the ink at the tip of the nozzle sequentially, forming positive and negative jet successively. During the positive pulse of AC voltage, negative charged particles accumulates on the meniscus of ink, as shown in Stage I. Once the electrical force of charged particles are greater than surface tension, negatively charged droplets will be ejected, forming jet and removing charge. The negative silver dots will be printed on insulating Ajinomoto build-up films (ABF) substrate first. As electrode polarity changes, positive charged particles accumulate and generate a positive jet (Stage II) and printed along the negative charged dots. Since the duty ratio of the signal is one, the negative printed tracks would be neutralized by these same amounts of positive particles. The printed tracks return to an electrically neural state that is ready for another period of ejections.

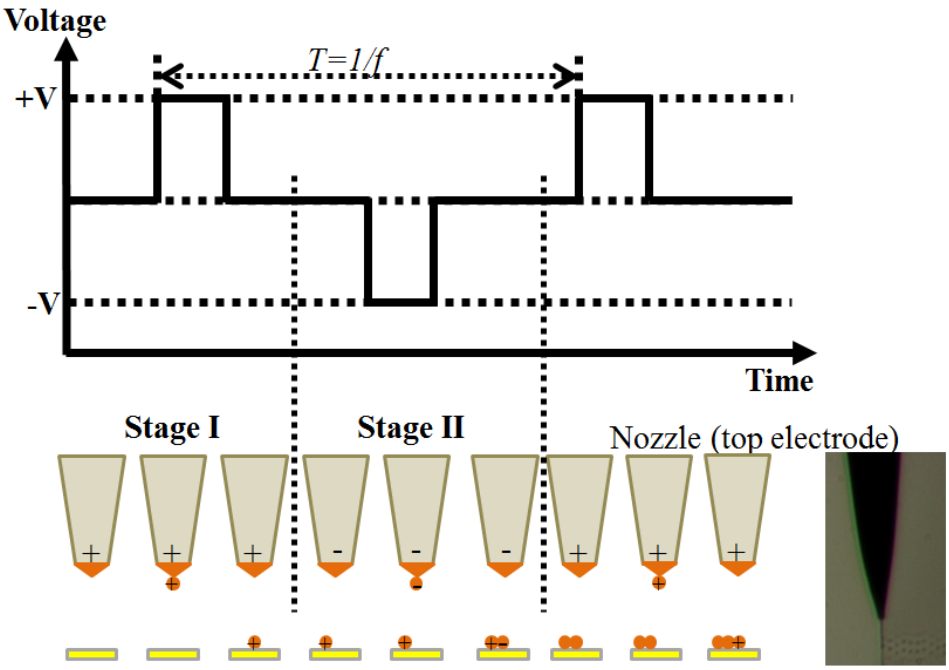

Figure 3.3 Mechanism of ac-pulse modulated e-jet printing on highly insulating substrate: adjacent alternative positive and negative charged droplets will neutralize residual charges on the substrate for stable printing of continuous patterns

For e-jet printing, it is a critical issue to obtain both high resolution and low resistivity of printed filaments in micro scale manufacturing. First, silver nano ink is different from bulk silver. The inevitable voids generated between particles and additives in the nano ink reduced conductivity and increased dimension of silver filaments. Second, the desired nanocolloid ink jet is emitted from the stable cone of liquid meniscus, which is related to the dimension of the nozzle. A common sense of relationship between tip diameter of the nozzle and jet would be the smaller the outer diameter of the nozzle, the smaller the jet and line width, and the less conductive of silver tracks because of reduced cross sections and discontinuity of tracks.

Third, to acquire highly conductive micro tracks with good connectivity of printed metal particles, multilayered printing was attempted by direct placing the deposition on top of each other in the study with sacrificing of resolution.

3.2 Fundamental study of electrohydrodynamic inkjet printing

The detailed mechanism of AC-pulse modulated e-jet printing was demonstrated in previous section. I conducted a sequence of experiments to verify the concept and characterize droplet formation regards to amplitude, frequency and duty rate of input voltage. Experiments using e-jet printing for direct fabrication of conductive silver tracks including electrical characterization were conducted and details were presented in the following sections.

Figure 3.4 (a) shows experimental setup for e-jet printing. The additive printing system is capable of on-demand printing planner and three dimension micro structures using not only conductive inks, but also polymers [39], wax materials [32], etc. The positioning system was configured to move linear in three orientations with 0.1 μm repeatability and accuracy. As shown in Figure 3 (a), the position system can be programmed to provide planar movement for substrate in X-Y direction with a displacement range of 100 × 100 mm, and up-and-down motion for nozzle in Z direction with a displacement range of 50 mm. A pneumatic syringe is able to provide pressure for e-jet printing and keep required flow rate if necessary with maximum pressure of 5 psi and 0.05 psi resolution.

AC-pulse modulated voltage is applied between top electrode (nozzle) and bottom electrode. The nozzle, which is made of glass with a conical nozzle tip, has to be coated with gold and platinum first in order to function as top electrode. The bottom ground electrode is

made of silicon with aluminum coating outside. All electrical voltage input is programmed by signal generator (Agilent Technologies, Model 33220A) and amplified by high voltage source meter (Cole Parmer, Model 9741-50) before supplied to the electrodes.

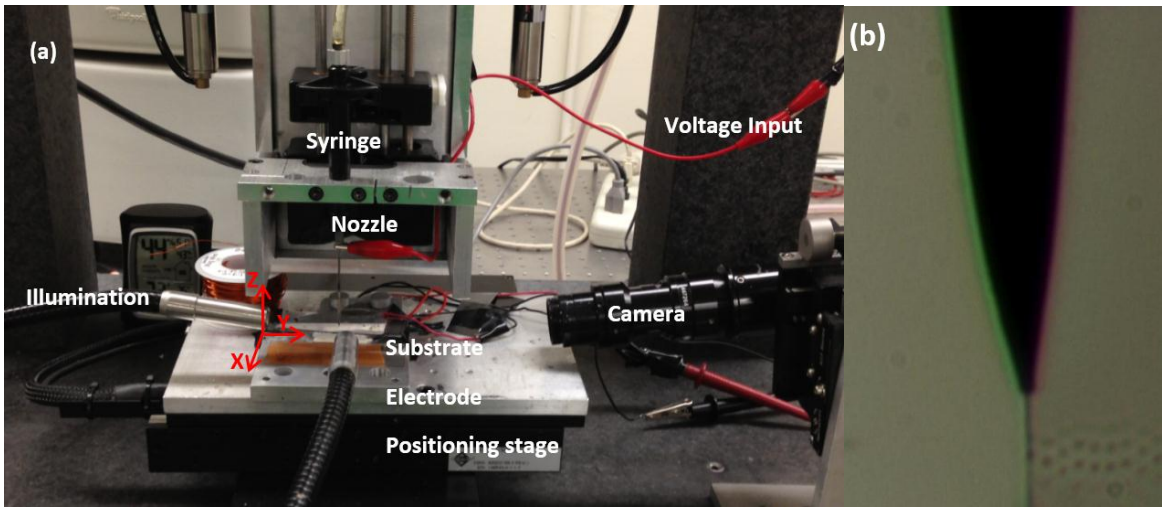

Figure 3.4 (a) Lab setup of e-jet printing for experiment, (b) optical image of nozzle and jetting generated

The optical camera (Newport Corp.) is adapted to monitor fabrication process with a 0.5 μm resolution, as shown in Figure 3.4 (b) with illumination on the other side posting shade of nozzle and jet. From the image of the camera, I was able to identify the cone-jet working mode of e-jet printing, in accordance with the functioning mode of electrohydrodynamic theory [12], indicating silver nanoink work well in our e-jet printing system.

It is essential for researchers to identify different materials for additive printing and I used silver nanoink in the e-jet printing system and characterize its property in my

experiment. The nanoink can easily produce electrode circuit with high-resolution compared with photolithography. I used silverjets purchased from Advanced Nano Product with 30~35 % solid content. The solvent is triethylene glycol monoethyl ether (TGME) with small amounts of lubricants and surfactants to prevent agglomeration between silver nanoparticles. The curing temperature is about 120~150 ℃ from company's data sheet, and viscosity is in the range of 10-1 cP. Three types of substrates used in the study are microscopic glass slides (100 mm × 25 mm × 1 mm), and two highly insulating substrates, 1 mm thick ABF film coated on glass slides, and 1 mm thick PET film, which is one of the most widely used materials used for flexible electronics.

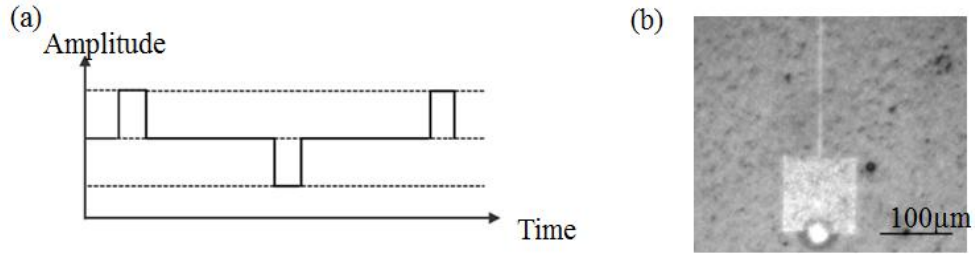

Figure 3.5 (a) AC voltage signal with duty ratio of one, (b) 30-layer straight silver track with line width of 2.3 μm printed on ABF

In the work, the experiments were conducted as follows. First, pulse frequency and pulse voltage amplitude were investigated to control printing process. The AC-pulse modulated waveform of input voltage was given in Figure 3.5 (a) to improve controllability of e-jet printing process and reduce residue charge accumulation problems. The AC-pulse frequency was used to control printing frequency because each positive or negative pulse will

produce a droplet, meaning printing frequency was expected to double pulse frequency. The amplitude of voltage determines electrical field to form droplets. An optimal frequency and voltage would be identified by obtaining stable nanoink jet. Second, plotting speed was characterized for continuous features of printed patterns with single layer. There was a corresponding maximum plotting speed for each fixed input voltage. By regulating amplitude, frequency of input voltage, and plotting speed, I was able to print continuous silver tracks with best resolution. Third, electrical characterization in terms of multi-lay printing was conducted, including effect of multi-layer effect. The following section discussed curing temperature and other factors on conductivity of printed patterns in details. The resistance of printed silver tracks was measured using two point probe methods and details would be discussed in the following section.

The process characterization was performed on glass slides. After the process conditions were identified, continuous silver tracks and silver interconnectors were directly printed on to glass substrates, as well as insulating PET and ABF film. The shape and dimension of printed patterns was observed using high-resolution microscope (KH 770 from Hirox, and infinite 1 from Lumenera Corp.) and atomic force microscope (AFM) (Park Systems).

3.2.1 Modeling of printing mechanism

Figure 3.6 showed a 3D AFM image of printed dots. Based on the measurements of printed silver droplets, I was able to calculate and analyze the track-formation mechanism of the AC modulated e-jet printing process. My assumptions include: (1) the falling droplets are perfect sphere, and average height h and diameter d of printed dots can be measured from

AFM image, as shown in Figure 3.6; (2) the volume loss of evaporated solvents during printing process is negligible; and (3) current in the meniscus is stable and proportion to voltage. During the printing process, the accumulated charges in the meniscus result in the formation of droplets. The total amount of charges in a droplet can be estimated by integral of electrical voltage and time. Based on my observation in my previous research presented in [38], the track line width turns out to be greater with an increased amplitude of voltage and a decreased frequency (increased cycle time), which means more charges accumulate during the time interval.

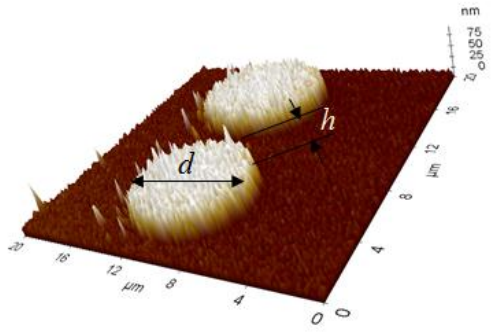

Figure 3.6 3D AFM image of printed dots

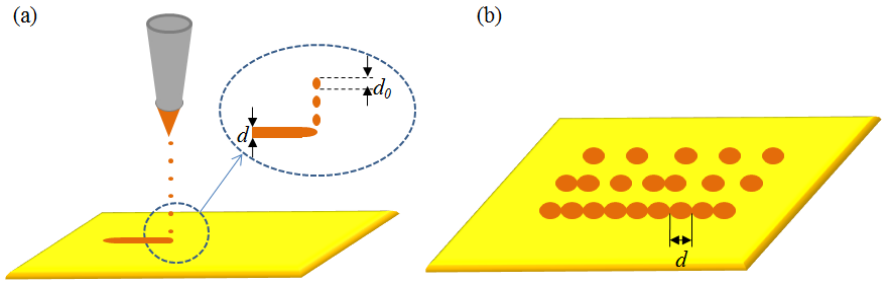

Figure 3.7 Sketches on a microscopic of (a) mechanism of falling droplets with actual diameter of falling droplets d_0 and diameter of printed droplets d; (b) requirements to obtain connective silver tracks printed on substrate

Figure 3.7 shows the mechanism of falling droplets and the patterns that these droplets form on the substrate. As shown in Figure 3.7 (a), once a droplet is formed, it will fall off and flatten on the substrate to form a dot. The volume of droplets and dots are equal. For a printed track width of *d*, we are interested in knowing what the initial drop size d_0 should be. The volume of a printed droplet is found to be:

$$V_{print} = \pi \times \left(\frac{d}{2}\right)^2 \times h \quad (1)$$

where V_{print} = volume of printed droplets, h = average height of printed droplets, d = diameter of printed droplets. The actual volume of a falling drop can be found to be:

$$V_{droplet} = \frac{4}{3} \times \pi \times \left(\frac{d_0}{2}\right)^3 \quad (2)$$

where $V_{droplet}$ = actual volume of falling droplets, and d_0 = actual diameter of falling droplets. Since the volume of the falling droplet is the same as the volume of the printed drop, one has the following:

$$V_{print} = V_{droplet}, \rightarrow \pi \times \left(\frac{d}{2}\right)^2 \times h = \frac{4}{3} \times \pi \times \left(\frac{d_0}{2}\right)^3 \quad (3)$$

By rearranging Equation (3), one can find the droplet size d_0 to be:

$$d_0 = 2 \times \sqrt[3]{\frac{3V_{droplet}}{4\pi}} = \sqrt[3]{\frac{3 \times d^2 \times h}{4}} \quad (4)$$

Equation (4) can be used to estimate the e-jet printing droplet size. Once we measure the average height and diameter of printed dot on the substrate, the actual size of falling droplet can be calculated using Equation (4).

As shown in Figure 3.7 (b), in order to print connective silver tracks instead of separate dots on substrates, two adjacent droplets has to be at least tangential to each other.

The time between two adjacent droplets is half of cycle time of AC voltage. The maximum plotting speed can be calculated using the following equation. Assuming *T* is the cycle time of AC voltage, and f is the frequency of AC voltage, the maximum plotting speed v_{max} can be found as following:

$$v_{max} = \frac{d}{T_d} = \frac{2d}{T} = 2df \text{ , and } T = \frac{1}{f}, T_d = \frac{T}{2} \quad (5)$$

where $T = 1/f$, f = frequency of AC voltage, $T_d = T/2$, T_d = time between two adjacent droplets, d = diameter of printed droplets, and v_{max} = maximum plotting speed.

Equation (5) can be used for plotting speed control of XY stage position in the AC modulated e-jet printing process. As shown in Equation (5), the plotting speed for e-jet printing is determined by the frequency of the AC used in modulating e-jet printing process.

3.2.2 Amplitude and frequency of AC-pulse voltage

As shown in Figure 3.8, in AC-pulse modulated e-jet printing, the fine jet down to nano scale is generated at the tip of ink meniscus when enough charge accumulates inside the meniscus. The system works at cone jet mode when electric stress resulting from applied voltage deforms the ink at the nozzle tip. A droplet forms when its electrical force is greater than surface tension.

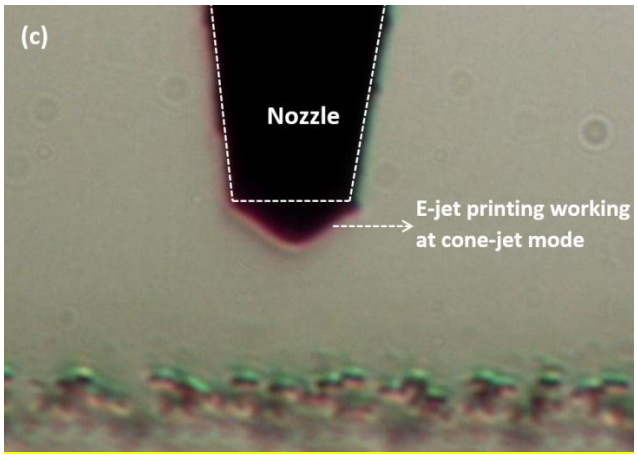

Figure 3.8 Optical image of e-jet printing working at cone-jet: the dimension of printed droplets is smaller than dimension of the nozzle

As shown in Figure 3.9, silver tracks were printed with changing pulse amplitudes of input pulse voltage while keep other parameters constant to find its effect on e-jet printing. The diameter of nozzle was 7 μm, feed rate was 9 mm/s, pulse frequency was fixed at 1000 Hz, and duty rate is 10%. The line width of printed silver with respect to pulse amplitude was shown in Figure 3.9 (b). It can be clearly observed that with increasing amplitude, line width of printed silver tracks was increased. The results are in accordance with results based on DC voltage. With larger amplitudes, there will be more charge accumulation at the meniscus, thus bigger droplet sizes.

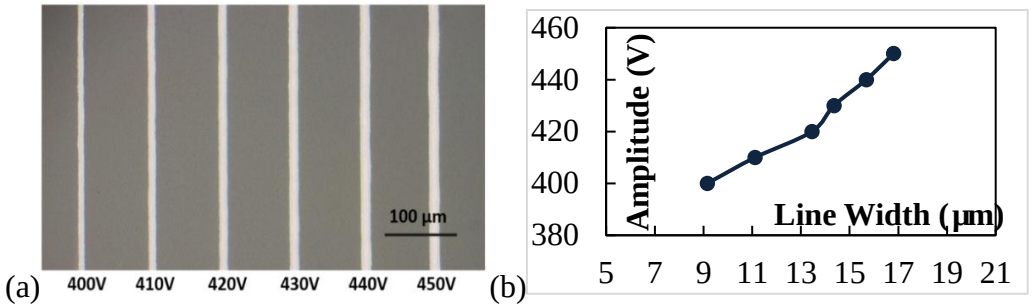

Figure 3.9 (a) Printed silver tracks at different pulse amplitude, (b) Line with of printed silver tracks in regarding to pulse amplitude

The printing frequency was double pulse frequency because each positive or negative pulse will produce a droplet. This was how I solve the residual charge problems of e-jet printing by neutralizing printed charges with alternative positive and negative droplets for continuous patterning. I used a fixed voltage of 400 V, a fixed duty rate of 10%, plotting speed of 9 mm/s with different pulse frequencies to study its effect, as shown in Figure 3.10. Based on the measurement from Figure 3.10 (b), a reduced line with of printed silver tracks was observed with increasing frequency. Larger pulse frequency means shorter duration for charge accumulation with same duty cycle and amplitude of input voltage, thus generating a smaller droplet. It was noticed that when frequency was larger than 1000 Hz, discontinuous pattern was formed because duration time was too short for charge accumulation. It was the balance between amplitude and frequency that generated best resolution with continuous features. With fixed pulse amplitude of 400 V, frequency of 1000Hz, and duty rate of 10%, I was able to print stable continuous silver tracks with smallest line width. These parameters were adapted in the following experiments.

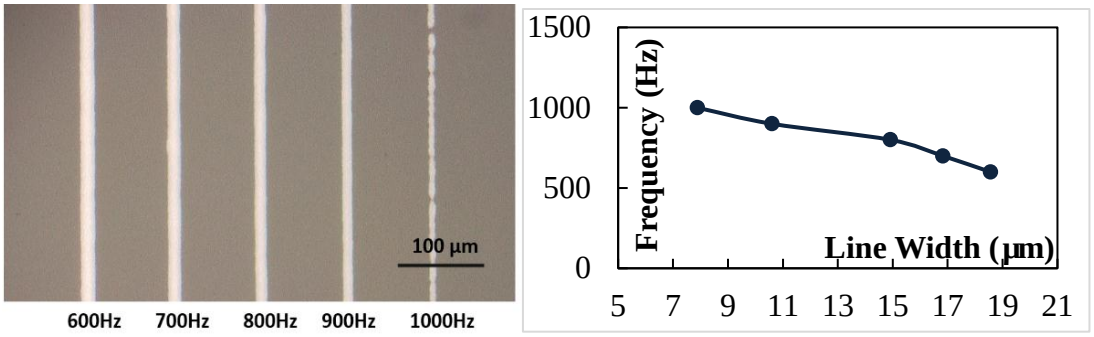

Figure 3.10 (a) Printed silver tracks at different pulse frequencies, (b) Line width of silver tracks in regarding to pulse frequency.

3.2.3 Plotting speed and droplet size

Based on the measurements of printed silver droplets, I was capable of calculating and analyzing the mechanism of printing process. One assumption is that the falling droplets are perfect sphere and printed dots are cylinder shape with average height and diameter measured from AFM image. I assumed that the triethylene glycol in the droplets would be volatilized during falling. During the printing process, the accumulated charges in the meniscus will result in formation of droplets. Assuming the current in meniscus is stable and proportion to voltage, the total amount of charges in a droplet can be estimated by integral of electrical voltage and time. In accord with my previous research [85-87], line width turned out to be greater with increased amplitude of voltage and decreased frequency (increased cycle time), which means more charges accumulate during the time interval.

With our previous analytical model, I was able to characterize plotting speed and estimate droplet size on single layer printing process. Using Equations (1) to (5), one can find

the maximum e-jet printing plotting speed v_{max} and the actual droplet size d_0 for the process, shown as follows:

$$f = 1000\ Hz, d = 6.06\ \mu m\ , h = 30.73\ nm$$

Using the process parameters and Equation (5), the maximum e-jet printing plotting speed v_{max} can be found as follows:

$$T = \frac{1}{f}\ , T_d = \frac{T}{2}\ , v_{max} = \frac{d}{T_d} = \frac{2d}{T} = 2df = 12.12\ mm/s$$

By using Equation (4), the droplet size d_0 can be found as follows:

$$d_0 = 2 \times \sqrt[3]{\frac{3V_{droplet}}{4\pi}} = \sqrt[3]{\frac{3 \times d^2 \times h}{4}} = 0.92\ \mu m$$

As shown in Figure 3.11, the cross section of printed silver dots has an average height of 30.73 nm and an average line width of 6.06 μm. By using Equations (4) and (5), the maximum speed v_{max} for connective silver tracks was 12.12 mm/sec, and the actual diameter of falling droplets was 0.92 μm. The ratio of diameter of nozzle and diameter of falling droplets was about 7.6.

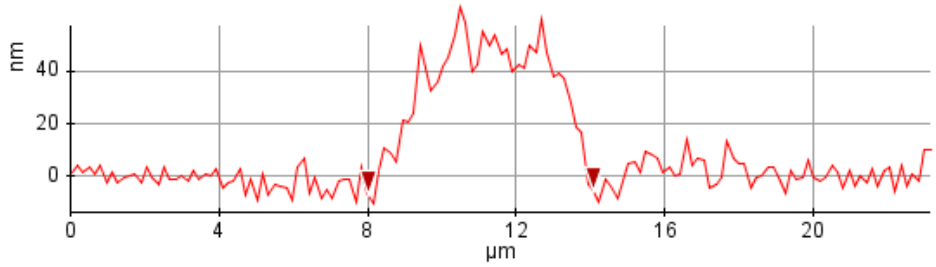

Figure 3.11 Cross section of cylinder-shape printed silver tracks

According to Figure 3.11, the cross section of printed silver dots had an average height of 30.73 nm and an average line width of 6.06 μm. Based on equations (1) and (2), The maximum speed for connective silver tracks was 12.12 mm/s and the actual diameter of falling droplets was 0.92 μm, as calculated in equation (3). The ratio of diameter of nozzle and diameter of falling droplets was about 7.6.

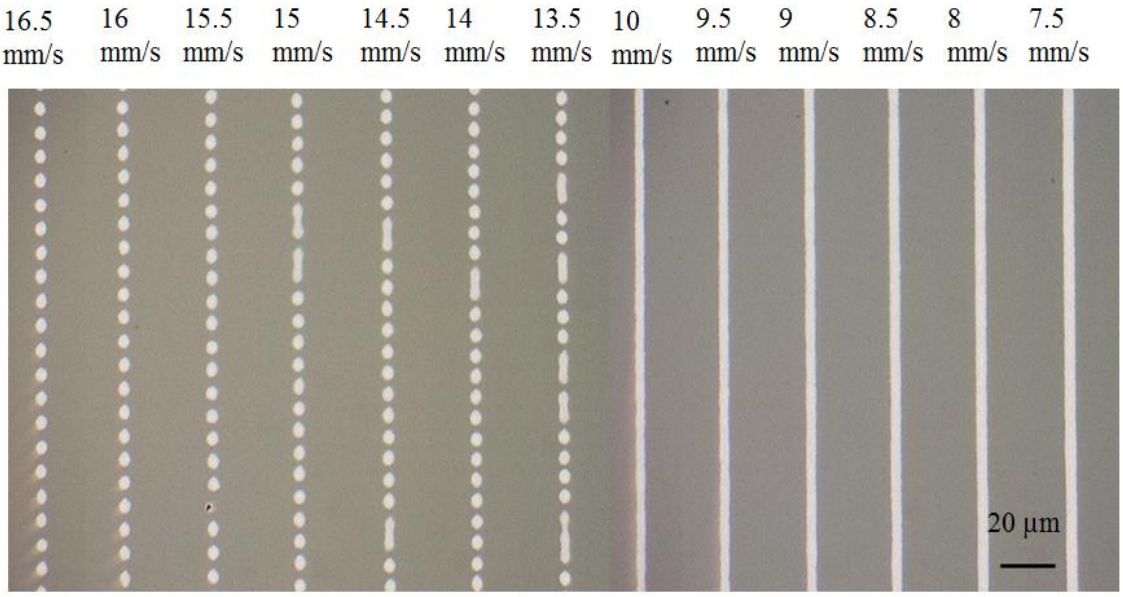

Figure 3.12 Effect of plotting speeds: plotting speed increased from 7.5 mm/s to 16.5 mm/s with reduced line width and discontinuous pattern

Plotting speed determines droplet spacing and overlap when all other parameters were kept constant. Figure 3.12 showed printed patterns from discontinuous silver dots to continuous silver with decreasing plotting speed from 16.5 mm/s to 7.5 mm/s. When plotting at a smaller plotting speed slower than the calculated v_{max} by Equation (5), I was able to

acquire stable and continuous silver tracks during my experiments. As the plotting speed increased, the width of silver tracks reduced gradually because of excess ink accumulation along printed silver tracks, as shown in Figure 3.12 with plotting speed increased from 7.5 mm/sec to 10 mm/sec. Two adjacent droplets had to have a minimum overlap in order for continuous patterns. As observed from experiments, with high plotting speed (13.5 – 16 mm/s), there was no or not enough overlap between two adjacent droplets, thus resulting in discontinuous patterns. Though some of droplets were connected, the overall continuity was interrupted. The results helped to prove that the maximum speed for connective silver tracks was about 12.12 mm/sec in this scenario based on Equations (5).

3.2.4 Multi-Layer printing

During the depositing process, the substrate was scanned over a distance of 50 mm for single layer and stable multi-layer printing in order to study the effect of connectivity on electrical performance. To achieve good conductivity of direct printing trackers, the connectivity is an important factor that needs to be controlled. The dimension of silver nanoparticles in the ink is about 30-50 nm, encapsulated by polymer shell to avoid coagulation. There are also certain amount of lubricants, surfactants, and solvent in the nano ink to keep it at stable suspension status. Silver nano ink will transfer from suspension status into solid status when most of solvents are evaporate. The effects of nano particle connectivity and its impact on the conductivity of direct printing tracks were studied and discussed in the following section. Figure 3.13 showed the effects of connectivity on conductivity.

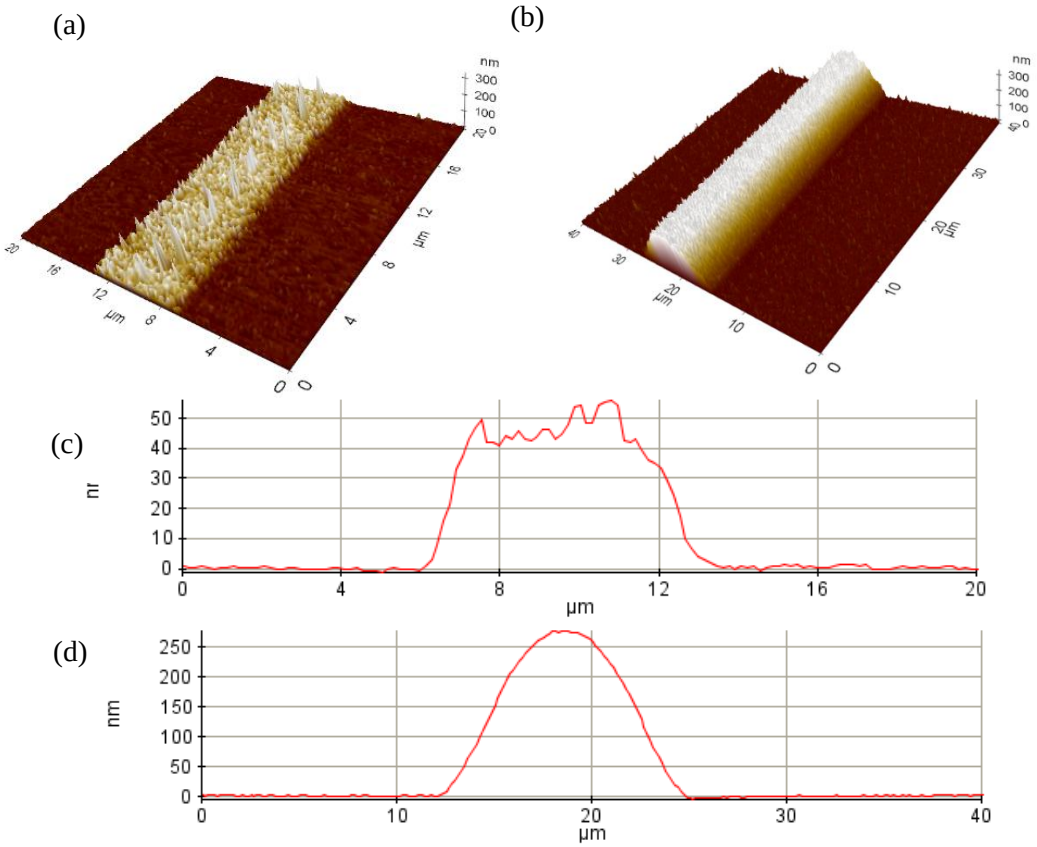

Figure 3.13 (a) Printed single layer silver track, (b) Printed multi-layers silver track, (c) Single layer pattern with average thickness of 46 nm for and line width of 5.9 µm (d) 20-layer pattern with average thickness of 187 nm and line width of 13.1 µm

Even though the silver nano ink is in stable suspension status, the viscosity of silver nano ink is relative low. As a droplet fall onto the substrate, the silver nano particles inside it will break out the surface tension and splash out. As shown in Figure 3.13 (a), single particle hillocks can be observed in single layer e-jet printed silver track. The separate existed particle hillocks resulted in a poor connectivity condition for silver tracks. As a result, these

cracks and gaps inside silver tracks would block current flow and significantly affect conductivity of printed patterns. From Figure 3.13 (c), the maximum height for printed single layer silver track was measured to be 46 nm. It was believed that only one or two nano particles were overlaid each other considering diameter of silver nanoparticles is about 30-50 nm.

By depositing multiple layers at the same position, I can print multiple silver layers (20 layers in this example) at the track with fine semi-ellipse cross section, as shown in Figure 3.13 (b). It was clearly shown in the figure that inter-connectivity of printed pattern was improved with multi-layer printing. A maximum height of 277 nm was measured as shown in Figure 3.13 (d). However, the average line width was increased from 5.9 μm for single layer printing to 13.1 μm for multi-layer printing because there were unavoidable particles creeping down to the edge when particles stack layer by layer. For a pattern with fixed length, the corresponding resistance was inversely proportional to cross-section area of the pattern. An increased cross-section area had the ability to drive higher current and consume lower power.

3.3 Electrical characterization and post-curing

The printed multi-layer silver tracks in previous section showed well inter connected profiles; however, they didn't show any electrical conductivity. The reason for its extremely large resistance was that there was still polymers shell and residual solvents impeding nano particles connecting with each other. A post curing process was necessary for e-jet printing in order to remove all impurities inside silver tracks and reform its structure for better electrical performance. As shown in Figure 3.14, curing process will first remove lubricants,

surfactants, solvents and polymers out of silver patterns. The next step is a diffusion mechanism, where the heat will reform the silver nanoparticles, creating necks between adjacent silver particles and later transforming the necks into grain boundaries. During curing, pores and interstices will be removed once grain boundaries forms, resulting in a denser structure of printed patterns and better conductivity as well.

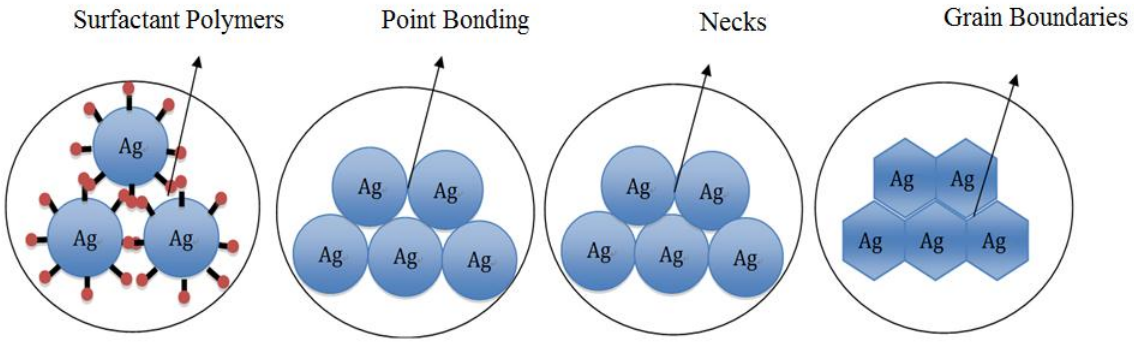

Figure 3.14 Sketches on a microscopic scale the changes that occur during sintering of silver nanoparticles

3.3.1 Effects of connectivity on conductivity

The silver ink consists of triethylene glycol, surfactants and silver nanoparticles. Nano particles are dispersed in the solvent, which would be evaporated during printing process. However, with smaller diameter of droplets to achieve better resolution, when they fall onto the substrate, they will splash out and transform into single particle bunches, as shown in Figure 3.15 (a). Since most of bunches were not interconnected, there was no electric conductivity of single layer silver tracks. By depositing multi layers on the same position, I can print 20 layers silver tracks with fine semi-ellipse cross section, as shown in

Figure 3.15 (b). The cross sectional measured maximum height of 60 nm for the single layer pattern with an average thickness of 27 nm and line width of 5.3 μm. Because the geometric diameter of silver nanoparticles was below 50nm, it was believed that there was only single nano particle printed on the substrate without any overlay. That was the reason why the inter connectivity was so poor that single layer silver tracks could not carry a current flow. The cross sectional measured maximum height of 310 nm for the 20 layers pattern with an average thickness of 167 nm and line width of 15.1 μm. By depositing the silver ink on the same position to acquire multi-layer pattern, line width, line thickness and connectivity were increased with sacrifice of resolution. After curing process, the 20 layers silver track showed good electric conductivity.

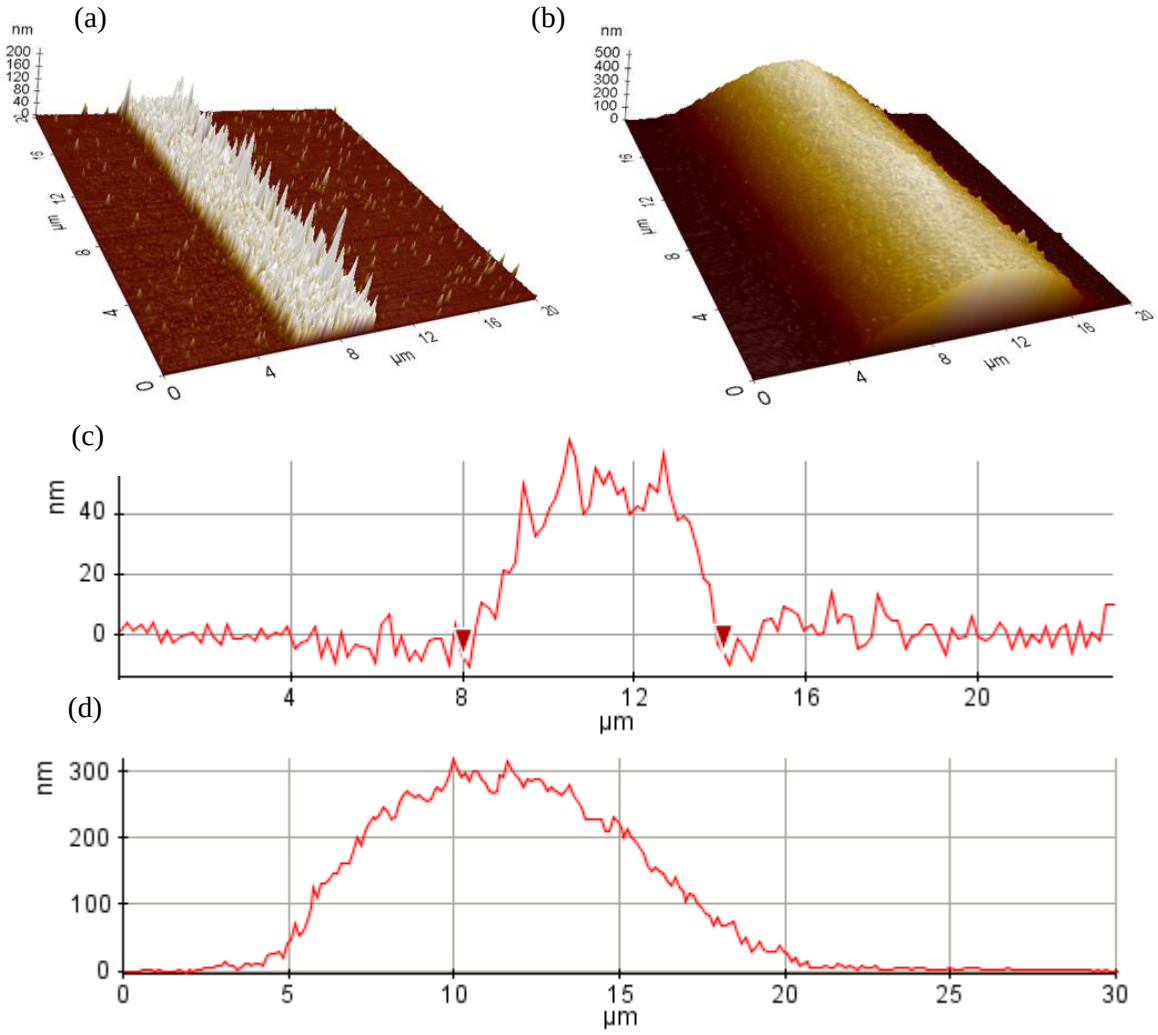

Figure 3.15 (a) 3D AFM image of single layer pattern, (b) 3D AFM image of 20 layers pattern. (c) Cross sectional measured maximum height of 60 nm for single layer pattern with an average thickness of 27 nm and line width of 5.3 µm (d) Cross sectional measured maximum height of 310 nm for 20 layers pattern with an average thickness of 167 nm and line width of 15.1 µm

3.3.2 Effects of curing temperature on conductivity

I compared influences of different curing temperature modalities on resistivity and morphography of printed patterns, as shown in Figure 3.16. 20-layer silver tracks were printed under the same condition where diameter of nozzle is 7 μm, frequency of voltage is 150 Hz, and amplitude is 800 volts. The first sets of samples were instantly cured at 220 ℃ for 30 minutes and the result was shown in Figure 3.16 (b). The morphography indicated that silver nanoparticles went through violent crystallization, forming particle clusters when impurities inside were removed drastically in instant. The independent undulating topography resulted in poor connectivity of printed patterns and thus poor conductivity.

A ramped curing temperature modality was adapted in which the silver tracks were cured from 40 ℃ to 220 ℃ at 30 minutes time interval in a linear growth pattern. The temperature was increased 18 ℃ per 3 minutes in the 30 minutes time frame, and then kept at 220 ℃ for 15 minutes. As we can see from the topography shown in Figure 3.16 (a), the ramped curing temperature led to a smooth diffusion and curing process for silver tracks. The ramped temperature modality was adapted in the fabrication process for the following sections.

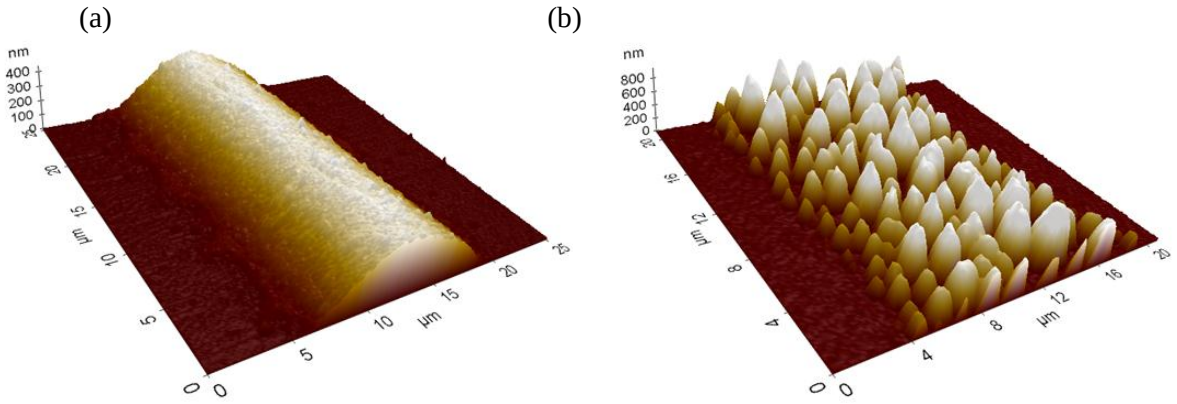

Figure 3.16 (a) 3D AFM image of 20 layers pattern cured with ramped temperature to 220 ℃, (b) 3D AFM image of 20 layers pattern cured instantly to 220 ℃

A contacting two probes method was adapted for measurement of resistance of printed silver patterns. An ohmmeter (Fluke) would detect the resistance when two contact probes were placed at two ends of silver tracks in a fixed length. The resistance of printed patterns can be calculated using Equation (6).

$$R = \rho \times L / A \tag{6}$$

where R = resistance of printed silver tracks, ρ = resistivity of printed silver tracks, A = area of cross-section of printed silver tracks, and L = length between the two contact probes.

To find the effect of curing temperature on resistivity of printed patterns, 10-layer silver tracks and 20-layer silver tracks were printed when the pulse frequency, amplitude, plotting speed and nozzle diameter were fixed at 150 Hz, 800 V, 7 mm/s and 7 μm, respectively. Five different curing temperatures (140 ℃, 160 ℃, 180 ℃, 200 ℃ and 220 ℃) were applied on 10-layer and 20-layer samples using ramped modality as shown in previous

section. After post curing, we measured each sample at five different positions and averaged for its resistance. The average cross-section area of samples was from AFM results.

Table 3.1 Electrical characterization of printed 10-layer and 20-layer silver tracks

Temperature (℃)	**Resistivity (ρ, Ω·μm)**		**Resistance (μΩ)**		**Line Length (μm)**		**Cross-Section Area ($μm^2$)**	
	10-Layer	20-Layer	10-Layer	20-Layer	10-Layer	20-Layer	10-Layer	20-Layer
25	∞	∞	∞				2.5885	3.88
140	0.888	1.288	40.4692	36.00	104.6	97.5	2.2952	3.49
160	0.612	0.547	28.0616	17.43	96.4	107.3	2.1024	3.37
180	0.322	0.251	15.2506	7.79	94.8	100.5	2.0016	3.24
200	0.142	0.051	7.58394	1.52	103.9	91.2	1.9454	3.06
220	0.159	0.07	9.46792	2.32	108.5	98.6	1.8221	2.98
Bulk Silver	0.016							

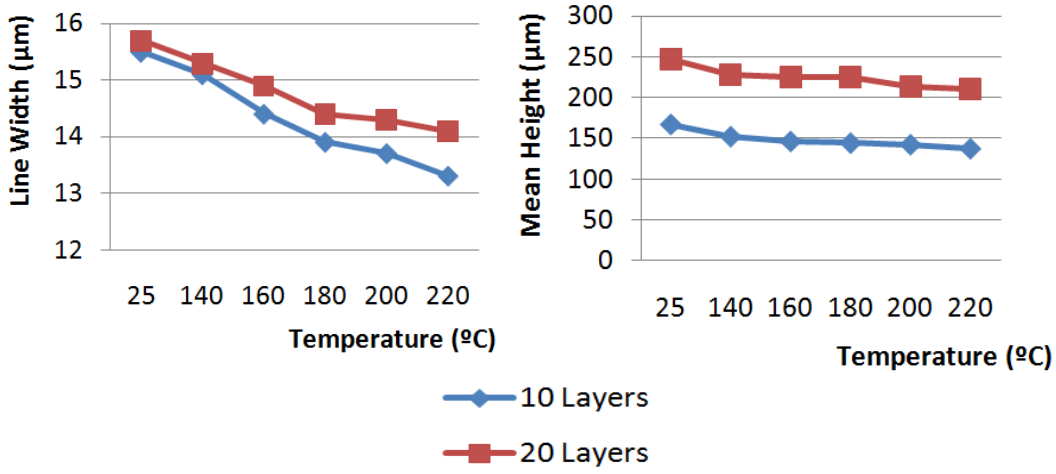

Figure 3.17 Line width and mean height reduction during curing process

Table 3.1 and Figure 3.18 demonstrated resistivity changes and constriction of printed silver tracks with respect to curing process. Shrinkage occurs during curing process as results of pore size reduction, lubricants and surfactants evaporation. This largely depends on the composition of silver ink, temperature and time. Silver tracks were printed with 10 lays and 20 lays using the same nozzle with glass tip outer diameter of 7 μm, using an AC voltage with 130 Hz frequency and 820 volts amplitude. The silver tracks were cured under temperatures of 140 ℃, 160 ℃, 180 ℃, 200 ℃ and 220 ℃ using ramped pattern. As shown in Figure 3.17, there was a reduction in both line width and mean height (similar to maximum height) due to shrinkage. As maximum curing temperature went high, the shrinkage was more obvious. A maximal 14.2% reduction of line width and 17.8% reduction of mean height were observed in 10 layers sample. A maximal 10.2% reduction of line width and 14.5% reduction of mean height were observed in 20 layers sample.

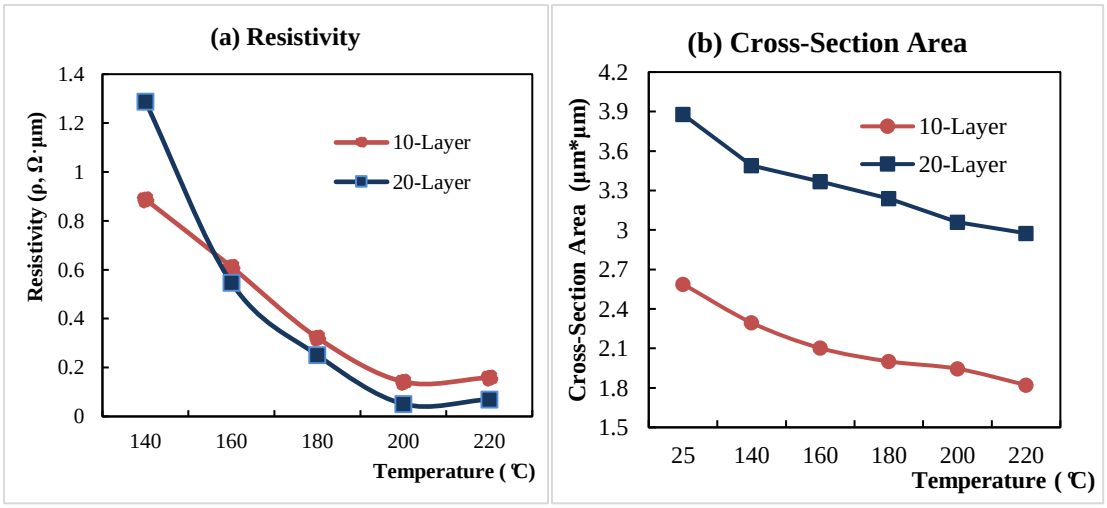

Figure 3.18 (a) Resistivity in regard to curing temperature, (b) Shrinkage of silver tracks with a reduction in cross-section area due to curing process

From Equation (6), resistance is a product of resistivity and cross-section area with fixed line length. The geometric dimension of printed plays a significant role in electrical performance. At room temperature of 25 ℃, the line widths of printed 10-layer silver tracks and 20-layer silver tracks showed almost same line width, but the thickness was increased from 167 nm to 247 nm with 10 more layers printing. Printed patterns shrinks during curing process to get rid of impurities inside, defusing and reforming nano particles, resulting in reduction of cross-section area. With higher temperature, the deduction ratio became higher. A maximal 29.6% reduction of cross-section area was observed in 10-layer sample at curing temperature of 200 ℃. But the resistance was tremendously reduced because of improved resistivity.

Curing process improved conductivity of printed patterns, as shown in Figure 3.18 (a). The optimal temperature for curing is 200 ℃ where conductivity of silver tracks reached a peak value. The minimum resistivity measured was 5.1 $\times 10^{-2}$ Ω· μm, about three times than that of bulk silver at room temperature. The electrical performance of printed silver patterns was no better than bulk silver because of unavoidable voids and inter coarse network between silver particles inside the track.

3.3.3 Electronic components printing

Figure 3.19 (a) showed high-resolution printed metal pads, interconnects for representative circuit patterns with critical dimensions as small as 18 μm showed great potential applications in microelectronic components fabrication. Figure 3.19 (b)

demonstrated silver tracks with line width of 12 μm printed on ABF, which was a highly insulating material. These can be applied for micro capacitor or inductor fabrication.

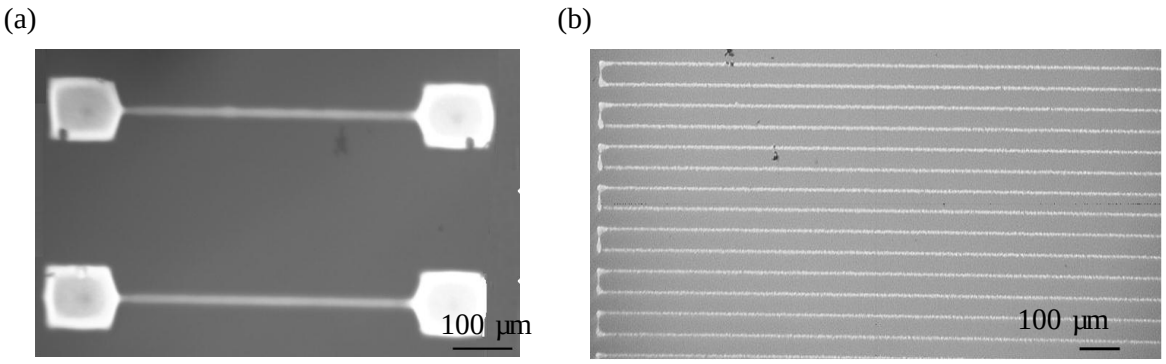

Figure 3.19 Printed electronic components: (a) printed metal pads and interconnects (b) an inductor

3.4 Summary

In this chapter, a novel AC-pulse modulated e-jet printing technique was developed with improved controllability, resolution and electrical performance for printed patterns. Fabrication process and detailed analytical track formation mechanism were investigated and validated experimentally. AC-pulse modulated e-jet printing alternates charge polarity of adjacent droplets to neutralize charges remained on the substrate for printing on highly insulating materials. Pulse frequency, pulse amplitude, and plotting speed can be controlled independently for continuous features with sub-10 μm resolution. Multi-layer printing technique and post curing process were applied for desired resistivity of silver tracks. It is demonstrated that the proposed printing technique can achieve both high-resolution and low

resistivity patterns on insulated surfaces, showing great potential in flexible electronic and printed electronic applications. The presented AC modulated e-jet technique is capable to fabricate resistors, inductors and micro interconnects, which offer a simple and versatile method to on demand direct fabricate conductive patterns in micro/nano electronic manufacturing.

In the following chapter, further improvement on electrical performance of printed patterns was studied and a prototype of capacitive touch sensor based on e-jet printing was fabricated and tested to valid the fabrication process.

CHAPTER 4 ELECTROLESS COPPER DEPOSITION OF PRINTED PATTERNS

From Chapter 3, e-jet printing demonstrated its great potential as a high-resolution rapid prototyping method for flexible electronics. However, there was still one major challenge before it can be used for device fabrication. The thickness of printed patterns was not high enough, and the area of cross section was too small which made it hard to carry current flow. As a result, the stability and resistivity of printed patterns were not good enough for device fabrication. In this chapter, I first introduced electroless copper deposition into e-jet printing to increase the thickness and cross section area of printed patterns. I demonstrated that AC-pulse modulated e-jet printing followed by electroless copper deposition can produce high resolution conductive patterns with improved thickness on insulating substrates and flexible substrates, which can be applied to direct printing and micro scale patterning for flexible electronics and wearable devices applications.

4.1 Mechanism of electroless copper deposition

As mentioned in previous section, the electrical performances of printed patterns were not good enough for electronic devices. The silver nano ink consisted not only silver nano particles, otherwise they will coagulate instead of forming stable solutions, but also polymer shells and solutions to avoid this problem. The solution would be evaporated during printing, while the polymer shell remains in the pattern. As a result, the interconnectivity and conductivity of printed patterns has to be improved first. Post-treatment of printed patterns were necessary to enhance electrical performance for electronic devices.

There are two kinds of post-treatment methods that can be adapted into the rapid prototyping method. First, curing process can remove impurities inside silver patterns and

reform the inner structures of silver nano particles, removing voids and generating grain boundaries between particles into denser structures. The temperature needed for curing process is between 150 °C and 250 °C for a better conductivity. However, for flexible electronics where substrates are made out of polymer, paper or wood, this high temperature would also be a problem since it will affect the polymer structure resulting in distortions.

To address this issue, electroless copper deposition was introduced into the fabrication process. E-jet printing was applied to deposit silver seeds on the substrate. The substrate was immersed in the plating solution. The electroless copper deposition occurred only where silver seeds were printed. Most lithograph methods are restricted to planar surfaces, which is especially difficult to extend photolithographic or e-beam techniques to curved substrate because of focal plane issues. I demonstrated printing of silver seeds to generating pattern on curved surfaces and afterwards copper deposition. The resolution of features on curved substrate was similar to that on planar substrates.

Pretreatments of substrates were necessary to ensure good adhesion of printed silver seeds and substrate to avoid washing away when placed into solution. It also helps strong interaction between catalyst and deposited layer. I used glass, silicon with oxide layer, polymers as substrates for electroless copper deposition. The first step is cleaning the substrate using water in an ultrasonic environment to remove particles and other contaminations. The second and third step is immersing the substrates in solution of acetone and ethanol, separately, to remove all organic contaminations that may reduce the adhesion between silver seeds and substrates. Then the substrate is put back into water under ultrasonic environment.

The mechanism of electroless copper deposition has been thoroughly studied [88]. There are plenty of empirical laws proposed to measure the reaction orders [89]. Traditional electroless plating baths are typically composed of a metal salt such as metal ion sources like $CuSO_4$ and $AgNO_3$, chelating agent to prevent formation of undesired compounds, and a reducing agent (formaldehyde). The reactions are typically catalyzed only on noble metals, including Pt, Pd, Ag, Au, Rh, or Ir [90]. Overall, electroless copper deposition can be generalized into the anodic and cathodic reactions [91]:

Anodic half reaction: $2HCHO + 4OH^- \rightarrow 2HCOO^- + 2H_2O + H_2\uparrow + 2e^-$

Cathodic half reaction: $CuL_n^{2-n*m} \leftrightarrow Cu^{2+} + nL^{-m}$, $Cu^{2+} + 2e^- \rightarrow Cu$

where L represents complexing agents, such as the most common complexing agents used for formaldehyde-based electroless copper deposition is ethylenediaminetetraacetic acid (EDTA) and triethanolamine (TEA), and m represents the charge of chelating agent.

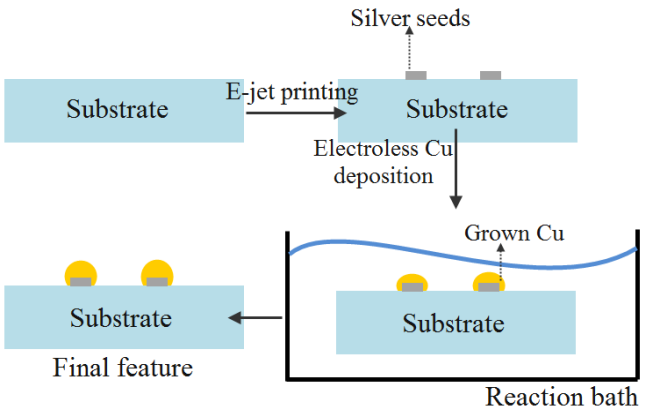

Figure 4.1 Schematic of electroless copper deposition with e-jet printed silver seeds

At alkaline conditions, copper ions tend to form copper hydroxide and precipitate out. It is the complexing ability of chelating agents to prevent that. That's why it is so important to carefully consider the concentration of each agent. The complexing agent must be strong enough to reduce free cupric ion concentration, so that copper hydroxide level is below its solubility. On the other hand, too much chelating agents would affect the deposition rate because of reduced free cupric ions. So as the first step for copper deposition using printed silver seeds, I performed a calibration to find out the optimal proportion of each reaction agent for best copper growth rate and topography.

4.2 Electroless copper deposition on silver seeds

In this section, I proposed a combined fabrication technique by printing silver patterns on the substrate followed with electroless copper deposition on printed silver seeds. The process is capable of fabricate sub-20 μm patterns with increased thickness up to 5 μm. I also focus on improving the copper electroless process for new pattern techniques and both organic and inorganic substrates. Submicron silver tracks were printed using e-jet printing as catalytic sites for subsequent electroless deposition of copper. The method of depositing copper based on silver catalyst turned out to be capable of growing copper with thickness up to 15 μm and resistivity about four times bulk copper, a good replacement of traditional palladium catalyst based deposition in terms of cost of process. The combined fabrication technique can be further adapted in integrated circuits, packaging substrates, interconnectors, transistors, and printed circuit boards for flexible electronic devices or prototyping. The process demonstrates a new strategy, combination of direct e-jet printing of silver seeds on the surface and electroless metal deposition, for fabrication of metal features with submicron

dimensions. The procedure can be generalized by varied patterns. Copper can be patterned using electroless deposition combined with electrohydrodynamic inkjet printing for fabrication of printed wiring boards. The approach consists of directly writing a silver seed layer with subsequent step of electroless copper plating to increase thickness and conductivity.

Figure 4.2 presents a schematic outline of the combined fabrication process with e-jet printing and electroless deposition. The whole process can be adapted into traditional continuous fabrication process or roll-to-roll manufacturing. I used e-jet printing to deposit silver seeds patterns on the substrate. The substrate was then immersed in the plating solution. The electroless copper deposition occurred only where silver seeds were printed. A challenge for e-jet printing at this moment is improving resolution of printed patterns while maintaining high conductivity at the same time. In our previous research [92-96], I reported printing of silver filaments with line width down to 2 μm and good conductivity. However, the thickness of printed line is about 300 nm even though with multi-layer printing due to low viscosity of silver ink (tendency to split out instead of accumulate layer by layer). That's the motivation for introducing electroless copper deposition into the procedures to increase the thickness of patterns.

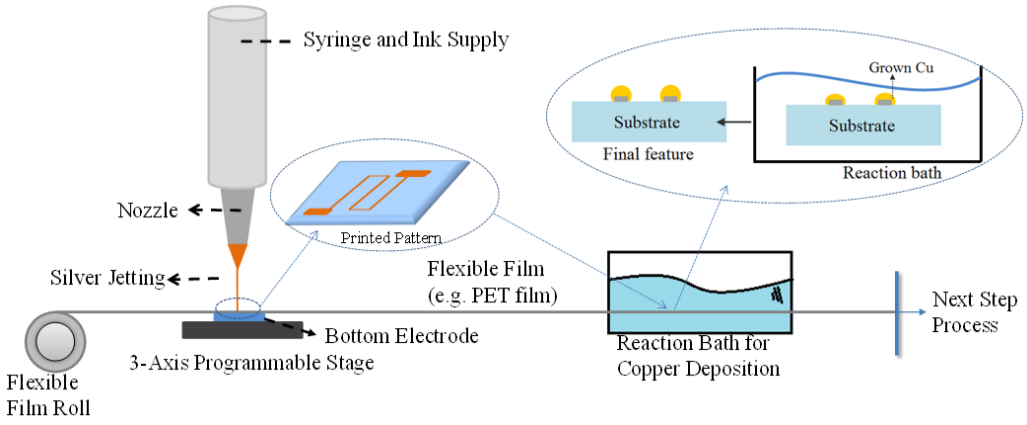

Figure 4.2 Schematic outline of procedures for e-jet printing of silver seeds and subsequent copper deposition. Metallization occurred only where substrate was activated with silver seeds

Electroless deposition of metal is based on reaction between copper ions and a chemical reducing agent in the electrolyte. The process is initiated by a catalyst on the substrate surface. Once the target metal is precipitated out at the first place, the process transforms into autocatalytic process. The precipitation will keep going on where the precipitated metals oxidize reducing agent [66]. The substrates or catalysts will no longer influence electroless copper plating after several atomic layers of copper deposition. The schematic of electroless copper deposition with e-jet printed silver seeds is shown in Figure 4.2.

In the study, substrates were cleaned in an ultrasonic bath for 10 minutes in water, 10 minutes in methanol and 10 minutes in acetone, and 10 minutes in de-ionized water to remove any organic and inorganic contaminants from the substrate. After writing the seed layers, samples were again cleaned using the ultrasonic cleaning steps described above. The substrates were immersed in an electroless copper plating bath. The copper plating bath

consisted of copper sulfate as metal ion source, EDTA and TEA as complexing agent, and formaldhyde as reducing agent. NaOH is used to adjust pH to alkaline environment.

4.2.1 Reaction bath and agents proportion

Electroless deposition of metal is based on reaction between copper particles and a chemical reducing agent in the electrolyte. The process is initiated by a catalyst on the substrate surface. Once the target metal is precipitated out at the first place, the process transforms into autocatalytic process. The precipitation will keep going on where the catalytic seeds and precipitated metals oxidize reducing agent [66]. The substrates or catalysts will no longer influence electroless copper plating after several atomic layers of copper deposition.

A dual complexing agent system using EDTA and TEA was employed in our process. I used the following copper plating bath: Solution A contains $CuSO_4$ (Alpha Chemical Inc.) as metallic source, EDTA and TEA (Sigma-Aldrich Inc.) as complexing agents, NaOH to adjust pH, and distilled water. Solution B is an aqueous formaldehyde solution (36.5% wt%, Thermo Fisher Scientific Inc.). The two solutions A and B were mixed before the bat was used. The deposit copper were immersed the patterned substrate in a mixture of 10 minutes to 40 minutes at different temperatures.

For the calibration, glass substrates were cleaned in an ultrasonic bath for 10 minutes in water, 10 minutes in methanol and 10 minutes in acetone, and 10 minutes in de-ionized water to remove any organic and inorganic contaminants from the substrate. Then straight silver lines are drawn on the substrate with line width around 200 μm. The substrates with straight lines were immersed in the electroless copper plating bath. The copper plating bath

consisted of copper sulfate as metal ion source, EDTA and TEA as complexing agent, and formaldehyde as reducing agent. NaOH is used to adjust pH to alkaline environment. Details of the bath composition matrix are shown in Table 4.1.

Table 4.1 Experimental details of electroless copper bath with different concentrations

EDTA(g/L) / TEA(mL/L)	0	6	12	18	24	30
0						
12						
18						
24						
30						
36						

I used $CuSO_4$ concentration 9g/L, making sure copper particles inside the solution are enough to grow on silver seeds. Each of the concentrations shown in Table 4.1.

Table 4.1 is replicated three times. Samples are immersed into the bath composition shown in the matrix at a constant temperature at 25^0C. The amount of copper in the solution A is enough to cover all silver lines on glass substrates. There was a total of 75 samples. The pH of each solution A is adjusted to 12.5. Solution B is added into solution. The substrate is

then immersed into mixed solution for 20 minutes. The grown copper is observed by Veeco Dektak 150 Profilometer for topography and copper grown. The optimal concentration was picked up for future experiment.

I used the optimal concentration as fixed variables. The substrates were immersed into solution at temperature from 15^0C to 65^0C with 10^0C intervals, extracted, rinsed in deionized water and dried at room temperature. All the samples were then examined by optical microscope and profilometer to find out the optimal temperature for copper growth.

With optimal concentration and temperature as fixed variables, I further immersed substrates for 5 to 30 minutes with 5 minutes intervals, extracted, rinsed in deionized water and dried at room temperature. All the samples were then examined by optical microscope and profilometer to find out the optimal time for copper growth.

With determined optimal concentration of solution, temperature, and time for copper growth on printed silver nanoparticles, I further analyzed resistivity of printed high resolution patterns after copper growth.

The copper deposition is induced by existing silver seeds at the beginning of the process. The copper only grows on silver seeds at this moment. After initial deposition, additional copper deposition will continue on most based on auto-catalytic effect from copper. After copper grains grow up and contact each other, it will form a film over the silver seeds, similar to a silver and outside copper encapsulated film structure.

For electroless copper deposition, I used the following copper plating bath: Solutin A contained different concentrations of CuSO4, NaOH in distilled water. Solution B was an aqueous formaldehyde solution. The two solutions A and B were mixed in a 10:1 (v/v) ration

before the bat was used. The deposit copper were immersed the patterned substrate in a mixture of different times) at room temperature. All the samples were then examined by optical microscope and profilometer. Table 4.2and Table 4.3 show changes of growth rate and surface roughness of grown copper onto printed silver seeds using different combination of these two agents, respectively.

Table 4.2 Growth rate (nm/min) of deposited copper using bath with different concentrations

EDTA(g/L) TEA(mL/L)	0	6	12	18	24	30
0		192.8	185.3	182.0	179.6	128.6
12	311.0	233.0	192.5	194.4	191.2	132.6
18	334.5	224.0	191.1	197.7	183.7	155.1
24	447.1	257.	225.2	209.8	205.2	136.2
30	484.2	318.7	278.3	263.9	222.0	138.4
36	408.6	405.4	410.7	317.3	240.6	137.7

Table 4.3 Standard deviation of thickness (μm) of deposited copper using bath with different

EDTA(g/L) TEA(mL/L)	0	6	12	18	24	30
0		2.246	1.870	1.889	1.826	0.451
12	2.996	2.121	2.188	2.219	1.760	0.615
18	3.400	2.607	2.093	2.194	1.700	0.885
24	3.801	2.787	2.284	2.450	1.693	0.837
30	4.368	3.740	3.113	2.546	1.860	1.346
36	4.625	3.686	3.643	2.277	2.386	1.260

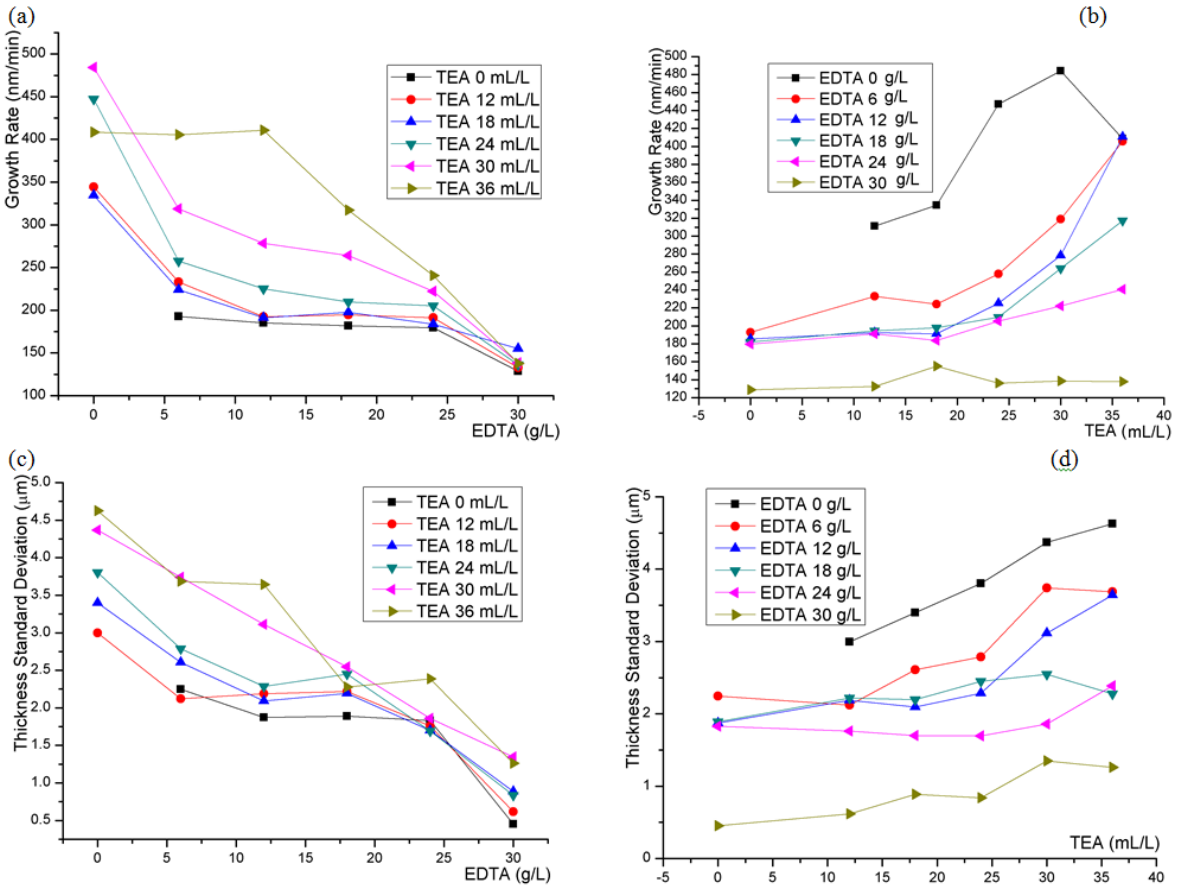

Figure 4.3 Growth rate changes due to different concentrations of EDTA and TEA: (a) Growth rate of copper with same EDTA concentration, (b) Growth rate of copper with the same concentration of TEA; Standard deviation of thickness (μm) changes due to different concentrations of EDTA and TEA: (c) Standard deviation with the same concentration of EDTA, (d) Standard deviation with the same concentration of TEA

Our plating bath contains two main chelating agents, TEA and EDTA, which are all able to chelate cupric copper ions. I first investigated the effect of these two chelating agents. The effects of EDTA and TEA on growth rate are shown in Figure 4.3 (a) and (b),

respectively. The effects of EDTA and TEA on surface roughness (reflected by standard deviation of thickness of deposited copper) are shown in Figure 4.3 (c) and (d), respectively.

The initial concentration of dual-chelating agent will affect the growth rate and overall reaction of copper growth. Electroless copper deposition continuously consumes copper ions while chelating agents remain in the bath, which changes from their initial status. The maximum thickness of metal features was between 2 μm and 17 μm, measured using profilometer. An average thickness d is calculated by averaging measurement from five different cross-section lines of each sample with a corresponding bath solution. Total copper growth area was calculated based on average thickness divided by total time which is 30 minutes. Growth rate R then can be calculated using the formula "$R=d/30$", where 30 minutes is the time used for copper growth.

As we can see from the Figure 4.3 (a), with the same concentration of TEA, the overall growth rate was decreased with increased concentration of EDTA. According to the figure, EDTA showed a negative affect with increasing concentration in terms of growth rate, because it is one of the strongest complexing agents of cupric ions. With increasing concentration of EDTA, dissociative cupric ions tended to complex form with Cu ions which affect formaldehyde oxidation and copper reduction. However, the overall standard deviation of thickness grown showed a decreased trend, which means surface roughness can be increased and the solution will be more stable with increased initial concentration of EDTA.

On the other hand, when the concentration of TEA reached 36 mL/L, the trend of curve became different from the other concentrations. We can also notice that with the same concentration of EDTA, the overall growth rate was increased with increased concentration

of TEA in Figure 4.3 (b). The plating rate of using TEA as a chelating agent showed a greater deposition rate than using EDTA. However, the plating solution converted to be unstable due to insufficient EDTA if only using TEA as complexing agents or with excess amount of TEA because of its weak ability for chelating, which resulted in an overall increased trend of standard deviation of thickness grown.

In this dual-chelating system, the existence of TEA can play a positive role for rate of copper deposition, while EDTA play a more significant role in terms of chelate and stabilize whole bath solution, affecting surface roughness. The adsorption of additives is a major effect on reducing plating rate as indicated. The actual values for reaction depend on experimental conditions and they are related to initial concentration of TEA as well in this dual-chelating system. In fabrication process, it is essential to figure out optimal initial concentration of these two agents in order to get optimal results for specific occasions. As shown in Figure 4.3, when concentration of TEA were 12 mL/L, 18 mL/L, and 24 mL/L and concentration of EDTA were 12 g/L and 18 g/L, there wasn't a distinct difference in terms of growth rate and standard deviation of thickness grown. For copper deposition onto silver nano particles, on the following section, I employed 12 g/L EDTA and 24 mL/L TEA in our bath in order to get a stable solution with both relative higher deposition rate and more stable solution reaction intensity. The effects of temperature and time in the fabrication process were discussed in the following section.

4.2.2 Effect of temperature and time on copper growth

The effect of temperature on copper deposition rate is shown in Figure 4.4 (a). As we can see from Figure 4.4 (a), we observe that temperature has a strong effect on deposition

rate. Deposition rate increases with increasing deposition temperature. The deposition rate at 65^0C was abnormal because adhesion force between metal filaments and substrate was not strong enough at this temperature. When samples were immersed into solution at 65 ^{0}C, metal filaments were partially peeled off and folded resulting in measurement error. With increasing temperature, peeling off problem will seriously affect final quality of samples. By balancing higher growth rate and good adhesion, a temperature of 35 ^{0}C was employed in the following section.

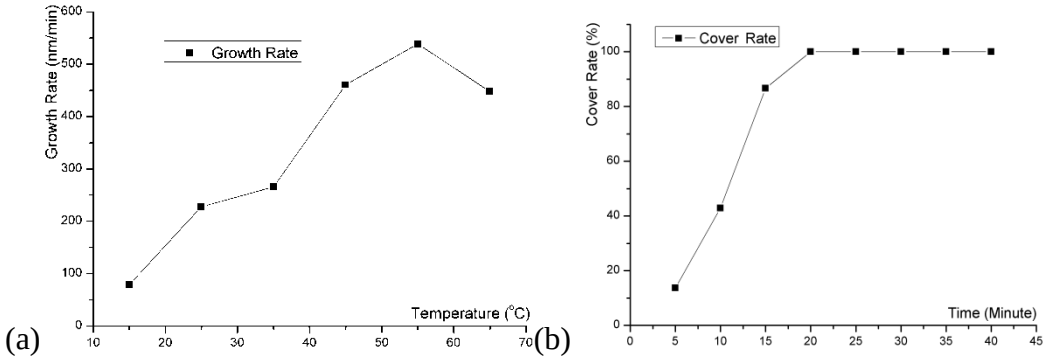

Figure 4.4 (a) Growth rate of copper using 24 mL/L TEA, 12 g/L EDTA for 30 minutes at 15^0C, 25^0C, 35^0C, 45^0C, 55^0C and 65^0C; (b) Cover rate of copper using 24mL/L TEA, 12g/L EDTA at 35C for 5, 10, 15, 20, 25, 30, 35 and 40 minutes

The plating time to achieve a certain film thickness depended on proportion of solution, and type of substrate. Figure 4.5 shows microscope pictures of copper growth on printed silver filaments with partially covered (a) and total covered (b) structures. With enough time for copper to grow, they will finally totally cover the whole printed silver surface. Substrates were immersed for 5 to 40 minutes with 5 minutes intervals, extracted,

rinsed in deionized water and dried at room temperature. Total copper growth area was calculated based on microscopic pictures using 50 μm grids to divide samples into small areas. If copper coverage is greater than half area of the cell, it will be counted as total cover of the cell. We were capable of calculating total area copper covered area as A and total filament area as A_0. The total cover rate is calculated by A/A_0. As we can see from Figure 4.5 (b), the overall reaction become very vigorous after about 10 minutes and will gradually reach a relative steady state after 15 to 20 minutes. To make sure that copper deposition will fully covered printed silver seeds, we will immerse samples in solution for at least 20 minutes in the following experiments.

(a) 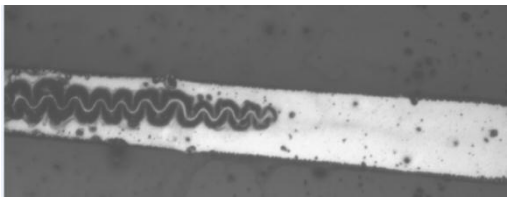 (b) 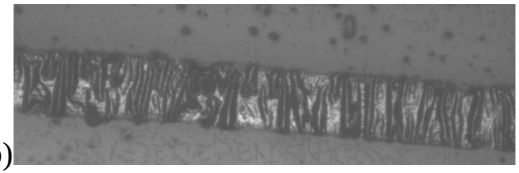

Figure 4.5 Microscope pictures of copper growth on printed silver filaments

4.2.3 Topography analysis and electrical characterization

Possible defects in the copper structures are because the ambient laboratory conditions, where dust and other contaminants from atmospheric and plating solution can lead to defects. The edge resolution of structures is determined by size of copper grains.

The resistance was measured with the help of an ohmmeter (Fluke 115) by contacting two probes on conductive tracks. Five measurements were taken at each sample at five

different locations and then averaged. The electrical resistivity ρ of the printed silver patterns was calculated by using the formula "$\rho=R\cdot A/L$", where "R" is the resistance of the pattern measured, "A" is cross section area of the printed pattern and "L" is the length between the two measuring points. The cross section A of the silver tracks was calculated using equation "$A= w \times t$", where "w" is the width of silver tracks and "t" is the average thickness of the tracks, measured through profilometer.

As for the printed silver filaments, these filaments have to be cured first in order to obtain high conductivity [92]. Silver tracks were cured at 200^0C for 20 minutes and then measured using two point method. The printed silver filaments have a minimum resistivity of 5.1 μΩ·cm under a curing temperature at 200 ºC, which is about 3.16 times that of bulk silver (1.587 μΩ·cm). The average thickness of printed silver tracks was 524nm.

However, as for flexible electronic fabrication techniques, 200^0C have already exceeded critical value of polymer-based substrates. That is a huge advantage if we can apply electroless copper deposition into the fabrication process to avoid curing of silver nanoparticles. The thickness and area of cross section of metal filaments will also be increased, resulting in lower resistor value and lower power consumption. The average resistivity of copper lines with two point method was measured to be 6.8 μΩ·cm. The value is about four times bulk copper (1.678 μΩ·cm) or bulk silver.

Possible defects in the copper structures are because the ambient laboratory conditions, where dust and other contaminants from atmospheric and plating solution can lead to defects. The edge resolution of structures is determined by size of copper grains. There might be voids inside the metal structures that increase the resistivity.

4.2.4 Printed patterns with silver core and copper shell

Our plating bath contains two main chelating agents, TEA and EDTA, which are all able to chelate cupric copper ions. I investigated the effect of these two chelating agents. The initial concentration of dual-chelating agent will affect the growth rate and overall reaction of copper growth. The calibration of different variables and how they affect copper growth rate and cover rate were demonstrated in the previous chapter. Electroless copper deposition continuously consumes copper ions while chelating agents remain in the bath, which changes from their initial status.

I immersed cured silver patterns in solution with 24 mL/L TEA, 12 g/L EDTA for 30 minutes at 35^0C. The maximum thickness of metal features was between 2 μm and 15 μm, measured using profilometer. The thickness of the patterns was increased from original value around 250 nm of printed silver seed layer to 2-15 μm after copper deposition, about 10 times thinker. The average resistivity of copper lines with two point method was measured to be 6.8 μΩ·cm, similar to printed silver patterns after curing process. The value is about four times bulk copper (1.678 μΩ·cm) or bulk silver, which may come from the possible defects of the deposited copper layer. These defects in the copper structures are because the ambient laboratory conditions, where dust and other contaminants from atmospheric and plating solution can lead to defects. The edge resolutions of structures are determined by size of copper grains. There might be voids inside the metal structures that increase the resistivity.

For ultra large scale integration (ULSI), increasing current density is essential because improvement in interconnect time delay will offer significant improvements in the speed of the system. The time delay for an interconnect means the time for the voltage at one

end of a metal line to come to 63% of its final value when an input is applied at the other end of the line. The delay time of an optimized interconnect line with length L is proportional to its resistance *R*. As I mentioned in previous section, the resistance of printed pattern can be calculated using formula "$R = \rho \times L / A$, and $A = w \times t$ ". For a pattern with length of *L* and width *w*, the corresponding resistance *R* will be reduced 10 times if thickness t is increased 10 times. As a result, it has the ability to drive higher current and consume lower power.

Figure 4.6 shows microscope pictures of microstructure of copper deposited on polyester (PET) film. Copper microstructures produced by combination of e-jet printing and electroless copper deposition on PET film were successfully fabricated. The average line width of printed features is around 20 μm on PET film. Figure 4.6 (a) shows microscopic pictures of part of silver patterns printed by e-jet printing with line width around 20 μm, followed by copper deposition as shown in Figure 4.6 (b). It is clear from Figure 4.6 (b) that copper is successfully grown on silver seeds.

(a) (b)

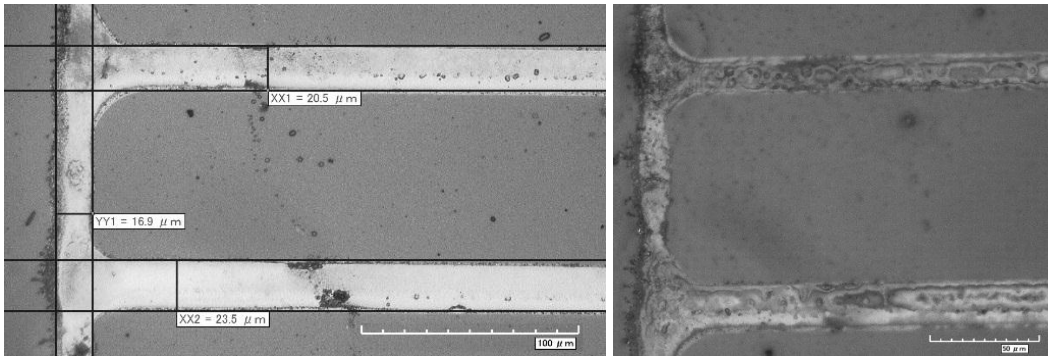

Figure 4.6 High resolution conductive filaments matrix (a) printed by e-jet printing, and (b) after copper deposition. The thickness of printed patterns was increased from original around 250 nm silver seeds to 2-15 μm with copper covered

As for the printed silver filaments without electroless copper deposition, these filaments have to be cured first in order to obtain high conductivity [92].As I mentioned earlier, silver tracks were cured at 200^0C for 20 minutes and then measured using two point methods. However, as for flexible electronic fabrication techniques, 200^0C have already exceeded critical value of polymer-based substrates. That is a huge advantage if we can apply electroless copper deposition into the fabrication process to avoid curing of silver nanoparticles.

4.3 Summary

In this chapter, the research examined how different concentration of chelating agents, temperature and time affect deposition rate and fabrication efficiency, thus providing basis for some predictions and tendencies. EDTA showed strong complexing ability to cupric ions, but played a negative role for deposition rate. TEA in the bath will help to balance the increased deposition rate and solution stability. Temperature in the solution will significantly affect deposition rate. With increased temperature, an obvious increase in deposition rate was observed. However, an increased temperature will result in peeling off problems between metal and substrate. Results in this study provided a valuable reference for electroless copper deposition recipe for specific applications in flexible electronics. Copper deposition was successfully applied on printed silver seeds to increase thickness of patterns up to 15μm with conductivity about four times bulk copper. Microstructures on PET film were also fabricated and reported.

Base on Chapter 3 and Chapter 4, I have demonstrated the new method of patterning surfaces with catalyst for selective deposition of copper. E-jet printing of silver seeds with

customized patterns delivers the catalysts to pretreated substrate surface. It is capable of generating metal structures with submicron dimensions. The technique is flexible to be used on different substrates such as polymers and glass, both planar and curved surfaces. Copper can be patterned using electroless deposition combined with e-jet printing for fabrication of printed wiring boards. The approach consists of directly writing a silver seed layer with subsequent step of electroless copper plating to increase thickness and conductivity. Thickness issues for e-jet printing are successfully resolved in the proposed process. In the follow chapter, rapid prototyping of an array of capacitive sensor based on the fabrication technique was discussed in the next chapter to test the concept in device and system integration level.

CHAPTER 5 DEVICE FABRICATION AND SYSTEM INTERGRATION

In Chapter 3, I demonstrated rapid prototyping of highly conductive micro patterns based on e-jet printing. To solve the thickness issues of printing technique and to improve conductivity of printed patterns, electroless copper deposition was applied on printed patterns to increase its cross section areas, as discussed in Chapter 4. Prototyping of microelectronic components based on the techniques I proposed needed to be fabricated to show the versatility and capability of the rapid prototyping methods. In Chapter 5, the rapid prototyping method was further investigated in device and system level. Capacitive sensors were fabricated onto PET film. An analytical model was developed to predict capacitive sensor characteristics for coplanar interdigitated structure, and experiments were conducted to study the effects of sensor design. Sensitivity of high-resolution capacitance sensor was investigated for droplet and humidity detection applications. The rapid prototyping method was proved to possibly make a significant impact in enabling simultaneously (1) customized and flexible touch sensors, (2) cost-effective manufacturing, and (3) high-resolution and good sensitivity. The techniques can be further used for on-demand fabrication of customized conductive patterns and components for flexible and wearable electronics.

5.1 Flexible electronics and capacitive sensor

Indium tin oxide (ITO) is the current industry standard material used as transparent conductor electrodes. ITO is a brittle ceramic material which makes it unsuitable for flexible electronics. ITO in most cases is fabricated through a vacuum deposition process. A most distinguishing feature of flexible electronics is the possibility to print or coat the device

directly onto thin flexible carrier substrates using roll-to-roll manufacturing or printing methods that enable simple handling and fast processing [97]. The ideal ITO replacement material should be a printable or coatable conductor material. There are groups that working on poly(3,4-ethylenedioxythiophene):poly(styrenesulfonate) (PEDOT:PSS) [98-100], the only available material that is remarkably transparent that may replace ITO for flexible electronics. The resistivity of PEDOT: PSS is 5-12 Ω μm [101, 102] (compared to bulk silver with a resistivity of 0.0159 Ω μm). The conductivity of PEDOT: PSS is too low to enable large area electrode arrays. Nanowires and other forms of metal meshes have emerged as ITO replacement materials. On one hand, they offer benefits for large-area flexible displays where conductivity and flexibility of ITO on plastic substrates is an issue. On the other hand, the overall manufacturing cost can be reduced as they all have flexibility in printing or coating.

Capacitive sensing represents the second most widely used sensing method. Touch activity is identified by detecting minor changes in electrical charge generated by the contact with an object. Substrates for capacitive touch sensors may be glass or flexible polymers, or combination of them [19]. The sensors are usually constructed as narrow strips of conductors. Interdigitated electrodes are among the most commonly used sensor structures. The change in capacitance caused by proximity of a finger near an intersection is 1pF or less, and the effect on adjacent electrode may be less than 0.1 pF [20]. Analysis of capacitance changes at or near intersections of electrode reports the touch action if change in capacitance exceeds the system threshold. Capacitive sensors show excellent sensitivity, and are unaffected by

most contaminations. These advantages have provided particularly attractive options for them to be applied into next generation flexible electronics and in microfluidic devices [103].

Capacitive structures have been broadly used in electronics covering applications from touch detection to energy storage and humidity sensing. The most common structures are planner parallel plate and interdigitated electrodes. Planner parallel plate is characterized by simplicity of geometry and ease of modeling and calculation. Interdigitated electrodes present more interesting features, e.g. control of signal strength easily by design dimensions, multifunction detection including electric or acoustic features. All these two structures can be fabricated with multiple materials and by different manufacturing processes, from integration in wafers to printing on flexible substrates.

The challenge for modern flexible electronics is to find new solutions for producing large area electronic with full mechanical and electrical functions while reducing costs. Many research groups are working on alternative fabrication method to replace conventional process such as photolithography and vacuum deposition while meeting high-performance, resolution, manufacturing needs and cost requirements. Among them, additive printing shows its potential to be the best fabrication process for flexible devices in prototyping domain. It can be scaled to very large areas with full microelectronic function. Additive printing is a noncontact jet printing process that is capable of fabricating both silicon based and polymeric based TFTs and electronic components. By incorporating it with roll-to-roll fabrication, additive printing can help to reduce process and material cost for flexible electronic fabrication. Feature resolution of traditional inkjet printing is limited by the size of droplets, which is typically above 30 μm.

There are still plenty of challenges before inkjet printing can be applied for rapid prototyping of electronic components for flexible electronics. First, most of complex, multi-functional metal or alloy inks have to be characterized before they can be adapted into real applications. Second, there are resolution issues with current inkjet printing methods, and the electrical performance of printed patterns needs to be investigated.

In this chapter, the focus was at device and system integration level to test products from e-jet printing on underlying of structure of electrodes, materials, and fabrication process. The capacitance sensor design, sensitivity, and electrical performance on flexible substrates were investigated in the study. Integrated capacitance sensors using additive e-jet printing with conductive silver nano-ink was fabricated and tested. With the help of e-jet printing, sub-20μm features can be on-demand printed on PET film. The presented prototyping amd fabrication method can be adapted into rapid prototyping of touch pads or micro fluid detecting sensors in micro scale. The interdigitated design maximizes the capacitive signals for sensor applications in 2D domain. The over-all performance was characterized using an RC relaxation oscillator circuit. The analysis of electrical performance of parallel coplanar patterns and high-resolution pattern was conducted to test electrical properties of direct printed patterns.

The results of experimental tests confirmed that capacitive sensors fabricated by the proposed additive e-jet printing could be effective for sensor applications. The sensors exhibited great stretchability, high sensitivity, and fast response time. Both high resolution and electrical properties were achieved in the work. The proposed fabrication technique is

capable of rapid prototyping of electronic components for flexible electronic, medical sensors, wearable devices, and radio frequency identification devices.

5.2 Capacitive touch sensor

Projected capacitive technology is a technology based on capacitive coupling effect, which can detect anything that is conductive or has different dielectric effects from air [21]. The technology has been widely used in modern touch screens. A basic construction of a typical projected capacitive touch screen includes a top layer touch surface (chemically strengthened cover glass with holes and slots cut into it), optical bonding adhesives, touch sensor arrays (usually a glass separator with indium tin oxide deposited on both sides), and the bottom LED/LCD screen [12], as shown in Figure 5.1. Projected capacitive technology provides advantages such as multi-touch detection, excellent optical properties, and long life. Projected capacitive touch sensors are easy to integrate into systems to eliminate coordinate drift [22]. Projected capacitive touch sensors can be adapted into both glass and plastic, and flat and curved surface. Most touch applications are immune to chemical attacks and extreme temperatures because sensors are usually sealed by the protection layers.

For traditional optoelectronic touch devices with top layer glass surface, capacitive touch sensor arrays, ad bottom LED/LCD screen, the dielectric strength and thickness of cover glass plays an important role on sensitivity of projected capacitive touch screen. A thinner cover glass and higher dielectric constant will have better performance. However, for flexible electronics, polymers usually have a lower dielectric constant; thus, it has to be thicker than glass to achieve the same performance. One of the most common used cover materials is PET film.

A simple capacitive touch sensor that has been used on touch displays is shown in Figure 5.1. As we can see, the touch sensors consist of rows of ITO electrodes on one side of separator and columns on the other side. The common materials that currently used for micro electrodes usually are ITO. However, ITO is fragile and indium is scarce resource on earth. Researchers have been tried to find out other materials to replace ITO electrodes and metal has shown its advantages. It would be a great idea if I can adapt the proposed rapid prototyping method for the fabrication of touch sensor array as a replacement of traditional ITO microelectrodes for touch screen applications.

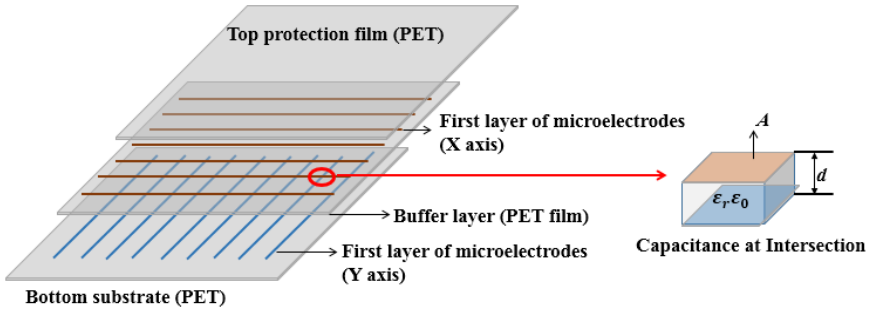

Figure 5.1 Schematic of structures in projected capacitive touch screens: row and column stack up layers

The electrodes are active conductive elements of the sensor. Many electrode patterns can be used to create projected capacitive sensor. The electrode pattern geometries are an important factor in sensitivity and resolution of the sensor. For the projected capacitive touch sensor pattern shown in Figure 5.1, The touch sensor arrays are “scanned” in working conditions. Each individual electrode or electrode intersection is measured one-by-one. In a

typical scanning for touch sensor arrays, the controller will drive a single column (Y) and then scan every row (X) that intersects with the column. The capacitance value at each X-Y intersection will be measured and compared with initial values to determine location of objects [104]. The process is repeated for every column until the entire pattern is scanned. The columns and rows of touch displays are physically fixed. Since each intersection is responsible for a small area. The capacitive touch sensors are more precise than any other methods. The development of capacitive touch displays has evolved since the past 10 years with patents and introduction of iPhone from Apple in 2007.

The actual functioning area is shown on the right in Figure 5.1. The active functioning components are the intersection areas. It can be modeled using the simple capacitor model:

$C = \frac{\varepsilon_r \varepsilon_0 A}{d}$, where C is the capacitance of intersection, ε_0 is permittivity of free space ($8.85* 10^{-12}\ F/m$), ε_r is the relative permittivity to space of filling material.

The value of capacitance is related to surface area of plates, distance between plates, and materials constant for insulating films. In this design, patterning ITO on glass with line widths of 20μm and resistivity of 2-6 Ω *μm is commonly accomplished using photolithography. Micro level metal wires (sub-20μm) can be a good substitute for sputtered ITO in most cases. When it comes to flexible electronics, e.g. pattern on flexible PET film, line width based on screen-printing or laser ablation are typically 100-200μm. There are increasing demands for developing new techniques to fabricate high-resolution capacitance sensors on flexible substrates with both good conductivity and sensitivity.

From 2D point of view, coplanar electrode arrays offer a compact design for capacitive touch sensors. The use of interdigitated electrode arrays also helps increase capacitive signals, which is perfect for ultra-small signal detections. Several research groups have been focused on interdigitated sensors consisting of metallic electrodes with uniform width [105]. Capacitive sensing is based on the contrast of dielectric property between different phases. In this chapter, several electrode designs were tested with a range of size, spacing, number of electrode, proximity of fingers, and curing temperature.

To maximize sensitivity for detection, an effective sensor design and fabrication method was required. The capacitance sensor with single pair of interdigitated electrodes was shown in Figure 5.2. Chen et al. analyzed droplets detection using coplanar capacitance sensors assuming droplets were in direct contact with electrodes [106]. In my case, there was a protecting polypropylene film outside electrodes for protection of electrodes from contaminations. The thickness of polypropylene film was about 40 μm. It was desired to take this into consideration when developing an analytical model of detection.

Chen et al. [106] applied conformal mapping techniques, and calculated capacitance created by a single pair of coplanar electrodes in semi-infinite domain with same liquid cover as:

$$C = \frac{Q}{2V_0} = \frac{2\varepsilon_r \varepsilon_0 l}{\pi} ln\left\{\left(1 + \frac{w}{a}\right) + \sqrt{\left(1 + \frac{w}{a}\right)^2 - 1}\right\} \quad (1)$$

where C is the capacitance, ε_r is dielectric constant, ε_0 is the electric constant, l is the length of the electrodes, w is the width of electrodes, a is half-gap between electrodes.

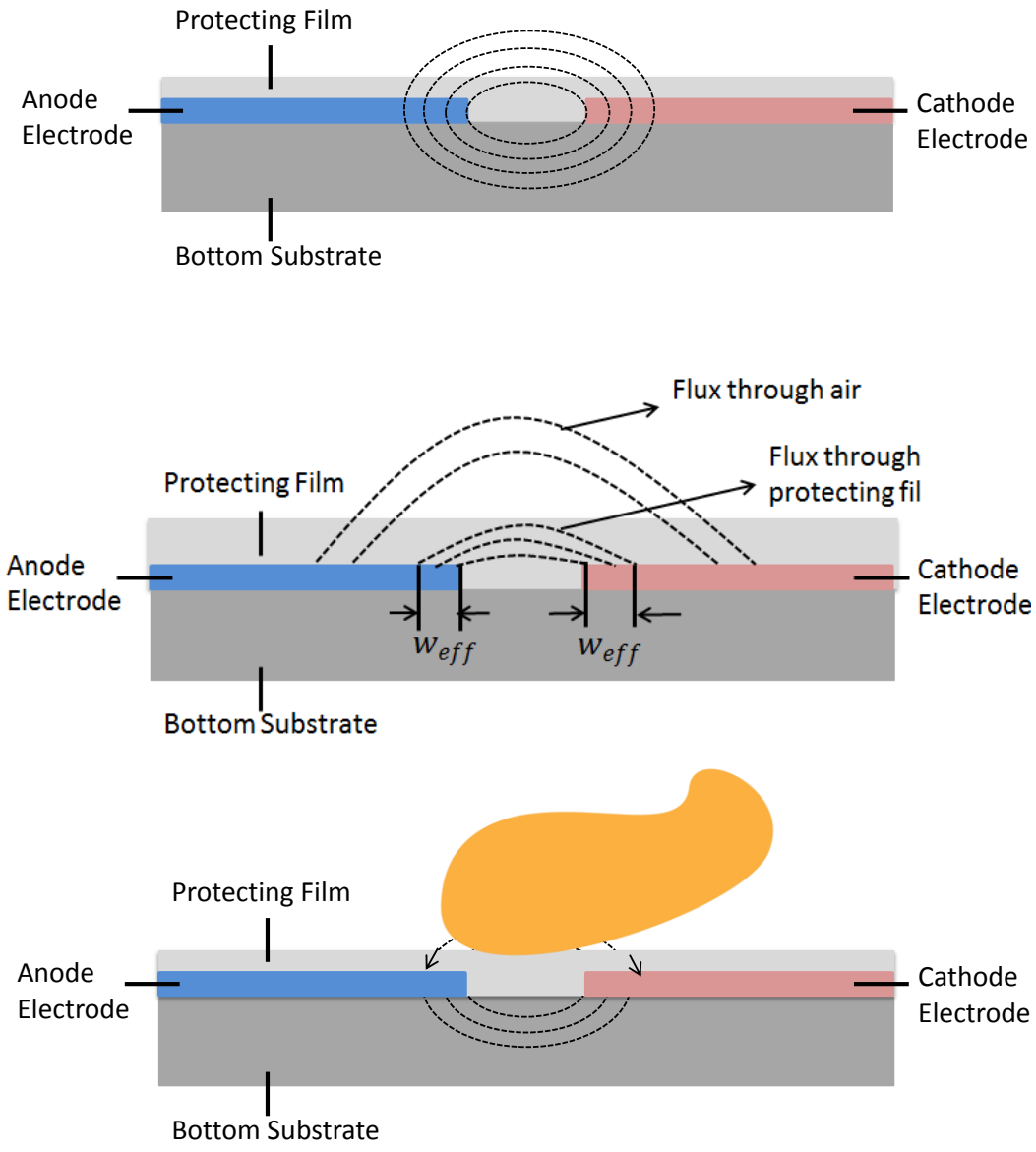

Figure 5.2 Working principle of capacitors with single coplanar electrode

The equation was valid in the limit of *w/a>>1*. Based on simulation, the ratio *w/a=1.1* produces a deviation from the semi-infinite model approximately 10.4%. The approximation was reduced to about 0.2% for *w/a =1000*. In real fabrication, *w/a=1* was

adapted in the research. A 10.4% compensation in terms of capacitance calculation was used in the research. From Equation (1), the relation suggested that the maximum capacitive signal can be achieved by minimizing electrode gap spacing. The protecting layer, which was polypropylene film, has ε_r=2.2-2.36. The field lines passing through the cover do not contribute to changes in capacitance detected by sensor. There must be an effective electrodes width in the design that generated electrical flux only coming through protecting films. The model was proposed as following:

$$w_{eff} = a\left(\sqrt{1+\left(\frac{w}{a}\right)^2}-1\right) \tag{2}$$

In the model, the capacitance must be calculated considering the effect of protecting layer. The total capacitance from single pair of coplanar electrodes can be formulated as follows:

$$C_{air} = \frac{Q}{2V_0} = \frac{2\varepsilon_{air}\varepsilon_0 l}{\pi} ln\left\{\left(1+\frac{w}{a}\right)+\sqrt{\left(1+\frac{w}{a}\right)^2-1}\right\} \tag{3}$$

$$C_{film} = \frac{2\varepsilon_{film}\varepsilon_0 l}{\pi} ln\left\{\left(1+\frac{w_{eff}}{a}\right)+\sqrt{\left(1+\frac{w_{eff}}{a}\right)^2-1}\right\} \tag{4}$$

The effective width w_{eff} was calculated by Equation (2). Using Equations (3) and (4), the capacitance was found as follows:

$$C = C_{air} + C_{film} \tag{5}$$

With our design as shown in Figure 5.2, assuming the number of electrodes for single polarity was *N*, the total pairs of coplanar electrodes can be considered as *2N-1*. So the total capacitance of printed coplanar electrodes can be estimated as:

$$C_{total} = (2N-1) * C \tag{6}$$

As shown in Figure 5.2, when a finger touches the sensor, the finger functions as a media (ground electrodes) for the system, and modifies the electrical field around the sensor to decrease total capacitance. Assuming there was an intrinsic frequency of any conducting objects, the system can be modeled as a coplanar capacitance in parallel with finger capacitance. The actual effect from the finger was difficult to model because of variability in electrical properties of human fingers, which may also vary with personal conditions for an individual [107]. As a result, I considered the properties of a finger as a purely dielectric material with relative permittivity to be 60 [108].

5.3 Materials and fabrication process

As shown in Figure 5.3, the direct e-jet printing system developed at the lab was used following previous research results. The e-jet printing system consisted of a three-axis stage, a dispensing system with pressure regulator, nozzle, and substrate. The three-axis stage can be programmed to provide relative displacement in X-Y directions between substrates and nozzle, simultaneously controlling plotting speed of nozzle and trajectory of tracks. Note that the fabrication process was capable of on demand printing multi-layers on substrate by programming the movement of the 3-axis stage.

Following preliminary results from previous chapters, I used silver nanoink for e-jet printing of capacitive sensors. The silver nanoink was from Advanced Nano Products Co., Ltd. It is composed of silver nanoparticles with 20-35% in weight, triethylene glycol with 65-80% in weight, and other small amounts of surfactants and lubricants to prevent agglomeration of nanoparticles. Silver nanoparticles have diameters below 50 nm, and they were uniformly dispersed in the solvent. The viscosity was 10-18 cP and surface tension was

35-38 dyn/cm. Highly insulating polyethylene terephthalate (PET) films were used as substrates in the experiments. PET films are widely used for high density circuit, electronic packaging and flexible electronics.

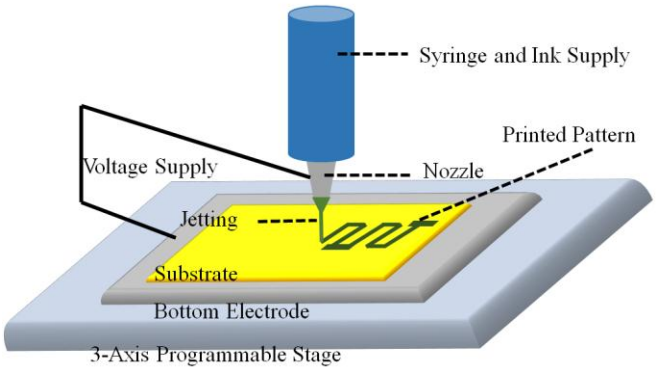

Figure 5.3 - Fabrication platform for E-jet printing

In my previous research published in [93, 109, 110] and discussion from previous chapters, I have demonstrated applying electrohydrodynamic inkjet printing (e-jet printing) to fabricate sub-20 μm conductive patterns on insulating substrates. In e-jet printing, I applied a voltage between nozzle and substrates. When the liquid was supplied to a sufficiently high electrical potential, the liquid at the tip of the nozzle formed a stable cone and emitted a jet on its summit. The technique that used electric fields instead of thermal or acoustic offered some advantages of patterning compared with other direct write technologies. The dimension of the jet generated by e-jet printing was much smaller than the dimension of the nozzle, thus improving the resolution of printed patterns.

In the chapter, three sets of experiments were conducted: (1) fabrication conditions and curing process, (2) investigation of capacitive touch sensor in large-area scale for flexible electronics, (3) investigation of high-resolution printing and performance of printed sensor array for droplet detection.

5.4 High-resolution printing and multi-layer printing

Figure 5.4(a) demonstrated the nozzle used in printing. The outside diameter at the tip of the nozzle was 20 μm. At steady state after ink was supplied to the nozzle, surface tension of the ink prevented droplet formation, as discussed in previous section. The applied voltage generated electric fields between nozzle and substrates. Once electrical force was greater than surface tension at the needle tip, droplets formed at the meniscus as shown in Figure 5.4(b). The dimensions of printed patterns were much smaller than dimensions of the nozzle. Based on voltage applied, the nozzle/droplet ratio was from 7 to 2. The testing pattern printed was shown in Figure 5.4 (c) and (d). The pads were 100 μm square for interconnector with outside circuits. The line width was 10um shown as single layer printing. The line length was 500 μm in Figure 5.4(c) and 3.5mm in Figure 5.4(d) to demonstrate ability of the technique in both small and large scale.

(a) (b) (c)

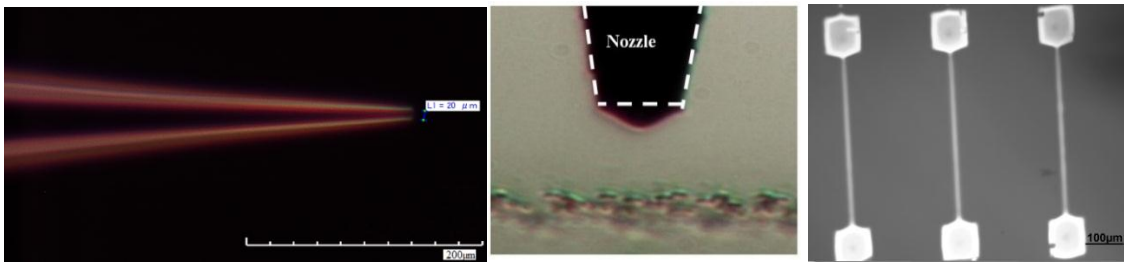

(d)

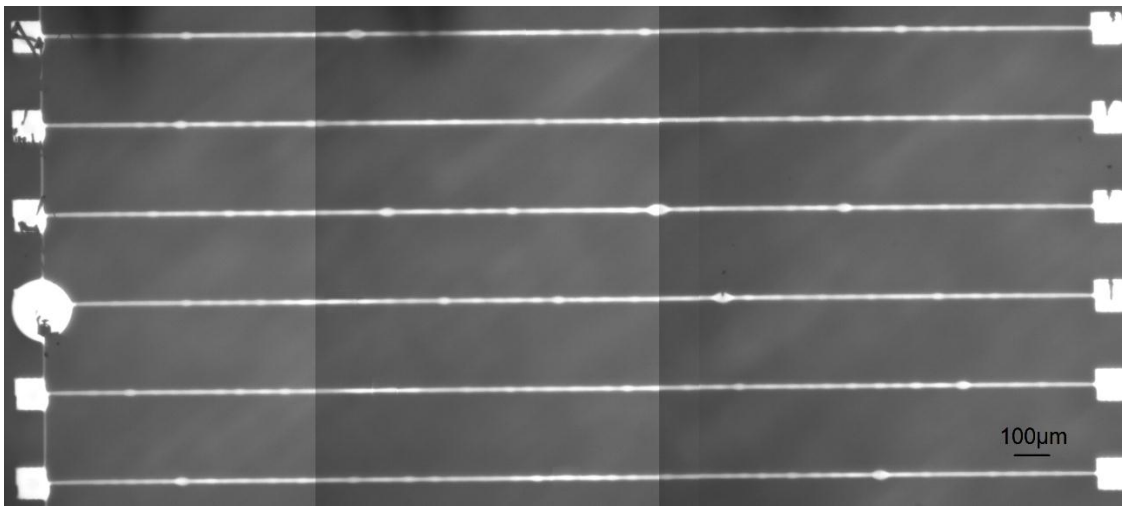

Figure 5.4 (a) Nozzle applied in e-jet printing, (b) Printing condition: meniscus formed at the tip of nozzle to overcome surface tension because of electrical force, (c) (d) printed patterns: 100 μm square pads, 10 μm line width.

The conductivity of single layer printing wasn't high enough for sensor applications. There were two reasons for this insulating phenomenon. First, single layer printing only generated line thickness of 45nm. The nanoparticles in silver ink has a diameter of 30-50nm, indicating there was only single particle layer printed on substrate, as shown in Figure 5.5 (a)

and (b). There were inevitable voids between particles resulting in poor connectivity and conductivity. Second, the ink consisted of lubricants to avoid particles agglomeration. The nanoparticles also have polymer shells outside. Most of lubricants and polymers inside the ink needed to be removed by curing process. In the experiments, the printed pattern on PET film were cured at 100 ℃ for 12 hours before testing to ensure silver particles can form grain boundaries and good conductivity. From the table, the resistivity of printed silver patterns was 9.48*10-2 Ω ·μm, around 6 times bulk silver. The line width and thickness of printed silver pattern were both reduced during curing process because of shrinkage, as shown in Figure 5.5 (b) and (c). The reason was that polymers and lubricant were removed, and voids between silver nanoparticles were removed to form grain boundaries.

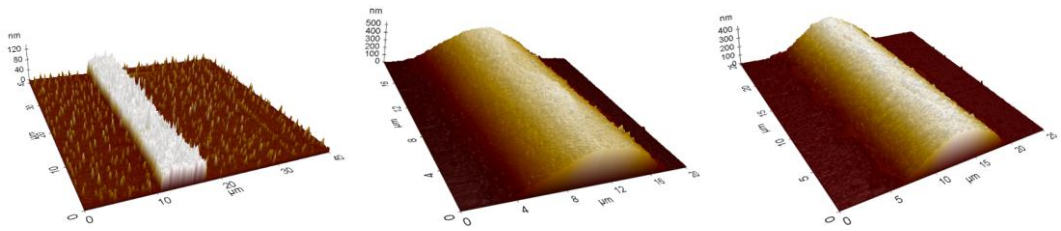

Figure 5.5 (a) Single-layer printing, (b) 30-layer printing before curing, (c) 30-layer printing after curing

Applying a 400 V AC voltage with frequency of 1kHz, the nozzle diameter was 20 μm. The comparison charts was shown in Table 5-1. By setting up voltage amplitude, frequency, plotting speeds, height between nozzle and substrates, and curing temperature and time, high resolution pattern with conductivity similar to bulk silver and better than ITO film

can be achieved. For the following printing process, over-lapping printing and multi-layer printing were applied for both large-scale fabrication and high-resolution device testing.

	Before Curing			**After Curing**		
	Width μm	Thickness nm	Resistivity Ω* μm	Width μm	Thickness nm	Resistivity Ω* μm
Single-layer	8.621	45.113	N/A	N/A	N/A	N/A
30-layer	14.728	364.325	N/A	13.949	274.556	$9.48*10^{-2}$

Table 5-1 Comparison charts of single-layer printing vs 30-layer printing, before and after curing process

5.5 Sensor test circuit layout

Capacitive touch sensor is a transducer with a touch responsive surface that interacts with electrical signals. It is desirable for the touch sensor to be flexible and provides enough sensitivity to touch. A detector (Arduino Nano ATmega 328) is controlled by microprocessor, providing excitation signals for the sensor and receiving signals from the sensor in response to a touch, converting the received signal into the presence of the touch and communicated with system.

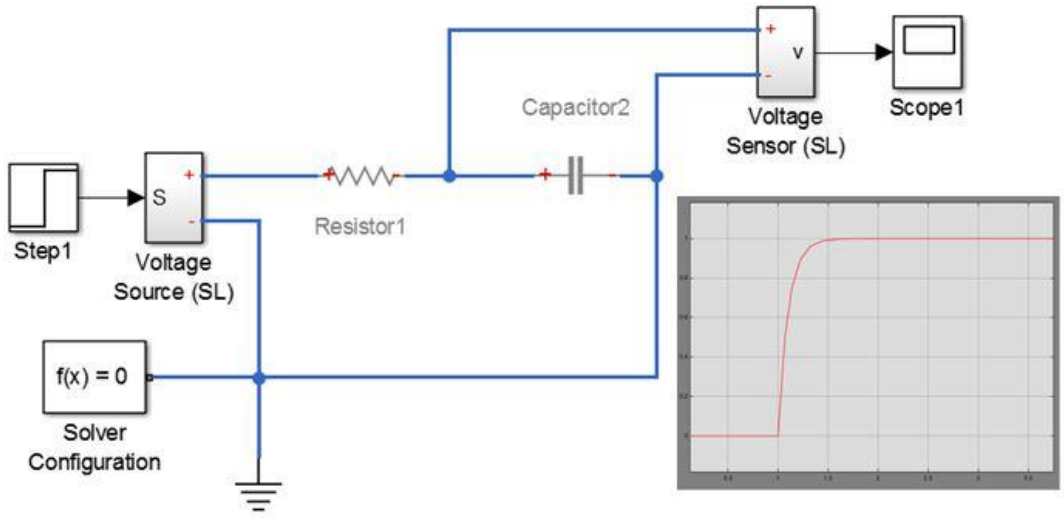

Figure 5.6 - Schematic of capacitive touch sensor test system.

Figure 5.6 demonstrated sensor circuit layout as an RC-delay circuit. The touch sensor can be represented as capacitance *C* cascaded with a high-value 80MΩ resistor *R*, and a signal generator. The microchip was used to send signals to electrodes and extract time delay signal from the capacitor. The time constant was defined as the time for the voltage to be raised to *1-1/e*, or 63.21% of the maximum value. The applied signal was shown to the right of the circuits.

Based on Kirchhoff's current law, the capacitance of a printed touch sensor can be calculated as:

$$C * \frac{dv}{dt} + \frac{V}{R} = 0 \tag{7}$$

$$V_c(t) = V(1 - e^{-\frac{t}{RC}}) \tag{8}$$

$$C_{sensor} = \frac{\tau}{R} \tag{9}$$

where C is the capacitance, R=80MΩ, τ is the time for the voltage to be 63.21% of the maximum value of input voltage.

5.6 Large scale fabrication and testing

Figure 5.7 showed a schematic view of the touch sensor structure design used for large-area scale flexible electronics in 2D scale. The coplanar interdigitated design was a common design to maximize capacitance for the structure. The design variables included the number of electrodes, electrode length, and electrode distance. The output parameter was capacitance of printed coplanar capacitance touch sensors. A high-resolution prototyping of microelectrodes array on flexible substrate in a multi-layer structure was demonstrated and tested in the last section to demonstrate the versatility and capability of rapid prototyping using e-jet printing.

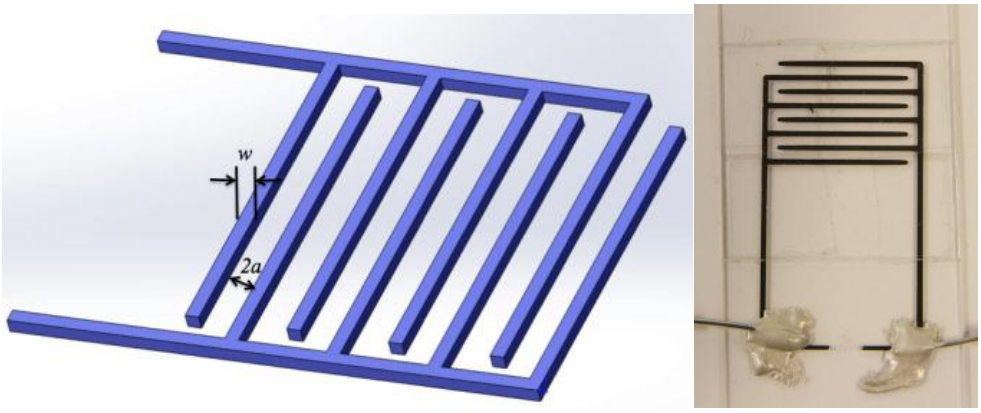

Figure 5.7 - Schematic view of touch sensor structure, and the patterns printed in the lab setup

The touch sensors were printed by e-jet printing applying a AC voltage of 100V and 500Hz on PET film. Multi-layer and overlapping printing was adapted to achieve a line width of 300 μm. In this study. The experiments were conducted as follows:

(1) To study the effect of electrode numbers on touch sensor capacitances, the length of each electrodes were printed as l=10mm, the distance between two adjacent same polarity were printed as $4a$=1.5mm, the number of printed electrodes of the same polarity N are 2, 3, 4, 5, and 6.

(2) To study the effect of the length of electrodes on touch sensor capacitances, the number of electrodes N was set as 4, the distance $4a$ was set as 1.5mm, and length l was printed as 5mm, 7.5mm, 10mm, 12.5 mm and 1.5mm.

(3) To study the effect of the distance on touch sensor capacitance, the number of electrode N was set as 4, length l is set as 10mm, and distance $4a$ is printed as 1 mm, 1.25mm, 1.5mm, 1.75mm and 2mm.

(4) To study the sensitivity of printed touch sensor, one set of electrodes was printed with the number of electrodes N set as 4, length l set as 10mm, and distance $4a$ set as 1mm. The time constant was measured before and after a finger touched on the sensor.

4.3.1 Effect of number of electrodes on capacitance

The effect of number of electrodes on touch sensor capacitance was investigated in the study. As shown in Figure 5.8, the capacitance of printed sensor was increased with increased active number of electrodes. The calculated results based on the model in previous section were the dotted line in the figure. The results indicated the overall trending and value of printed touch sensor matched the proposed model.

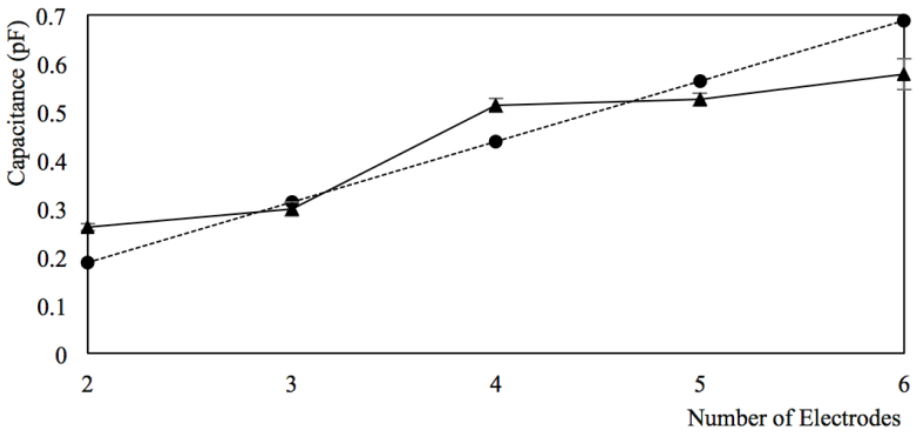

Figure 5.8 - Effect of number of electrodes on touch sensor capacitance

The capacitance of a coplanar comb-like touch sensor is proportional to the number of electrodes. As a result, for a fixed area, active greater number of electrodes will result in better electrical performance. That is the reason it is desirable to improve the resolution of printed electrodes. We can have more active number of electrodes on the touch area if we can further reduce the dimension of each electrode.

4.3.2 Effects of length on capacitance

In the study, I investigated the effect of length of electrodes on capacitance of printed touch sensor, as shown in Figure 5.9. The dashed line was the calculated value from our model. As we can see from the figure, with increased active length of printed electrodes, the capacitance was slight increased. In real applications, since most touch sensors are for human fingers, a touch pad usually comes with the size of 1 cm^2 that provides a good enough user experience. The electrodes inside each touch unit usually come with 10mm dimension. There

are also applications that require large-scale fabrication of electrode arrays, e.g. humidity sensors or RFID tags in a train or plane. In those cases, an increasing length of electrodes will results in a stronger capacitive signal.

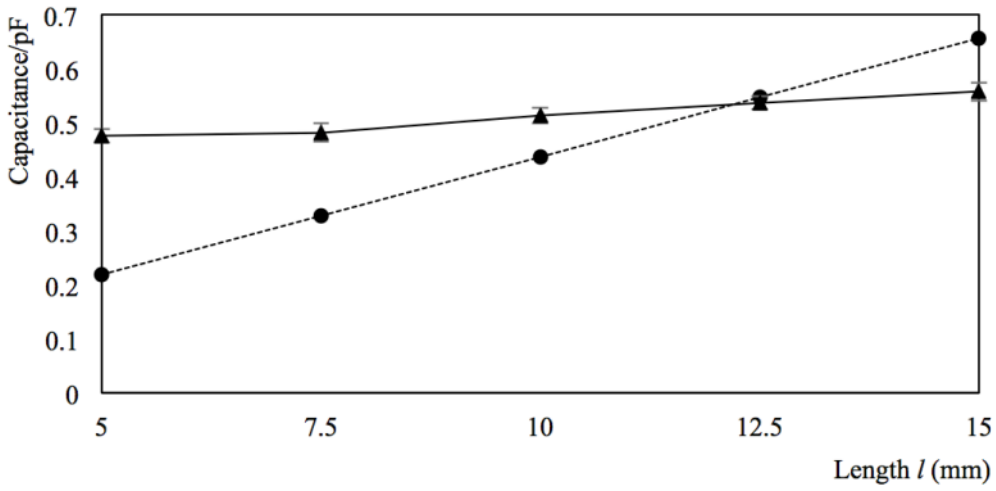

Figure 5.9 - Effect of length of electrodes on touch sensor capacitance

4.3.3 Effects of distance on capacitance

Figure 5.10 demonstrated the effect of distance between electrodes on touch sensor capacitance. The dashed line was calculated capacitance value based on our mathematical model. The experimental results matched the predicted value. With increased distance, the capacitance of printed patterns was decreased. This was due to the fact that with larger gap between adjacent electrodes, the coupling effect between them became weaker because air has much larger permittivity. The design of distances between functional components was extremely critical in RFID applications, where signal strength will determine final working distance of the product.

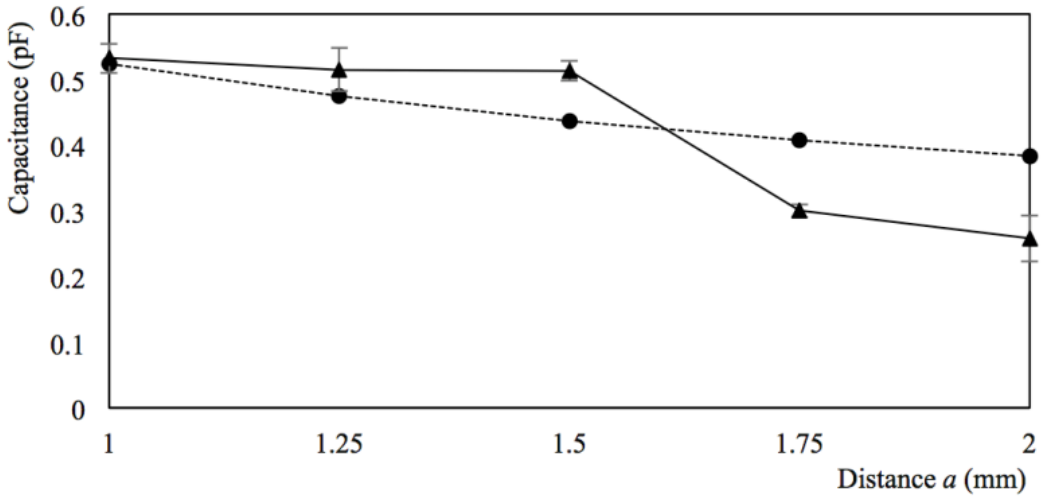

Figure 5.10 - Effect of distance between electrodes on touch sensor capacitance

4.3.4 Sensitivity with finger touch

I sampled the time constant with/without finger on the touch sensor to test its sensitivity for interaction with human fingers Figure 5.11 (a) showed response time with two finger touches and two without touches in 200 sampling points. As we can see, there was significant difference with or without finger on the touch sensor in terms of response time. The touch response can be further applied into electrical system design and circuit design. My proposed touch sensor can be further applied into touch screens and medical devices applications.

Figure 5.11 (b) revealed the capacitance changes with finger approaching the sensor from 10cm away until touching the sensor to investigate the effect of interacting between finger and distance. As we can see from the figure, a shorter distance and contacting led to an obvious change in capacitance because of interception of electric field due to finger

approaching. There was a slightly capacitance disturbance after finger left the sensor in my setups. The reason was that forces from finger touch were inevitable that deflected flexible sensors. The distance between top and bottom electrodes was reduced due to touching force. The presentence of finger dominated capacitance decrease by disturbing electric field. It also revealed that e-jet printing may be further applied into stress sensor applications. In my case, the capacitance sensor demonstrated its advantages that it can detect objects as long as they are in proximity within a certain range.

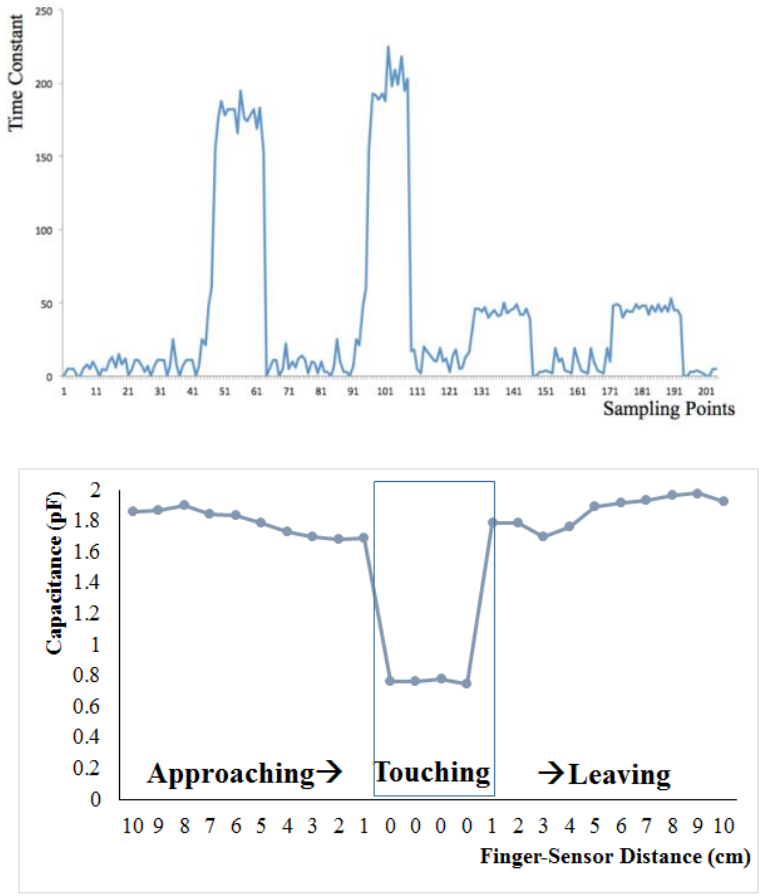

Figure 5.11 (a) Response time with finger touch/not touch the sensor, (b) Capacitance change due to proximity of finger with distance from 10cm to contacting

5.7 High-resolution capacitance pattern for droplet detection

Figure 5.1 demonstrated one type of commercial layout for touch display and touch sensor applications. The multi-layer structure of capacitive sensor was fabricated and tested in the research. A schematic view of the prototype was demonstrated in Figure 5.12 (a) and (b). The micro electrode layer in horizontal direction was first printed on bottom PET film. The printed electrode was covered by the second layer of PET film Another layer of micro electrode was printed on to the second layer PET film in perpendicular direction. The whole pattern was covered by the third layer of PET film for protection purpose.

(a) (b) (c)

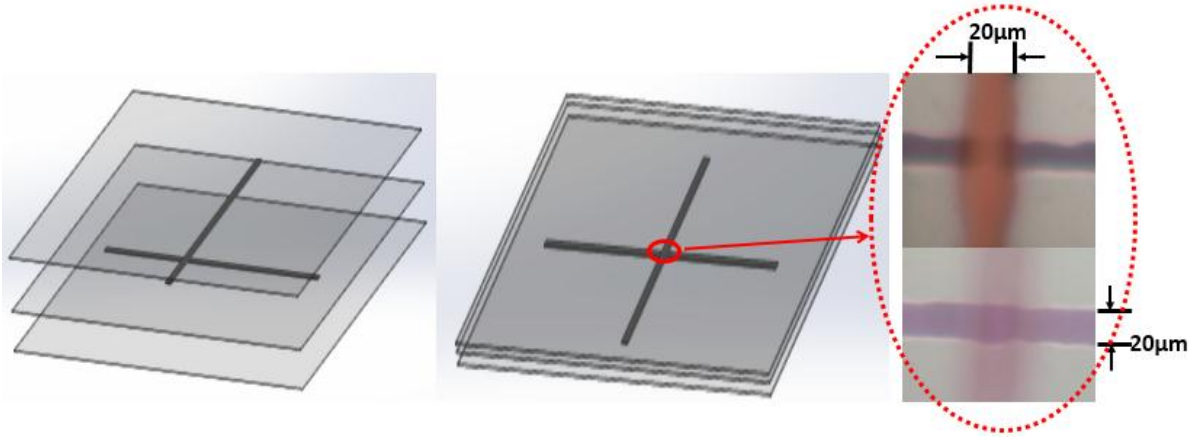

Figure 5.12 (a) (b) Schematic view of multi-layer electrodes array, (c) high-resolution capacitance touch sensor

In the study, high-resolution multi-layer structure sensor prototype was fabricated using e-jet printing on PET film, as shown in Figure 5.12 (c). The width of electrodes was 20 μm in two separate layers. The fabricated sensor was bended for 100 times in the experiment. Resistivity and capacitance of electrodes were measured to test the stretchability. Water droplets were deposited onto intersection area shown in Figure 5.12 (b) and (c). Capacitance changes due to presentence of water droplets were measured to test sensitivity of the sensor prototype.

Figure 5.13 demonstrated the stretchability test of the sensor prototype. As we can see from the Figure 5.13 (a), the resistivity maintained an average of $9.79*10^{-2}$ Ω ·μm and standard deviation of 0.008 during the 100 times bending test, while the capacitance maintained an average of 0.813pF and standard deviation of 0.333. The bending almost had no side effect on resistivity. Capacitance during bending demonstrated a slightly larger deviation. The reason was that adhesion between multi-layer structures wasn't strong enough in the experiments. The adhesion analysis would be a future topic for this research.

The response was almost simultaneous in the experiments. The key factor here was capacitance sensitivity. We applied four droplets on the intersection area of the prototype shown in Figure 5.12 (b). The changes of capacitance were shown in Figure 5.13 (b). At phase I, there was no droplet. With each droplets falling on the intersection, an obvious increase of capacitance change was observed.

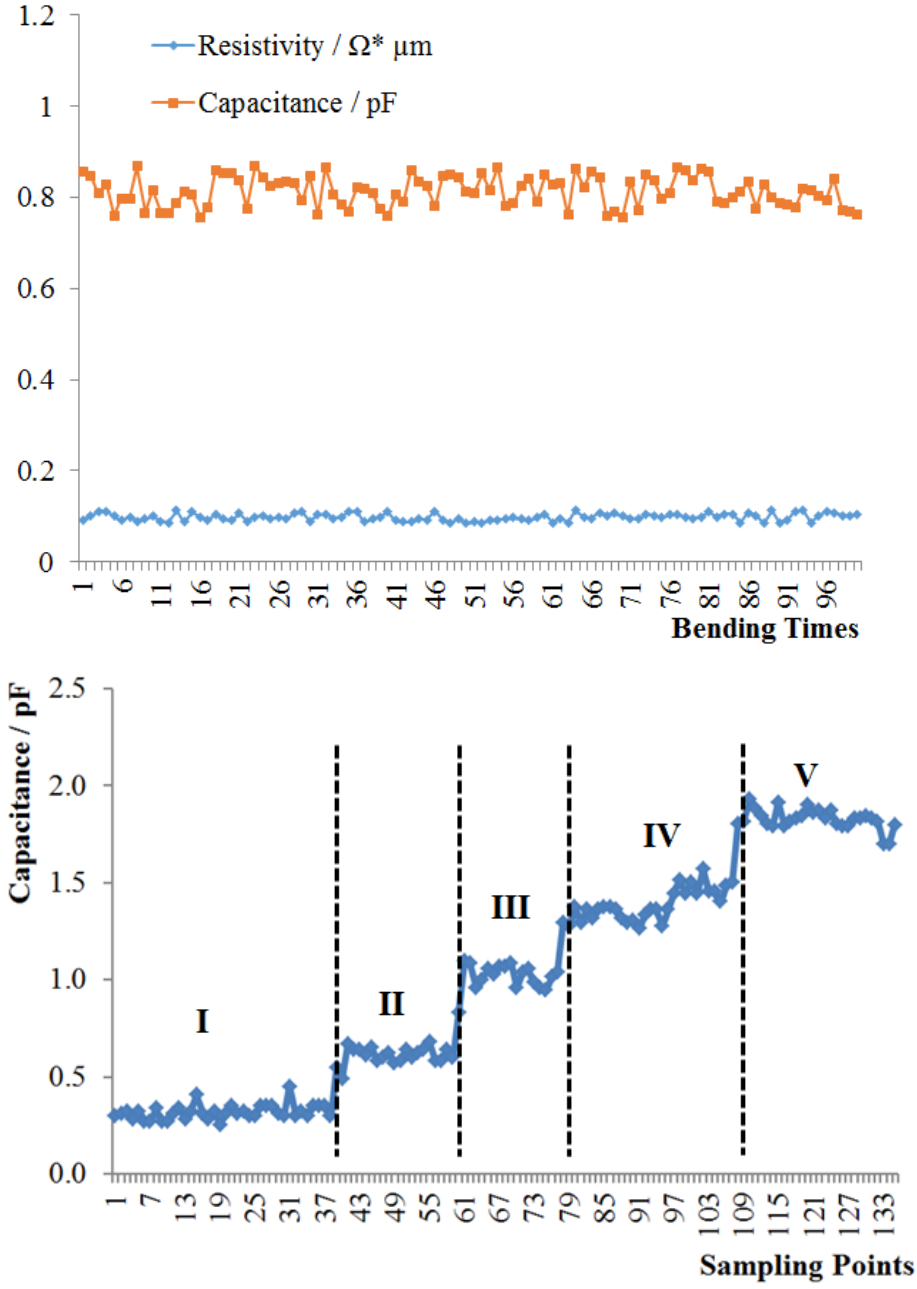

Figure 5.13 (a) Stretchability test of sensor prototype, (b) Response of capacitance to water droplets

Very few capacitance sensor can simultaneously achieve good conductivity, high-resolution, high sensitivity, and good stretchability. The rapid prototyping methods presented in the disseration can also be adapted for curved substrates, which is another advantages over traditional lithography methods. With metal ink used in the presented process, it can potentially be a good replacement for the traditional ITO film in current flexible display technologies.

I have demonstrated that e-jet printing using silver nano ink offers a lot more possibilities to meet customized needs in diverse applications.

5.8 Microelectrodes fabrication

In order to demonstrate the capability and versatility of our proposed e-jet printing followed by electroless copper deposition, I printed several electronic component patterns. An electronic pattern with a 100 μm width pad and a 2.3 μm silver track was obtained on ABF using AC voltage with nozzle outer diameter of 7 μm and inner diameter of 5 μm, as shown in Figure 5.14. Using ac-pulse modulated e-jet printing, I successfully printed high resolution metal pads, interconnects for representative circuit patterns with critical dimensions as small as 2 μm showed great potentials in microelectronic components fabrication. These can be applied for micro capacitor or inductor fabrication. The printed features are continuous, with micro-scale dimension, indicating charges accumulation problem are well solved using my technique.

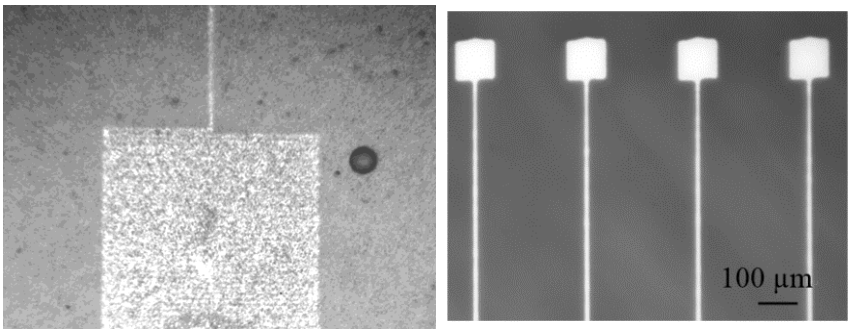

Figure 5.14 Printed electronic patterns with a 100 µm width pad and a 2.3 µm wide silver track on ABF

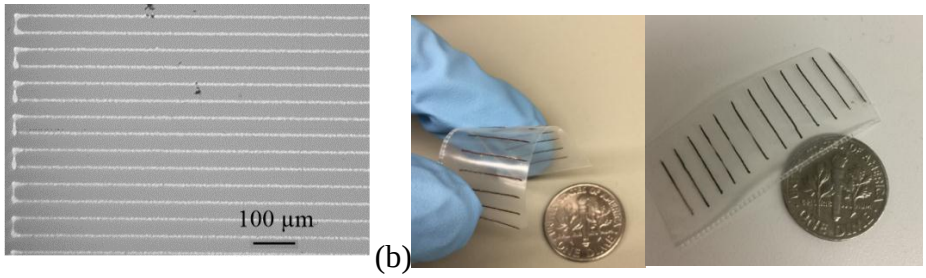

(a) (b)

Figure 5.15 Printed electronic components on highly insulating substrates: (a) an inductor pattern on ABF film, (b) Microstructures produced by combination of e-jet printing and electroless copper deposition on PET film with good conductivity

Most lithograph methods are restricted to planar surfaces, which make it especially difficult to be extended to curved substrate [99]. The process in this dissertation does not have this limitation. I demonstrated printing of silver seeds to generate patterns on flexible surfaces and afterwards copper deposition. The resolution of features on curved substrate is similar to that on planar substrates. Figure 5.15 (b) shows microscope pictures of

microstructure of copper generated on polyester (PET) film. Typical electrodes were produced by combination of e-jet printing and electroless copper deposition on PET film was successfully fabricated. The average line width of features is 20 μm with an average thickness of 7.3 μm on PET film.

To demonstrate the capability of e-jet printing as rapid prototyping method, microelectrodes array on PET film were fabricated with high resolution and transparency. As shown in Figure 5.16, I successfully printed high-resolution microelectrodes array with dimension as small as 15 μm. The patterns also demonstrated excellent transparency and flexibility on PET film using silver nanoink. The device I fabricated can be further applied for micro capacitor, inducer, or as electrodes array for flexible displays.

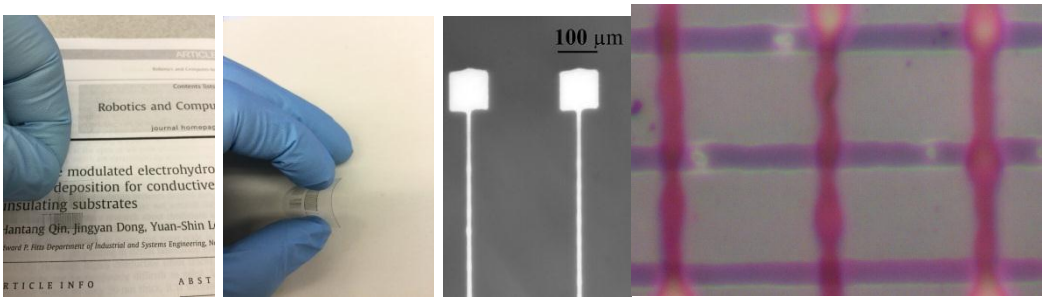

Figure 5.16 Printed microelectrodes array on PET film with good transparency, flexibility, and high resolution

5.9 Summary

In this chapter, I investigated the feasibility of rapid prototyping of capacitive touch sensor on flexible substrates based on e-jet printing using silver nanoink. From 2D point of

view, coplanar interdigitated electrode array were tested. From 3D point of view, a high resolution humidity sensor was tested. An improved mathematical model on my coplanar touch sensor design was developed to calculate the capacitance of printed sensor closely approximated measured values. I successfully fabricated touch sensors using comb like interdigitated structure. The effect of the design parameters, including the number of active electrodes, length of electrodes, and distance between electrodes were investigated in the study. With increasing number electrodes, active length, and smaller distance, the capacitance will increase, thus providing better sensing performance. Finally, I demonstrated rapid prototyping of sub-20 μm microelectrodes arrays using silver nanoink on PET film.

The successfully developed rapid prototyping method shows several distinct advantages and benefit to the community. It fills the gap between flexible electronics and rapid prototyping using metal ink. The touch sensor demonstrated in the chapter can be used as an alternative to fragile ITO film used in current touch display. The overall process is low cost, flexible, and avoid vacuum processing environment. The presented touch sensor and its rapid prototyping method can be further applied in medical and display applications, and it is also capable of on demand prototyping of any conductive patterns in flexible electronic manufacturing.

From Chapter 3, Chapter 4 and Chapter 5, a detailed study of AC modulated e-jet printing was presented for rapid prototyping of high resolution and high conductivity patterns on insulating substrates for flexible electronics. Fabrication process and detailed mechanism of e-jet printing using pulsed AC voltage was discussed. Feasibility of printing both high-resolution and low resistivity silver wires was demonstrated in these chapters. The presented

AC modulated e-jet printing technique is capable to fabricate resistors, inductors and micro wires, which offer a simple and versatile method to on demand direct fabricate conductive patterns in micro/nano electronic manufacturing. The proposed technique can be used for rapid prototyping of micro scale electronic circuits and devices. The patterns still need to be further improved in the future to meet industrial electronic standards.

CHAPTER 6 CONCLUSION AND FUTURE WORKS

The main objective of this research is to investigate and develop high-resolution rapid prototyping methods based on electrohydrodynamic inkjet printing and electroless copper deposition. Capacitance touch sensors were prototyped and tested from concept to product. The techniques can be used for prototyping of medical sensors, flexible electronics, wearable devices, droplet and humidity detectors, and other high-resolution or large-area applications. Some conclusion remarks and the future research were summarized and discussed in Chapter 6.

6.1 Conclusion

In this dissertation, I have presented the details of micro level rapid prototyping methods to fabricate high resolution electrical components for flexible electronics. In the study, I have investigated the modeling and process control of e-jet printing for high-resolution conductive patterns using silver nanoink, and electroless copper deposition onto printed silver seeds to increase cross section area of printed patterns. Capacitance sensors were fabricated to test feasibility of proposed techniques at device and system levels. The detailed accomplishments of the study can be summarized as follows:

- Fundamental studies of e-jet printing parameters using AC-pulsed voltage have been conducted to provide essential parameters for e-jet printing system. Silver nanoink was first characterized in the study for rapid prototyping of sub-20 μm conductive patterns. The parameters i.e. voltage, nozzle, plotting speed, were considered in my e-jet printing system to improve resolution compared to traditional inkjet printing. To solve the residual charge problems, I have introduced AC-pulse modulated voltage

into e-jet printing system by printing positive and negative charged droplets subsequently onto substrates. Analytical model of plotting speeds was developed to improve prediction of plotting speed for continuous patterns. This work made the lab-built e-jet printing system ready to fabricate microstructures.

- The electrical performances of printed patterns have been investigated for device production. Two post-treatments were proposed and studied in the research. Curing process can be applied to substrates that can stand high temperature to improve conductivity of printed patterns. However, for polymer based substrate with low melting temperature, curing might not work because it will cause reformation of polymer films. Electroless copper deposition was first introduced into e-jet printing to solve the electrical performance issues. The concentration of reaction agents for copper deposition was characterized in the research. With the help of electroless copper deposition, I was able to fabricate patterns with silver seeds and copper shell to improve overall electrical performance.

- Rapid prototyping of high-resolution electrode arrays to replace indium tin oxide (ITO) for flexible electronics was demonstrated. By direct printing silver nanoparticles on flexible substrates, capacitive touch sensors were fabricated onto polyethylene terephthalate (PET) film. An analytical model was developed to predict touch sensor characteristics for coplanar interdigitated structure, and experiments were conducted to study the effects of sensor design (e.g. number of electrodes, electrode length, and electrode distance) on the capacitance of printed touch sensors.

Sensitivity of high-resolution capacitance sensor was investigated in the study for droplet and humidity detection applications. The rapid prototyping method made a significant impact in enabling simultaneously (1) customized and flexible touch sensors, (2) cost-effective manufacturing, and (3) high resolution and good sensitivity. The presented techniques can be used for the on-demand fabrication of customized conductive patterns for flexible and wearable electronics.

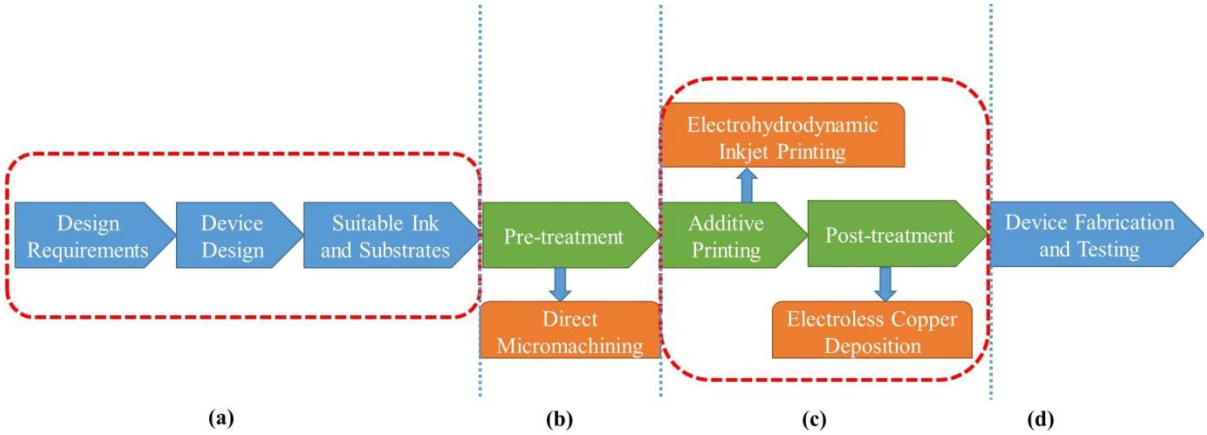

Figure 6.1 Overall processes proposed and conducted in the research

In conclusion, as shown in Figure 6.1, the overall proposal of the research included a whole product design flow. All works in this dissertation provided the road map of continuous development of high-resolution prototyping methods. The work started from concepts that planned to address current challenges in flexible electronics fields. Fabrication processes, e.g. e-jet printing, are the ways to achieve ultimate objectives. To develop the prototyping method, fundamental studies of the fabrication processes were conducted. The device fabrication and testing confirm the efficiency of proposed techniques and open up

new application possibilities. The dissertation not only has made contributions in fundamental science, but also forms the foundation for potential applications. From the contents in this research, I have published several conference and journal papers, and presented the research at conferences and seminars. The list of papers and presentations was shown in the following section.

6.2 Publications and presentations

The dissertation research so far have been conducted and submitted for journal and conference publications. Following is a list of the publications and presentations based on the results of the dissertation.

Journal Publications:

[1] H. Qin, Y. Cai, J. Dong, and Y-S. Lee, "*Direct Printing of Capacitive Touch Sensors on Flexible Substrates by Additive E-Jet Printing With Silver Nanoinks*." Journal of Manufacturing Science and Engineering 139.3: 031011, 2017.

[2] H. Qin, J. Dong, and Y-S. Lee. *"AC-pulse modulated electrohydrodynamic jet printing and electroless copper deposition for conductive microscale patterning on flexible insulating substrates."* Robotics and Computer-Integrated Manufacturing (2015), In Press, Accepted for publication on September 6th 2015, Available online November 6th 2015, ISSN 0736-5845.

[3] H. Qin, C. Wei, J. Dong, and Y-S. Lee, "*Direct Printing and Electrical Characterization of Conductive Micro Silver Tracks by AC-Pulse Modulated Electrohydrodynamic Jet (E-Jet) Printing"*, Journal of Manufacturing Science and Engineering (2016), Available online June 7th 2016, doi:10.1115/1.4033903.

[4] H. Qin, Y. Cai, J. Dong, and Y-S. Lee, *"Rapid Prototyping of High-Resolution Capacitive Touch Sensor Based on Electrohydrodynamic Inkjet Printing for Wearable and Flexible Electronics"*, manuscripts to Journal of Micromechanics and Microengineering in July 2016.

[5] C. Wei, H. Qin, N. A. Ramirez-lglesias, C-P. Chiu, Y-S. Lee, and J. Dong, *"High-Resolution AC-Pulse Modulated Electrohydrodynamic Jet Printing on Highly Insulating Substrates"*, Journal of Micromechanics and Microengineering, 24(4), 045010 (9pp), 2014.

[6] C. Wei, H. Qin, C-P. Chiu, Y-S. Lee, and J. Dong, *"Drop-on-Demand E-Jet Printing of Continuous Interconnects with AC-Pulse Modulation on Highly Insulating Substrates"*, Journal of Manufacturing Systems (2014), In press, Accepted for publication on July 14th 2015, Available online 6 August 2014, ISSN 0278-6125.

Conference Proceedings and Abstracts:

[7] H. Qin, C. Wei, J. Dong, Y-S. Lee, *"AC-Pulse Modulated Electrohydrodynamic (EHD) Jet Printing of Conductive Micro Silver Tracks for Micro-Manufacturing,"* The FAIM 2014 Flexible Automation and Intelligent Manufacturing Conference, San Antonio, TX, Paper # 231, May 20-23, 2014.

[8] C. Wei, H. Qin, C-P. Chiu, Y-S. Lee, J. Dong, *"E-Jet Printing on Highly Insulating Substrates with AC-Pulse Modulation"*, 2014 Industrial and Systems Engineering Research Conference (ISERC2014), Montreal, Canada, June 2014.

[9] H. Qin, C. Wei, J. Dong, Y-S. Lee, *"Direct Fabrication of Highly Conductive Micro Silver Tracks Using Electrohydrodynamic Jet Printing for Sub-20 μM Micro-*

Manufacturing", ASME 2014 Manufacturing Science and Engineering Conference (MSEC2014), Detroit, MI, Paper # 4163, June 9-13, 2014.

[10] C. Wei, H. Qin, C-P, Chiu, Y-S. Lee, J. Dong, *"Modulated Drop-on-Demand E-Jet Printing of Continuous Features on Electronic Insulation Substrates"*, Proceeding of NAMRI/SME North American Manufacturing Research Conference, Vol. 42, Page 345-353, ISBN: 978-1-63439-417-8, Detroit, MI, June 9-13, 2014.

[11] H. Qin, J. Dong, Y-S. Lee, *"Electrohydrodynamic Jet Printing of Silver Seeds: Micro Scale Patterning by Electroless Copper Deposition"*, Proceedings of the ASME 2015 Manufacturing Science and Engineering Conference, Volume 1, ISBN: 978-0-7918-5682-6, Charlotte, NC, June 8-12, 2015.

[12] H. Qin, J. Dong, and Y-S. Lee. *"Direct Printing of Capacitive Touch Sensors on Flexible Substrates by Additive E-jet Printing with Silver Nanoinks"*, Proceedings of the ASME 2016 International Manufacturing Science and Engineering Conference, Paper #8740, Blacksburg, VA, June 27-July 1, 2016.

Presentation:

[13] H. Qin, Rapid Prototyping Using Conductive Ink: Micro Scale Patterning Based on E-Jet Printing and Electroless Copper Deposition, ASME 2015 International Manufacturing Science and Engineering Conference. Charlotte, NC, June 2015.

[14] H. Qin, Rapid Prototyping of High-Resolution Capacitive Touch Sensor Based on Electrohydrodynamic Inkjet Printing for Wearable and Flexible Electronics, ASME 2016 International Manufacturing Science and Engineering Conference, Blacksburg, VA, June 2016.

6.3 Future researches

There are several possible research works that I can continue to do after this dissertation because the dissertation has opened up new area of fabrication of electronic components in flexible applications based on e-jet printing. The proposed techniques can also be further improved by incorporating micromachining into overall fabrication. Following is the list of interesting future researches that can be extended:

6.3.1. Aspect ratio and microgrooves

Even though I was able to print high resolution conductive patterns on substrate, there was still one challenge remaining to be solved. The cross section of printed patterns was still not good enough even with the help of electroless copper deposition. For microelectrodes that can be used as capacitive sensor, the required cross section would be perfect square shape or rectangular shape with high aspect ratio. The copper growth on printed silver patterns was unpredictable.

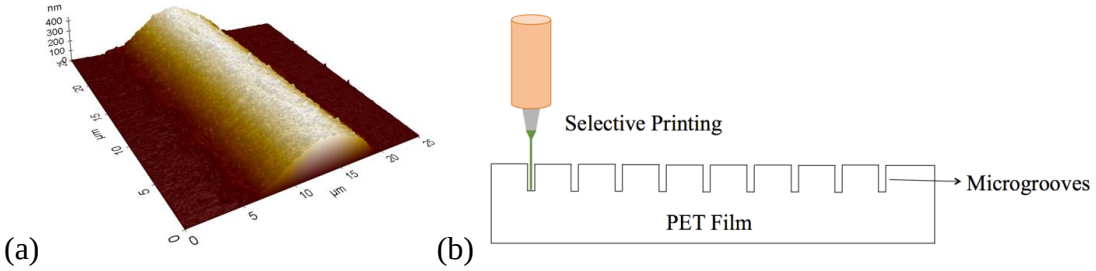

Figure 6.2 (a) Aspect ratio of printed patterns, and (b) schematic of selective printing into microgrooves on PET film

One of the methods to solve the two issues would be a pretreatment of PET film by fabricating microgrooves first on the substrates, as shown in Figure 6.2 (b). The microgrooves on the substrates can be selectively deposited with silver ink. It is either by fully filled with silver ink or can be followed by electroless copper deposition to fill the gap. To fabricate these microgrooves, two techniques can be integrated.

6.3.2. Micromachining and laser ablation

The fabrication of these microgrooves can be realized using mechanical force based micromachining or laser ablation. Mechanical based micromachining is capable of fabricating fine features on metal substrates.

Another technique to fabricate microgrooves would be laser ablation. Polymer films such as PET film show great elasticity but poor machinability due to hassle to remove chips. The term “laser” refers to “light amplification by simulated emission of radiation”, which was first developed by Maiman et. al in 1960. [100] Laser is generated when molecules of active laser medium is stimulated by excitation source into excited state. Once they go back to steady state, photon energy will be released which will then be accumulated as high-energy beam. Laser can be characterized according to wavelength in vacuum, such as UV or visible lights. The most commonly used lasers in industry are CO_2 laser, Nd:YAG laser and Excimer laser.

The platform of e-jet printing and laser ablation shares certain level of similarity. They both comes with fixed source (e.g. printing head and laser source), programmable platform for substrate. At the same time, they both work well on flexible polymer substrate.

The pre-treatment of substrate based on laser ablation is capable of fabricating micro-grooves on substrates for subsequent e-jet printing to selectively deposit silver ink into grooves. Fine features with increased cross section area can be achieved using this method.

Excimer laser is a specific type of pulsed laser that emits ultraviolet light with high energy. Most excimer lasers are based on inert gas and halogen gas in laser system. The wavelength of these UV laser is determined by its combination. Laser ablation is one kind of laser micromachining techniques that uses a mask to fabricate on particular area on workpiece [111]. The pattern is a reverse shape of mask by projection lens.

Figure 6.3 shows a schematic diagram of laser ablation. Different from traditional micromachining, there are much more parameters will affect final results of laser ablation. It is critical to study laser ablation on each material before we can develop any micro devices.

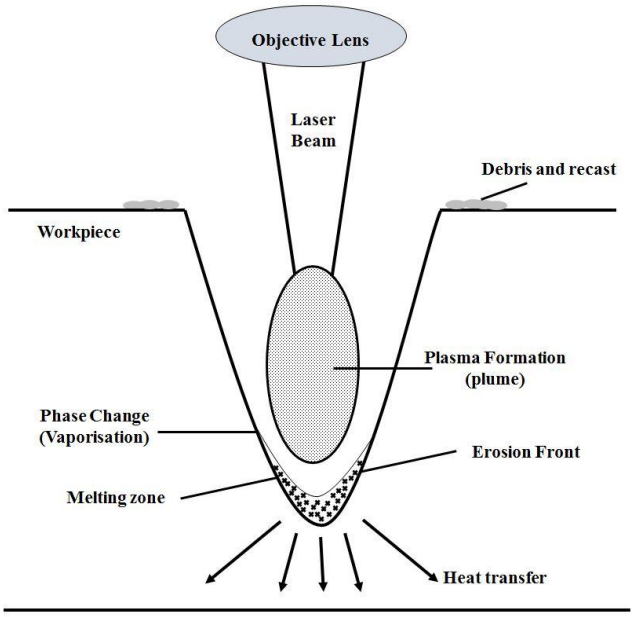

Figure 6.3 Schematic of laser ablation

Because of the complexity of laser ablation, the parameter study of laser ablation system is required before developing any devices. The excimer laser machine (COMPexPro 201, Coherent, Inc.) is able to emit UV laser pulse at a wavelength of 193 nm. The energy of output laser pulse can be up to 400 mJ and the maximum frequency was 10 Hz. Similar to e-jet printing platform, the laser ablation also uses 3-axis micro positioning platform to provide 3-axis synchronous motions with laser. In this case, the laser ablation and e-jet printing share similar configuration and thus can be combined into a rapid prototyping flow.

6.3.3. Multi-material and multi-scale fabrication

The capacitive touch sensor based on our proposed rapid prototyping method has been fabricated. There are plenty of groups from materials science also working on functioning materials. It would be very interesting topics if those new materials can be applied into the e-jet printing for flexible electronics. This application driven research will lead to product development, from lab to industry.

The future research listed here is by no means a complete list. There will be more research topic coming out from fundamental study of e-jet printing with new materials. It is expected that related research will continue to boom in various engineering and science disciplines.

REFERENCES

[1] M. Melzer, J.I. Mönch, D. Makarov, Y. Zabila, G.S. Cañón Bermúdez, D. Karnaushenko, S. Baunack, F. Bahr, C. Yan, M. Kaltenbrunner, Wearable Magnetic Field Sensors for Flexible Electronics, Advanced Materials, 27 (2015) 1274-1280.

[2] J. van den Brand, M. de Kok, A. Sridhar, M. Cauwe, R. Verplancke, F. Bossuyt, J. De Baets, J. Vanfleteren, Flexible and stretchable electronics for wearable healthcare, in: Solid State Device Research Conference (ESSDERC), 2014 44th European, IEEE, 2014, pp. 206-209.

[3] H.C. Chang, C.L. Liu, W.C. Chen, Flexible Nonvolatile Transistor Memory Devices Based on One‐Dimensional Electrospun P3HT: Au Hybrid Nanofibers, Advanced Functional Materials, 23 (2013) 4960-4968.

[4] K.L. Lin, K. Jain, Design and fabrication of stretchable multilayer self-aligned interconnects for flexible electronics and large-area sensor arrays using excimer laser photoablation, Electron Device Letters, IEEE, 30 (2009) 14-17.

[5] M. Kaltenbrunner, M.S. White, E.D. Głowacki, T. Sekitani, T. Someya, N.S. Sariciftci, S. Bauer, Ultrathin and lightweight organic solar cells with high flexibility, Nature communications, 3 (2012) 770.

[6] L. Leonat, M.S. White, E.D. Głowacki, M.C. Scharber, T. Zillger, J. Rühling, A. Hübler, N.S. Sariciftci, 4% Efficient Polymer Solar Cells on Paper Substrates, The Journal of Physical Chemistry C, 118 (2014) 16813-16817.

[7] K.-S. Kim, J.-O. Bang, S.-B. Jung, Electrochemical migration behavior of silver nanopaste screen-printed for flexible and printable electronics, Current Applied Physics, 13 (2013) S190-S194.

[8] S. Lee, S. Jeon, R. Chaji, A. Nathan, Transparent Semiconducting Oxide Technology for Touch Free Interactive Flexible Displays, Proceedings of the IEEE, 103 (2015) 644-664.

[9] C. Mariotti, W. Su, B.S. Cook, L. Roselli, M.M. Tentzeris, Development of Low Cost, Wireless, Inkjet Printed Microfluidic RF Systems and Devices for Sensing or Tunable Electronics, Sensors Journal, IEEE, 15 (2015) 3156-3163.

[10] R. Crabb, F. Treble, Thin silicon solar cells for large flexible arrays, (1967).

[11] K.A. Ray, Flexible solar cell arrays for increased space power, IEEE Transactions on Aerospace and Electronic Systems, 1 (1967) 107-115.

[12] W.S. Wong, A. Salleo, Flexible electronics: materials and applications, Springer Science & Business Media, 2009.

[13] Y. Chen, J. Au, P. Kazlas, A. Ritenour, H. Gates, M. McCreary, Electronic paper: Flexible active-matrix electronic ink display, Nature, 423 (2003) 136-136.

[14] M. Yano, K. Suzuki, K. Nakatani, H. Okaniwa, Roll-to-roll preparation of a hydrogenated amorphous silicon solar cell on a polymer film substrate, Thin Solid Films, 146 (1987) 75-81.

[15] T.P. Brody, The thin film transistor—A late flowering bloom, Electron Devices, IEEE Transactions on, 31 (1984) 1614-1628.

[16] M. Eltaib, J. Hewit, Tactile sensing technology for minimal access surgery—a review, Mechatronics, 13 (2003) 1163-1177.

[17] G. Walker, A review of technologies for sensing contact location on the surface of a display, Journal of the Society for Information Display, 20 (2012) 413-440.

[18] P.J. Kyberd, P.H. Chappell, Characterization of an optical and acoustic touch and slip sensor for autonomous manipulation, Measurement Science and Technology, 3 (1992) 969.

[19] M.H. Lee, H.R. Nicholls, Review Article Tactile sensing for mechatronics—a state of the art survey, Mechatronics, 9 (1999) 1-31.

[20] R. Phares, M. Fihn, Introduction to Touchscreen Technologies, Handbook of Visual Display Technology, (2012) 935-974.

[21] G. Barrett, R. Omote, Projected-capacitive touch technology, Information Display, 26 (2010) 16-21.

[22] L. Chenchi, M.A. Borkar, A.J. Redfern, J.H. McClellan, Compressive Sensing for Sparse Touch Detection on Capacitive Touch Screens, Emerging and Selected Topics in Circuits and Systems, IEEE Journal on, 2 (2012) 639-648.

[23] Z. Wu, Z. Chen, X. Du, J.M. Logan, J. Sippel, M. Nikolou, K. Kamaras, J.R. Reynolds, D.B. Tanner, A.F. Hebard, Transparent, conductive carbon nanotube films, Science, 305 (2004) 1273-1276.

[24] D. Zhang, K. Ryu, X. Liu, E. Polikarpov, J. Ly, M.E. Tompson, C. Zhou, Transparent, conductive, and flexible carbon nanotube films and their application in organic light-emitting diodes, Nano Letters, 6 (2006) 1880-1886.

[25] M. Zhang, S. Fang, A.A. Zakhidov, S.B. Lee, A.E. Aliev, C.D. Williams, K.R. Atkinson, R.H. Baughman, Strong, transparent, multifunctional, carbon nanotube sheets, Science, 309 (2005) 1215-1219.

[26] K.S. Kim, Y. Zhao, H. Jang, S.Y. Lee, J.M. Kim, K.S. Kim, J.-H. Ahn, P. Kim, J.-Y. Choi, B.H. Hong, Large-scale pattern growth of graphene films for stretchable transparent electrodes, Nature, 457 (2009) 706-710.

[27] J. Wu, M. Agrawal, H.A. Becerril, Z. Bao, Z. Liu, Y. Chen, P. Peumans, Organic light-emitting diodes on solution-processed graphene transparent electrodes, ACS nano, 4 (2009) 43-48.

[28] J.-H. Huang, D. Kekuda, C.-W. Chu, K.-C. Ho, Electrochemical characterization of the solvent-enhanced conductivity of poly (3, 4-ethylenedioxythiophene) and its application in polymer solar cells, Journal of Materials Chemistry, 19 (2009) 3704-3712.

[29] J.E. Yoo, K.S. Lee, A. Garcia, J. Tarver, E.D. Gomez, K. Baldwin, Y. Sun, H. Meng, T.-Q. Nguyen, Y.-L. Loo, Directly patternable, highly conducting polymers for broad

applications in organic electronics, Proceedings of the National Academy of Sciences, 107 (2010) 5712-5717.

[30] J. Meiss, M. Riede, K. Leo, Towards efficient tin-doped indium oxide (ITO)-free inverted organic solar cells using metal cathodes, Applied Physics Letters, 94 (2009) 013303.

[31] B. O'Connor, C. Haughn, K.-H. An, K.P. Pipe, M. Shtein, Transparent and conductive electrodes based on unpatterned, thin metal films, Applied Physics Letters, 93 (2008) 223304.

[32] A.R. Madaria, A. Kumar, F.N. Ishikawa, C. Zhou, Uniform, highly conductive, and patterned transparent films of a percolating silver nanowire network on rigid and flexible substrates using a dry transfer technique, Nano Research, 3 (2010) 564-573.

[33] J.-Y. Lee, S.T. Connor, Y. Cui, P. Peumans, Solution-processed metal nanowire mesh transparent electrodes, Nano letters, 8 (2008) 689-692.

[34] S. De, T.M. Higgins, P.E. Lyons, E.M. Doherty, P.N. Nirmalraj, W.J. Blau, J.J. Boland, J.N. Coleman, Silver nanowire networks as flexible, transparent, conducting films: extremely high DC to optical conductivity ratios, ACS nano, 3 (2009) 1767-1774.

[35] Y. Zhou, L. Hu, G. Grüner, A method of printing carbon nanotube thin films, Applied Physics Letters, 88 (2006) 123109.

[36] F.P. Melchels, J. Feijen, D.W. Grijpma, A review on stereolithography and its applications in biomedical engineering, Biomaterials, 31 (2010) 6121-6130.

[37] X. Yan, P. Gu, A review of rapid prototyping technologies and systems, Computer-Aided Design, 28 (1996) 307-318.

[38] D. Bourell, J. Beaman, M.C. Leu, D. Rosen, A brief history of additive manufacturing and the 2009 roadmap for additive manufacturing: looking back and looking ahead, Proceedings of RapidTech, (2009) 24-25.

[39] J.-H. Shim, J.-S. Lee, J.Y. Kim, D.-W. Cho, Bioprinting of a mechanically enhanced three-dimensional dual cell-laden construct for osteochondral tissue engineering using a

multi-head tissue/organ building system, Journal of Micromechanics and Microengineering, 22 (2012) 085014.

[40] B.J. de Gans, P.C. Duineveld, U.S. Schubert, Inkjet printing of polymers: state of the art and future developments, Advanced materials, 16 (2004) 203-213.

[41] D. Lee, E. Hwang, T. Yu, Y. Kim, J. Hwang, Structuring of micro line conductor using electro-hydrodynamic printing of a silver nanoparticle suspension, Applied Physics A, 82 (2006) 671-674.

[42] R. Parashkov, E. Becker, T. Riedl, H.-H. Johannes, W. Kowalsky, Large area electronics using printing methods, Proceedings of the IEEE, 93 (2005) 1321-1329.

[43] M.J. Heller, DNA microarray technology: devices, systems, and applications, Annual review of biomedical engineering, 4 (2002) 129-153.

[44] A. Bietsch, J. Zhang, M. Hegner, H.P. Lang, C. Gerber, Rapid functionalization of cantilever array sensors by inkjet printing, Nanotechnology, 15 (2004) 873.

[45] Z. Wang, H. Shang, G.U. Lee, Nanoliter-scale reactor arrays for biochemical sensing, Langmuir, 22 (2006) 6723-6726.

[46] J.-U. Park, M. Hardy, S.J. Kang, K. Barton, K. Adair, D. kishore Mukhopadhyay, C.Y. Lee, M.S. Strano, A.G. Alleyne, J.G. Georgiadis, High-resolution electrohydrodynamic jet printing, Nature materials, 6 (2007) 782-789.

[47] N. Stutzmann, R.H. Friend, H. Sirringhaus, Self-aligned, vertical-channel, polymer field-effect transistors, Science, 299 (2003) 1881-1884.

[48] C. Wei, J. Dong, Direct fabrication of high-resolution three-dimensional polymeric scaffolds using electrohydrodynamic hot jet plotting, Journal of Micromechanics and Microengineering, 23 (2013) 025017.

[49] J. Zeleny, Instability of electrified liquid surfaces, Physical Review, 10 (1917) 1.

[50] M. Cloupeau, B. Prunet-Foch, Electrohydrodynamic spraying functioning modes: a critical review, Journal of Aerosol Science, 25 (1994) 1021-1036.

[51] D.-Y. Lee, Y.-S. Shin, S.-E. Park, T.-U. Yu, J. Hwang, Electrohydrodynamic printing of silver nanoparticles by using a focused nanocolloid jet, Applied Physics Letters, 90 (2007) 081905-081905-081903.

[52] B.Y. Ahn, E.B. Duoss, M.J. Motala, X. Guo, S.-I. Park, Y. Xiong, J. Yoon, R.G. Nuzzo, J.A. Rogers, J.A. Lewis, Omnidirectional printing of flexible, stretchable, and spanning silver microelectrodes, Science, 323 (2009) 1590-1593.

[53] S. Lee, J. Song, H. Kim, J. Chung, Time resolved imaging of electrohydrodynamic jetting on demand induced by square pulse voltage, Journal of Aerosol Science, (2012).

[54] J.H. Yu, S.Y. Kim, J. Hwang, Effect of viscosity of silver nanoparticle suspension on conductive line patterned by electrohydrodynamic jet printing, Applied Physics A, 89 (2007) 157-159.

[55] S.-H. Lee, X.H. Nguyen, H.S. Ko, Study on droplet formation with surface tension for electrohydrodynamic inkjet nozzle, Journal of mechanical science and technology, 26 (2012) 1403-1408.

[56] V.D. Nguyen, D. Byun, Mechanism of electrohydrodynamic printing based on ac voltage without a nozzle electrode, Applied Physics Letters, 94 (2009) 173509.

[57] Y. Jang, I. Hartarto Tambunan, H. Tak, V. Dat Nguyen, T. Kang, D. Byun, Non-contact printing of high aspect ratio Ag electrodes for polycrystalline silicone solar cell with electrohydrodynamic jet printing, Applied Physics Letters, 102 (2013) 123901-123901-123904.

[58] Y. Jang, J. Kim, D. Byun, Invisible metal-grid transparent electrode prepared by electrohydrodynamic (EHD) jet printing, Journal of Physics D: Applied Physics, 46 (2013) 155103.

[59] X. Wang, L. Xu, G. Zheng, W. Cheng, D. Sun, Pulsed electrohydrodynamic printing of conductive silver patterns on demand, Science China Technological Sciences, 55 (2012) 1603-1607.

[60] K. Wang, J.P. Stark, Direct fabrication of electrically functional microstructures by fully voltage-controlled electrohydrodynamic jet printing of silver nano-ink, Applied Physics A, 99 (2010) 763-766.

[61] D.-H. Youn, S.-H. Kim, Y.-S. Yang, S.-C. Lim, S.-J. Kim, S.-H. Ahn, H.-S. Sim, S.-M. Ryu, D.-W. Shin, J.-B. Yoo, Electrohydrodynamic micropatterning of silver ink using near-field electrohydrodynamic jet printing with tilted-outlet nozzle, Applied Physics A, 96 (2009) 933-938.

[62] D.-Y. Lee, J.-C. Lee, Y.-S. Shin, S.-E. Park, T.-U. Yu, Y.-J. Kim, J. Hwang, Structuring of conductive silver line by electrohydrodynamic jet printing and its electrical characterization, in: Journal of physics: conference series, IOP Publishing, 2008, pp. 012039.

[63] C.-C. Yang, C.-C. Wan, Y.-Y. Wang, Synthesis of Ag/Pd nanoparticles via reactive micelles as templates and its application to electroless copper deposition, Journal of colloid and interface science, 279 (2004) 433-439.

[64] N. Fritz, H.-C. Koo, Z. Wilson, E. Uzunlar, Z. Wen, X. Yeow, S.A.B. Allen, P.A. Kohl, Electroless deposition of copper on organic and inorganic substrates using a Sn/Ag catalyst, Journal of The Electrochemical Society, 159 (2012) D386-D392.

[65] P.C. Hidber, W. Helbig, E. Kim, G.M. Whitesides, Microcontact printing of palladium colloids: micron-scale patterning by electroless deposition of copper, Langmuir, 12 (1996) 1375-1380.

[66] M. Schlesinger, M. Paunovic, Modern electroplating, John Wiley & Sons, 2011.

[67] E. Uzunlar, Z. Wilson, P.A. Kohl, Electroless Copper Deposition Using Sn/Ag Catalyst on Epoxy Laminates, Journal of The Electrochemical Society, 160 (2013) D3237-D3246.

[68] N.S. Dellas, K. Meinert Jr, S.E. Mohney, Laser-enhanced electroless plating of silver seed layers for selective electroless copper deposition, Journal of Laser Applications, 20 (2008) 218-223.

[69] C.-Y. Kao, K.-S. Chou, Electroless copper plating onto printed lines of nanosized silver seeds, Electrochemical and solid-state letters, 10 (2007) D32-D34.

[70] T. Masuzawa, State of the art of micromachining, CIRP Annals-Manufacturing Technology, 49 (2000) 473-488.

[71] L. Alting, F. Kimura, H.N. Hansen, G. Bissacco, Micro engineering, CIRP Annals-Manufacturing Technology, 52 (2003) 635-657.

[72] M. Heckele, W. Schomburg, Review on micro molding of thermoplastic polymers, Journal of Micromechanics and Microengineering, 14 (2004) R1.

[73] E.S. Kim, Analysis and Fabrication of Microfluidic Systems by Excimer Laser Micromachining and Its Applications for Microfluidic and Bio-Medical Devices, (2010).

[74] P. Wongwiwat, R. Narayan, Y. Lee, Laser Micromachining and Quality Improvement by Cyanoacrylate Coating on Silicon Wafer, Transactions of NAMRI/SME, 37 (2009) 41-48.

[75] P. Wongwiwat, R.J. Narayan, Y.-S. Lee, Improving Biocompatibily of Laser Micromachined Silicon Wafer by Surface Coating With Poly (Ethylene Glycol) Diacrylate and Diamond-Like Carbon for Biomedical Devices, in: ASME 2010 International Manufacturing Science and Engineering Conference, American Society of Mechanical Engineers, 2010, pp. 273-280.

[76] P. Wongwiwat, R.J. Narayan, Y.-S. Lee, Laser Micromachining Modeling and Laser Machined Surface Errors Prediction for Biomedical Applications, in: ASME 2012 International Manufacturing Science and Engineering Conference collocated with the 40th North American Manufacturing Research Conference and in participation with the International Conference on Tribology Materials and Processing, American Society of Mechanical Engineers, 2012, pp. 59-68.

[77] A. Khan, K. Rahman, M.-T. Hyun, D.-S. Kim, K.-H. Choi, Multi-nozzle electrohydrodynamic inkjet printing of silver colloidal solution for the fabrication of electrically functional microstructures, Applied Physics A, 104 (2011) 1113-1120.

[78] D.-Y. Lee, D.-H. Lim, Y.-J. Kim, J. Hwang, Electrical Characterization of a Microstrip Line Patterned by Electrohydrodynamic Jet Printing of Silver Nanoparticles, Journal of Imaging Science, 53 (2009) 41203-41203.

[79] K. Rahman, A. Khan, N.M. Muhammad, J. Jo, K.-H. Choi, Fine-resolution patterning of copper nanoparticles through electrohydrodynamic jet printing, Journal of Micromechanics and Microengineering, 22 (2012) 065012.

[80] M.W. Lee, N.Y. Kim, S. An, J.-Y. Huh, H.Y. Kim, S.S. Yoon, Effects of pulsing frequency on characteristics of electrohydrodynamic inkjet using micro-Al and nano-Ag particles, Experimental Thermal and Fluid Science, (2012).

[81] P. Galliker, J. Schneider, H. Eghlidi, S. Kress, V. Sandoghdar, D. Poulikakos, Direct printing of nanostructures by electrostatic autofocussing of ink nanodroplets, Nature communications, 3 (2012) 890.

[82] B. Kim, H. Nam, S.J. Kim, J. Sung, S.W. Joo, G. Lim, Control of charged droplets using electrohydrodynamic repulsion for circular droplet patterning, Journal of Micromechanics and Microengineering, 21 (2011) 075020.

[83] M. Lee, D. Kang, N. Kim, H. Kim, S. James, S. Yoon, A study of ejection modes for pulsed-DC electrohydrodynamic inkjet printing, Journal of Aerosol Science, 46 (2012) 1-6.

[84] H.T. Yudistira, V.D. Nguyen, P. Dutta, D. Byun, Flight behavior of charged droplets in electrohydrodynamic inkjet printing, Applied Physics Letters, 96 (2010) 023503.

[85] C. Wei, H. Qin, R. Nakaira, C.-P. Chiu, Y.-S. Lee, J. Dong, High Resolution AC-Pulse Modulated Electrohydrodynamic Jet Printing on Highly Insulating Substrates, Journal of Micromechanics and Microengineering, (2014).

[86] H. Qin, C. Wei, J. Dong, Y.-S. Lee, AC-Pulse Modulated Electrohydrodynamic (EHD) Direct Printing of Conductive Micro Silver Tracks for Micro-Manufacturing, in: Flexible Automation and Intelligent Manufacturing (FAIM2014), San Antonio, Texas, 2014.

[87] H. Qin, C. Wei, J. Dong, Y.-S. Lee, Direct Fabrication of Highly Conductive Micro Silver Tracks Using Electrohydrodynamic Jet Printing for Sub-20 μm Micro-Manufacturing, in: 2014 Manufacturing Science and Engineering Conference (MSEC2014), Detroit, Michigan, 2014.

[88] G.O. Mallory, J.B. Hajdu, Electroless plating: fundamentals and applications, William Andrew, 1990.

[89] Y. Shacham-Diamand, V. Dubin, M. Angyal, Electroless copper deposition for ULSI, Thin Solid Films, 262 (1995) 93-103.

[90] Y.-M. Lin, S.-C. Yen, Effects of additives and chelating agents on electroless copper plating, Applied Surface Science, 178 (2001) 116-126.

[91] Z. Hu, T. Ritzdorf, Electroless Deposition Processes and Tools, in: Advanced Nanoscale ULSI Interconnects: Fundamentals and Applications, Springer, 2009, pp. 413-433.

[92] H. Qin, C. Wei, J. Dong, Y.-S. Lee, Direct Fabrication of Highly Conductive Micro Silver Tracks Using Electrohydrodynamic Jet Printing for Sub-20 μM Micro-Manufacturing, in: ASME 2014 International Manufacturing Science and Engineering Conference collocated with the JSME 2014 International Conference on Materials and Processing and the 42nd North American Manufacturing Research Conference, American Society of Mechanical Engineers, 2014, pp. V002T002A026-V002T002A026.

[93] C. Wei, H. Qin, N.A. Ramírez-Iglesias, C.-P. Chiu, Y.-s. Lee, J. Dong, High-resolution ac-pulse modulated electrohydrodynamic jet printing on highly insulating substrates, Journal of Micromechanics and Microengineering, 24 (2014) 045010.

[94] C. Wei, J. Dong, Development and Modeling of Melt Electrohydrodynamic-Jet Printing of Phase-Change Inks for High-Resolution Additive Manufacturing, Journal of Manufacturing Science and Engineering, 136 (2014) 061010.

[95] C. Wei, H. Qin, C.-P. Chiu, Y.-S. Lee, J. Dong, Drop-on-demand E-jet printing of continuous interconnects with AC-pulse modulation on highly insulating substrates, Journal of Manufacturing Systems, (2014).

[96] H. Qin, C. Wei, J. Dong, Y.-S. Lee, AC-Pulse Modulated Electrohydrodynamic (EHD) Jet Printing of Conductive Micro Silver Tracks for Micro-Manufacturing, in: The FAIM 2014 Flexible Automation and Intelligent Manufacturing Conference, San Antonio, TX, 2014.

[97] N. Espinosa, M. Hösel, D. Angmo, F.C. Krebs, Solar cells with one-day energy payback for the factories of the future, Energy & Environmental Science, 5 (2012) 5117-5132.

[98] G. Greczynski, T. Kugler, W. Salaneck, Characterization of the PEDOT-PSS system by means of X-ray and ultraviolet photoelectron spectroscopy, Thin Solid Films, 354 (1999) 129-135.

[99] W. Hong, Y. Xu, G. Lu, C. Li, G. Shi, Transparent graphene/PEDOT–PSS composite films as counter electrodes of dye-sensitized solar cells, Electrochemistry Communications, 10 (2008) 1555-1558.

[100] Y.H. Kim, C. Sachse, M.L. Machala, C. May, L. Müller‐Meskamp, K. Leo, Highly conductive PEDOT: PSS electrode with optimized solvent and thermal post‐treatment for ITO‐free organic solar cells, Advanced Functional Materials, 21 (2011) 1076-1081.

[101] N. Kim, S. Kee, S.H. Lee, B.H. Lee, Y.H. Kahng, Y.-R. Jo, B.-J. Kim, K. Lee, Highly Conductive PEDOT:PSS Nanofibrils Induced by Solution-Processed Crystallization, Advanced Materials, 26 (2014) 2268-2272.

[102] S. Ouyang, Y. Xie, D. Wang, D. Zhu, X. Xu, T. Tan, J. DeFranco, H.H. Fong, Photolithographic patterning of highly conductive PEDOT:PSS and its application in organic light-emitting diodes, Journal of Polymer Science Part B: Polymer Physics, 52 (2014) 1221-1226.

[103] C. Elbuken, T. Glawdel, D. Chan, C.L. Ren, Detection of microdroplet size and speed using capacitive sensors, Sensors and Actuators A: Physical, 171 (2011) 55-62.

[104] F.R. Tolmasky, R. Williamson, C. Blumenberg, P.L. Coffman, Portable multifunction device, method, and graphical user interface for translating displayed content, in, Google Patents, 2011.

[105] A.V. Mamishev, K. Sundara-Rajan, F. Yang, Y. Du, M. Zahn, Interdigital sensors and transducers, Proceedings of the IEEE, 92 (2004) 808-845.

[106] J.Z. Chen, A.A. Darhuber, S.M. Troian, S. Wagner, Capacitive sensing of droplets for microfluidic devices based on thermocapillary actuation, Lab on a Chip, 4 (2004) 473-480.

[107] R.M. Mutiso, M.C. Sherrott, A.R. Rathmell, B.J. Wiley, K.I. Winey, Integrating simulations and experiments to predict sheet resistance and optical transmittance in nanowire films for transparent conductors, ACS nano, 7 (2013) 7654-7663.

[108] S. Gabriel, R. Lau, C. Gabriel, The dielectric properties of biological tissues: III. Parametric models for the dielectric spectrum of tissues, Physics in medicine and biology, 41 (1996) 2271.

[109] H. Qin, J. Dong, Y.-S. Lee, AC-pulse modulated electrohydrodynamic jet printing and electroless copper deposition for conductive microscale patterning on flexible insulating substrates, Robotics and Computer-Integrated Manufacturing, (2015).

[110] H. Qin, C. Wei, J. Dong, Y.-S. Lee, Direct Printing and Electrical Characterization of Conductive Micro Silver Tracks by AC-Pulse Modulated Electrohydrodynamic Jet (E-Jet) Printing, Journal of Manufacturing Science and Engineering, (2016).

[111] E.C. Harvey, P.T. Rumsby, M.C. Gower, J.L. Remnant, Microstructuring by excimer laser, in: Micromachining and Microfabrication, International Society for Optics and Photonics, 1995, pp. 266-277.